IDENTIFICATION OF NOVEL THERAPEUTIC TARGETS AND RATIONAL DEVELOPMENT OF IMMUNOTHERAPEUTICS FOR RECURRENT GLIOBLASTOMA

IDENTIFICATION, VALIDATION, AND IMMUNOTHERAPEUTIC TARGETING OF NOVEL TUMOR-ASSOCIATED ANTIGENS FOR TREATMENT-REFRACTORY GLIOBLASTOMA

By

NAZANIN TATARI, (H)B.Sc., M.Sc.

A Thesis Submitted to the School of Graduate Studies of McMaster University in Partial Fulfillment of the Requirements for the Degree of

DOCTOR OF PHILOSOPHY in BIOCHEMISTRY AND BIOMEDICAL SCIENCES

DESCRIPTIVE NOTES

DOCTOR OF PHILOSOPHY (2021)
Biochemistry and Biomedical Sciences
Faculty of Health Sciences, McMaster University
Hamilton, Ontario, Canada

TITLE: Identification, validation and immunotherapeutic targeting of novel tumor-associated antigens for treatment-refractory Glioblastoma

AUTHOR: Nazanin Tatari, (H)B.Sc, M.Sc.
SUPERVISOR: Dr. Sheila Kumari Singh
NUMBER OF PAGES: xvii, 189

ABSTRACT

Glioblastoma (GBM) is the most common and aggressive brain tumor in adults which is characterized by extensive cellular and genetic heterogeneity. Even with surgery, chemotherapy with temozolomide, and radiation, tumor re-growth and patient relapse are inevitable. The extensive inter- and intra-tumoral heterogeneity (ITH) of recurrent GBM emerges from dysregulation at multiple -omic levels of the tumor. ITH exits at the cellular level due to a small subpopulation of chemo- and radio-resistant cells, called brain tumor initiating cells, which may drive GBM treatment resistance. Although a wealth of literature describes the biology of primary GBM (pGBM), we currently lack an understanding of how GBM evolves through therapy to become a very different tumor at recurrence, which may explain why therapies against primary GBM fail to work in recurrent GBM (rGBM). Thus, understanding the tumor evolution from a multi-omic perspective is critical for the development of effective therapeutic approaches.

The current work focuses on identification and validation of novel predictive and prognostic biomarkers for rGBM using proteomics analysis on a large cohort of patient-matched pGBM-rGBM samples. This work allowed for detailed characterization of rGBM and its cognate TIME toward a better understanding of the molecular players driving recurrence which can be further used for instructing effective targeted and personalized therapies for the treatment of therapy-resistant GBM.

In another part, we developed a novel immunotherapeutic modality called dual antigen T cell engager, to target Carbonic Anhydrase 9, a highly enriched hypoxia-inducible enzyme

in GBM. We demonstrated that this immunotherapeutic strategy which allows for targeting tumor cells while recruiting and triggering T cells through simultaneously, is highly effective in eliminating tumor cells and can be a complementary component of combinatorial therapy for GBM patients.

Altogether, this study provided key data for instructing novel and rational combinatorial polytherapeutic approaches for the treatment of therapy-resistant GBM.

DEDICATIONS

I dedicate my doctoral dissertation with sincere gratitude to**:**

My Father, Farhad (04/1955 – 04/2013), to whom I promised I would never stop dreaming, never stop believing, never give up, never stop trying, never stop learning and never stop growing. Every time I faced challenges along my way, thinking about our last conversation lifted me up… "Do not allow the challenges along the way stop you from pursuing what you want to achieve and never be scared of tough days along the way, your god is with you wherever you go". Though you left us in the beginning of my journey, your love and memory has been my guide every single day. I miss you with all my heart, but I am happy I am walking the path you put me on, Dad.

My mother, Fahimeh, who taught me to believe in hard work and that so much can be done with little. You have been my constant source of encouragement since I've gotten to know myself. I am forever grateful for your incredible support, sacrifice, and for engineering this belief in my head that there is only one way to succeed: to find your purpose in life and to dedicate yourself to it. My most sincere and deepest thanks to you mom, for all you have done with so much understanding, compassion and love that made it possible for me to be where I am today.

My brother, Aydin, who has been my all-time best cheerleader and has never left my side. Thank you wholeheartedly for always believing in me with a kind, caring and loving heart and selflessly supporting me in such a way that made it possible for me to step and continue

in this path. No matter how old I become, whenever I am with you, everything feels as sweet as our childhood.

ACKNOWLEDGEMENTS

As we journey through life, we learn that very little of what we accomplish is a solitary act. It is through cooperation and collaboration and our interactions with others that we invariably create our art.

As such, I would like to acknowledge those who made my doctoral journey possible. First and foremost, I would like to express my sincere gratitude to my supervisor, Dr. Sheila Singh, for giving me the great opportunity of joining her renowned laboratory 4 years ago and supporting me in every possible way ever since to grow and develop as an independent scientist. I am most grateful for the nurturing environment she provided me with which allowed me to expand my knowledge and broaden my skills in translational brain tumor research field. I have learned very much from her in many ways both scientifically and non-scientifically and above all has been how to be highly achieved yet very down to earth. Thank you for all your incredible support. I am also very grateful for Dr. Chitra Venugopal's guidance and encouragement and insightful contributions which made this journey possible. She was not only my second mentor and supervisor in the lab but also my best friend and lab mother who was there for me in any situation through all ups and downs of the process. I owe much of my scientific achievements and success to her incredible support, guidance, and compassion. I am very appreciative of my committee members, Dr. Kjetil Ask, Dr. Bradley Doble and Dr. Jonathan Bramson for their enriching perspective which helped me to shape my thesis and expedite the process. Thank you for your constant help and support during the past 4 years.

I am also very thankful to all Singh Lab collaborators, especially Dr. Thomas Kislinger, Dr. Jason Moffat, and Dr. Shahbaz Khan as well as all the past and present members of the Singh Lab who have contributed their expertise to this thesis. Last but not the least, my sincere and deepest gratitude to the patients who kindly donated their samples for tumor study without whom this work would have not been possible. You are true heroes. Sincere thanks to funding agencies who generously supported the work conducted throughout my Ph.D. particularly The Terry Fox Research Institute (TFRI), The Ontario Graduate Scholarship (OGS) and Mitacs.

Finally, my deep and sincere gratitude to my family for their continuous help and support and unconditional love. Your words of encouragement and push for tenacity ring in my ears. I am forever grateful to my parents and brother for always being there for me and giving me great opportunities in life that have made me who I am today.

"I am convinced that knowledge is power - to overcome the past, to change our own situations, to fight new obstacles, to make better decisions"_Ben Carson

TABLE OF CONTENTS

LIST OF FIGURES & TABLES

Chapter 1

Chapter 2

Chapter 3

LIST OF ABBREVIATIONS

ACT – Adoptive Cell Transfer
AKT – protein kinase B
ALL – Acute Lymphoblastic Leukemia
Astro – Astrocytoma
BBB – Blood-Brain Barrier
bFGF – Basic Fibroblast Growth Factor
BiTEs – Bispecific T Cell Engagers
BT – Brain Tumor
BTICs – Brain Tumor Initiating Cells
BTSCs – Brain Tumor Stem Cells
CAR – Chimeric Antigen Receptor
CA IX – Carbonic anhydrase IX
ccRCC – clear cell Renal Cell Carcinoma
CD – cluster of differentiation
CDR – complementarity-determining region
EDTA – ethylenediaminetetraacetic acid
CNA – copy number alterations
CNS – Central Nervous System
CRS – Cytokine release syndrome
CSCs – cancer stem cells
CTLA-4 – cytotoxic T lymphocyte-associated antigen-4
CTLs – cytotoxic T Lymphocytes
CYTOF – Cytometry by time of flight
DATE – Dual Antigen T Cell Engager
DCs – Dendritic Cells
DNA – deoxyribonucleic acid
ECM – extra cellular matrix
EGFR – Epidermal Growth Factor Receptor
ELISA – Enzyme Linked Immunosorbent Assay
EOR – extent of resection
FFPE – formalin-fixed paraffin-embedded
GAPDH – glyceraldehyde 3-phosphate dehydrogenase
GBM – Glioblastoma
GSCs – Glioma Stem Cells
GSEA – gene set enrichment analysis
H&E – hematoxylin and eosin
Hh – Hedgehog
HHS – Hamilton Health Sciences
HIF – Hypoxia-Inducible Factor
hrEGF – human recombinant epidermal growth factor
HRP – horseradish peroxidase

ICIs – Immune Checkpoint inhibitors
IDH – isocitrate dehydrogenase
IFN – interferon
IHC – Immunohistochemistry
IL – Interleukin
IMDM – Iscove's Modified Dulbecco's Medium
ITH – intra-tumoral heterogeneity
KO – Knock Out
LDH –lactate dehydrogenase
MDSCs – Myeloid-Derived Suppressor Cells
MET – Mesenchymal-Epithelial Transition
MGMT – O6-methylguanine methyltransferase
MHC – Major histocompatibility complex
MIBI-TOF – multiplexed ion beam imaging by time of flight
MMR – DNA mismatch repair
MRI – magnetic resonance imaging
NAT _ normal adjacent tissue
NCC – NeuroCult complete
NES – normalized enrichment scores
NHA – Normal Human Astrocyte
NMF – non-negative matrix factorization
NPC – neural-progenitor cell
NSCs – Neural Stem Cells
OG – oligodendroglioma
OS – overall survival
pAKT – phosphorylated protein kinase B
PBMCs – Peripheral blood mononuclear cells
PBS – Phosphate Buffer Saline
PDGFR – Platelet Derived Growth Factor Receptor
PD-1 – programmed cell death protein-1
pGBM – primary GBM
PI3K – phosphatidylinositol 3-kinase
PTEN – phosphatase and tensin homolog
RB1 – Retinoblastoma
RFS – relapse-free survival
rGBM – recurrent GBM
RNA – Ribonucleic acid
RPMI – Roswell Park Memorial Institute medium
RT – radiotherapy
RTK – Receptor tyrosine kinase
scFvs – single-chain variable fragments
sci-RNA-seq3 – Single-cell combinatorial indexing RNA sequencing
SoC – Standard of Care
SVZ – subventricular zone

TAA – Tumor Associated Antigen
TAM – Tumor Associated Macrophages
TCGA – The Cancer Genome Atlas
TCR – T cell receptor
TILs – Tumor-infiltrating lymphocytes
TIME – Tumor immune microenvironment
TMA – Tissue Microarray
TME – Tumor Microenvironment
TMZ – temozolomide
TNF – tumor necrosis factor
Treg – T regulatory cells
VEGF – Vascular Endothelial Growth Factor
VEGFR – Vascular Endothelial Growth Factor Receptor
WHO – World Health Organization
WT – Wildtype

DECLARATION OF ACADEMIC ACHIEVEMENTS

This thesis represents the original work that I conceptualized and performed throughout my PhD. I designed and conducted experiments, performed data analysis and interpretation, and wrote the manuscripts and all sections of this thesis. My entire PhD work was conducted under the supervision of Dr. Sheila Singh. Contributions of co-authors to each publication have been listed below. This thesis is presented in the format of a sandwich thesis as outlined in the Guide for Preparation of Master's and Doctoral Theses (v2016).

Chapter 1 provides an overview of the field of glioblastoma research.

Chapter 2 is an original article focused on preclinical testing of Dual Antigen T cell Engagers (DATEs), as a novel immunotherapeutic approach, for targeting Carbonic Anhydrase 9 (CA9) expressing brain tumor initiating cells in Glioblastoma (GBM) and cancerous cells in Renal Cell Carcinoma (RCC). This manuscript is in the process of getting submitted to prestogiuos journals in the field and the citation is as follows:

Tatari N, Xang S, Keith Lawson, Minomi Subapanditha, Vassem Shaikh, Maleeha Qazi, Mathieu Seyfrid, Chitra Venugopal, Jason Moffat, SHEILA K. SINGH. Immunotherapeutic targeting of Carbonic Anhydrase 9 (CA9) in treatment refractory Glioblastoma using Dual Antigen T cell Engagers (DATEs)

The DATE was engineered and constructed by Dr. Jason Moffat at the University of Toronto. The *in vitro* experiment related to the RCC project was performed by Sally Zhang in Dr. Jason Moffat's laboratory.

Chapter 3 is an original article focused on investigating the malignant modifications generated in GBM from primary to the recurrent stage under the therapeutic pressure for the development of rational therapeutic targets and predictive and prognostic biomarkers for recurrent GBM. This study was performed using advance proteomics techniques on one of the largest primary-recurrent GBM matched patient samples in the world collected form the Hamilton Health sciences (2001-2016). This manuscript will be submitted to Nature Cancer in October 2021. The citation is as follows:

Nazanin Tatari[*], Shahbaz Khan[*], Julie Livingstone[*], Dillon Mckenna, Chirayu Chokshi, William D Gwynne, Manoj Singh, Chenghao Zhu, Jennifer Chan, Cynthia Hawkins, Jian-Qiang Lu, John P. Provias, Kjetil Ask, Tobias Weiss, Micheal Weller, Jeffrey N Greenspoon, Chitra Venugopal, Paul C. Boutros[#], Sheila K. Singh[#], Thomas Kislinger[#]. Uncovering the evolution of Glioblastoma proteome landscape from primary to the recurrent stage for development of novel diagnostic and predictive biomarkers.

The proteomics run and analysis was performed in collaboration with Dr. Thomas Kislinger's laboratory (Dr. Shahbaz Khan) at the University of Toronto. The bioinformatics analysis was done in collaboration with Dr. Paul Boutros (Julie Livingstone) at the University of California.

Chapter 4 discusses the major implications of the research presented in this thesis and explores future research directions to improve our understanding of GBM with having specific focus on GBM immune microenvironment. The future direction explains my third PhD project which was conducted in collaboration with Dr. Jaosn Moffat's lab at the University of Toronto. This project is focused on a detailed survey of the tumor immune microenvironment in human rGBM and mouse models of brain cancer using multiple profiling technologies (i.e. IHC, flow cytometry, sci-RNA-seq3) for common populations of cells and gene expression patterns that will be leveraged for development of therapeutic strategies.

CHAPTER 1: Introduction

1.1 Glioblastoma

1.1.1. Clinical characteristics

Glioblastoma (GBM) is the most common malignant primary adult brain tumor which accounts for 60–70% of all gliomas and based on World Health Organization (WHO) classification is classified as a Grade IV tumor [1]. Between 2009-2013, 5,830 Canadians were diagnosed with GBM, at an incidence rate of 4.06 per 100,000 persons per year, making GBM the most commonly diagnosed and lethal primary malignant brain tumor in adults (59.2% of all neuroepithelial tumors) with a slight predominance in males [1, 2]. From a histopathological point of view, GBMs are known as extensively heterogeneous and infiltrative tumors. They show astrocytic features and are characterized by nuclear atypia, significant hypercellularity, mitotic activity with high Ki67 proliferation index, excessive angiogenesis and microvascular proliferation, and necrosis [1, 3]. The 2016 WHO classification divided GBMs into primary (*de novo*) and secondary tumors based on the mutational state of isocitrate dehydrogenase (*IDH*) genes. *IDH* wild type GBM was defined as primary (*de novo*) which makes up about 90% of GBMs. Primary GBMs arise in the absence of prior disease and are the aggressive, highly invasive neoplasms that are more commonly seen in older individuals (>45 years) and represents poor overall survival [4]. Secondary GBMs, bear IDH-mutant status, are less common and affect younger people (<45 years). Unlike primary GBMs, secondary GBMs develop from low-grade astrocytoma and tend to have a better prognosis. Morphologically, primary and secondary GBMs are

indistinguishable, however molecular profiling revealed that they develop from different cells of origin which results in distinct genetic alterations and underlying biological mechanisms for these two GBM types and consequently different clinical outcomes [5]. In 2021, the Consortium to Inform Molecular and Practical Approaches to CNS Tumor Taxonomy (cIMPACT-NOW) updated the Central Nervous System (CNS) tumor classification, such that IDH-mutant GBM is now separated from IDH wild-type GBM and is considered as IDH-mutant astrocytoma [6].

1.1.2. Current standard of care (SoC) for glioblastoma

Despite advanced diagnostic modalities and aggressive multi-modal treatment including maximal surgical resection, followed by chemotherapy using concomitant and adjuvant temozolomide (TMZ) plus radiotherapy (RT), GBM remains incurable [7, 8]. Almost all patients experience relapse 7-9 months post-diagnosis and median survival has not extended beyond 15 months over the past decade [9]. Addition of other therapeutics such as bevacizumab to the standard therapy regimen for GBM patients has shown no improvement in patients' overall survival (OS) [10, 11].

Unlike primary GBM (pGBM), there is no established SoC for recurrent GBM (rGBM) [12] due to the existing limitations in identification of effective therapies [13]. The current treatment options for rGBM mainly includes surgical reoperation, radiation, systemic chemotherapies and assigning patients to clinical trials, and combined modality therapy [14]. These treatment options are described as follows:

A. Re-operation: The initial and most crucial therapeutic step for rGBM is surgery when feasible, which allows for tumor debulking. Although there are several patient-related factors which determine the outcome of the treatment, the strongest one remains the extent of resection (EOR) [15]. The patients who receive maximal safe surgical resection followed by chemotherapy and radiation have shown longer survival advantage. However, as GBM is an invasive and diffuse tumor, tumor debulking should be done in a balanced way so that it does not damage normal brain tissue and as a result affect the patient's quality of life [16, 17]. To increase the efficiency of tumor resection, fluorescent agents such as 5-aminolevulinic acid (5-ALA) are being applied to surgical practice which has shown 91.4% sensitivity and 89.2% specificity in defining tumor borders and protecting normal brain [18].

B. Chemotherapy: In 2005, Stupp and colleague reported that the addition of alkylating agent TMZ to radiotherapy following surgical resection of pGBM results in a significant increase in patient survival advantage from 12.1 to 14.6 months. In addition, their findings revealed minimal toxicity associated with TMZ administration [19]. The current TMZ treatment for newly diagnosed GBM patients consists of oral administration of 75 mg/m2 per day for 6 weeks throughout radiotherapy followed by 150–200 mg/m2 per day for the first 5 days of a 28-day cycle for up to 6 maintenance cycles [20]. There are several available options for second line chemotherapy for GBM patients. As such we can refer to Nitrosourea DNA alkylating agents such as lomustine (CCNU) which have shown high efficacy due to their lipophilic features which allows them to cross the blood brain barrier,

therefore making them an efficient therapeutic agent for GBM patients. It has been suggested MGMT promoter methylation can predict the response to this class of agents [21]. Moreover, TMZ monotherapy and TMZ-based combination regimens, has been shown effectiveness in second line chemotherapy and is being used as a treatment option for patients with rGBM [14]. In 2009, bevacizumab got approved by FDA as an effective treatment regimen for patients with rGBM [22, 23]. Since then, several clinical trials have been conducted which have revealed the efficacy of bevacizumab alone or in combination with other agents, such as TMZ for patients with rGBM. A retrospective analysis of 468 GBM indicated the efficacy of bevacizumab independent of disease stage and showed its effectiveness at both primary and recurrent state [24].

C. Radiotherapy (RT): Designing the right RT plan for pGBM patients is dependent on initial gross tumor volume which can be determined by postoperative-enhanced MRI. This gives the possibility to delineate the surgical resection cavity as well as any residual tumor. Currently the suggested RT plan for GBM patients is 2- to 3-cm clinical target volume margin and a 3- to 5-mm planning target volume expansion with RT volume of 60 Gy in 30 fractions (2 Gy daily) [25]. This therapeutic regimen has been partially effective and has only led to prolonging patients' survival up to 15 months. Since the brain gets exposed to high dose radiation following the first surgical resection, re-irradiation with the same doses upon tumor recurrence has high toxicity risks. Therefore, the methods used for re-irradiation at recurrence are mainly hypofractionated stereotactic radiotherapy

(hfSRT) and stereotactic radiosurgery (SRS) as they allow for limited volume irradiating. SRS and hfSRT both have smaller margins and deliver more than 2 Gy per fraction with shorter durations than conventionally fractionated radiotherapy (cfRT) and have shown more promising outcomes for rGBM [26].

D. In addition to SoC, in the last decade, there has been an extreme attention in producing targeted therapies for GBM. Therefore, several clinical trials have been reported which have shown promising results in Phase I/II for GBM [27]. As such we can refer to immunotherapies including CAR T cell-based therapies, antibody therapies and immune check point inhibitors as well as vaccines, and. The summary of current clinical trials used for GBM patients has been listed in the table below:

CAR T cell clinical trials for GBM	
NCT Number	Treatment
NCT00730613	IL13(E13Y)-CD3ζ CAR T cells (first generation) for rGBM [28]
NCT02208362	IL13(E13Y)-41BBζ CAR T cells (second generation) for rGBM [29]
NCT01109095	HER2-CD28ζ CAR T cells (second generation) for GBM [30]
NCT02209376	EGFRvIII-41BBζ CAR T cells (second generation) for rGBM [31]
NCT01454596	EGFRvIII-CD28-41BBζ CAR T cells (third generation) for rGBM [32]
Antibody therapy / immune check point inhibitor clinical trials for GBM	
NCT Number	Treatment
NCT02017717	Nivolumab (anti-PD-1) or bevacizumab for rGBM [33]
NCT02617589	Nivolumab (anti-PD-1) + radiotherapy or TMZ + radiotherapy for pGBM
NCT02667587	Nivolumab (anti-PD-1) + TMZ + radiotherapy for pGBM
NCT02313272	Hypofractionated stereotactic irradiation + pembrolizumab (anti-PD-1) + bevacizumab for Recurrent high-grade glioma [34]
NCT02337491	Pembrolizumab (anti-PD-1) or pembrolizumab + bevacizumab for rGBM [35]
NCT02550249	Neoadjuvant nivolumab for GBM
NCT02336165	Durvalumab (anti-PD-L1) alone, with bevacizumab, or with radiotherapy for GBM [36]

NCT02658981	Anti-LAG-3 or anti-CD137 alone or with anti-PD-1 for rGBM [37]
Vaccine based clinical trials for GBM	
NCT Number	Treatment
NCT00643097	EGFRvIII peptide vaccine + DI-TMZ for pGBM [38, 39]
NCT00458601	EGFRvIII Peptide Vaccine + TMZ for pGBM [40]
NCT01480479	EGFRvIII peptide vaccine + TMZ for pGBM [41]
NCT01498328	EGFRvIII peptide vaccine + bevacizumab for rGBM [42]
NCT00639639	CMV pp65 DC vaccine + Td Toxoid + TMZ for pGBM [43]
NCT00639639	CMV pp65 DC vaccine + DI-TMZ for pGBM [44]
NCT02366728	CMV pp65 DC vaccine + 111In-labeled DC vaccine + Td Toxoid + basiliximab for pGBM [45]
NCT02454634	IDH1 peptide vaccine for high grade glioma [46]
NCT00045968	DCVax-L vaccine for pGBM [47]
NCT00293423	HSPPC-96 peptide vaccine for rGBM [48, 49]
NCT02122822	HSPPC-96 peptide vaccine + TMZ + radiotherapy for pGBM [50]
NCT00905060	HSPPC-96 vaccine + TMZ for pGBM [51]

Table 1.1. Summary of clinical trials for GBM

In addition, another efficient treatment modality which has shown favorable efficacy and safety for GBM patients is Tumor Treating Fields (TTFields). Addition of TTFields to TMZ was associated with increased overall survival in GBM patients at both primary and recurrent state. TTFields applies its therapeutic effect via various mechanisms including suppression of tumor cell proliferation, migration and invasion, antimitotic effects, disruption of DNA repair and angiogenesis, and induction of apoptosis and immunogenic cell death. This makes TTFields an attractive therapeutic modality that can be used in combination with SoC and immunotherapy [52].

1.1.3. GBM prognostic factors - MGMT promoter methylation

Currently several prognostic factors including patient's age, neurological status, IDH (isocitrate dehydrogenase) mutational status and O6-methylguanine methyltransferase (MGMT) promoter methylation status have been established for GBM patients, many of which also play a critical role in predicting the patient's response to treatment [14]. TMZ is an integral part of GBM standard-of-care therapy, however; at least 50% of patients do not respond to TMZ [53]. Therefore, assessing the tumor's MGMT promoter methylation status is one of the most important predictive factors for effective response to chemotherapy [54].

TMZ, a small (194 Da) lipophilic molecule, is an orally administered monofunctional DNA alkylating agent. It is stable at acidic pH and has the ability to cross the blood-brain barrier, which makes it a desirable drug for CNS tumors. TMZ acts as a prodrug and induces DNA methylation and tumor cytotoxicity through cell cycle arrest. The mechanism of action for tumor cytotoxicity relies on the ability of TMZ to methylate DNA at several sites including N7-methylguanine (70%), N3-methyladenine (9%) and O6-methylguanine (6%). However, DNA adducts can be repaired by several mechanisms. N7-methylguanine and N3-methyladenine are repaired by the base excision repair pathway and are not considered as the primary mediators of TMZ toxicity. TMZ applies its toxicity effect by methylating DNA at O6 guanine. This carcinogenic and toxic lesion leads to insertion of thymine instead of a cytosine opposite to guanine during DNA replication which results in activation of DNA mismatch repair (MMR). MMR recognizes and removes thymine while the O6-MeG remains intact [55]. This causes futile cycles of repair such as consecutive DNA

strand breaks with the goal of fixing the mismatch, resulting in G2/M arrest and eventually cell apoptosis [56]. On the other hand, MGMT activation results in rapid reverses in alkylation (demethylation) at the O6 position of guanine which neutralizes the cytotoxic effects of TMZ and eventually causes tumor resistance to TMZ as an alkylating agent [55]. Therefore, the therapeutic effect of TMZ is dependent on the reduced activity or absence of MGMT and an intact and fully functional MMR pathway. Therefore, MGMT status testing is being used in clinical settings as a way to predict patient's response to therapy [57]. However, MGMT promoter status does not modify the inclusion of TMZ in standard-of-care treatment due to lack of other effective therapies for GBM; in other words, TMZ is seen as the only possibly effective and safe chemotherapy and is thus offered to all GBM patients, regardless of MGMT promoter status [19].

1.1.4. Molecular classification of GBM

Cellular and molecular characterization of GBM has revealed extensive inter- and intra-tumoral heterogeneity caused by dysregulation at multiple "omic" levels. Therefore, comprehensive understanding of the genome, transcriptome and proteome alterations in GBM is a crucial step for deciphering tumor treatment resistance and designing empirical diagnostics, prognostics, and targeted therapeutics. Studies focused on Copy Number Alterations (CNA) conducted by different groups in the past two decades, identified regions of amplifications and deletions which play a significant role in GBM exacerbation and tumorigenesis [58-60]. The identified pattern of modifications revealed that amplifications were mainly detected in oncogenes such as Epidermal Growth Factor Receptor (EGFR,

[Chr.7]; 32.6%), Mesenchymal-Epithelial Transition factor (MET), Platelet Derived Growth Factor Receptor (PDGFR, [Chr.4]; 4.5%), Vascular Endothelial Growth Factor (VEGF) and Vascular Endothelial Growth Factor Receptor (VEGFR), Myc, and in TP53 signalling (MDM2 [Chr.12] and MDM4; 34.4%) [61] while the deletions were largely focused on tumor suppressors including retinoblastoma protein (RB1) and phosphatase and tensin homolog (PTEN [Chr.10]; 32%) [62]. In addition, the study conducted by Parsons *et al* in 2008 also introduced the Receptor Tyrosine Kinase (RTK) signalling pathways, P53 and RB1 signaling pathways as the most dominant alterations in the majority (74%) of GBMs [63].

RTK: RTKs which are transmembrane proteins have a critical role in controlling receptor activity in normal cells, and they regulate cell survival, cell growth, cell differentiation, and migration. However, the balanced functioning of the RTKs is affected in GBM in various forms of amplification, mutation or deletion. The main RTKs affected in GBM include:

1. EGFR: EGFR is amplified in 40–50% of tumors and is overexpressed in over 60% of patients. One of the most common variants of mutation in EGFR is EGFRvIII which causes the activation of the receptor independent of the ligand. Co-expression of EGFR and EGFRvIII leads to activation of STAT3/5 signaling pathway which ultimately results in tumor progression [64].
2. PDGFR: PDGFR consists of 2 isoforms including PDGFRα and PDGFRβ which play different roles in GBM progression. While PDGFRα is one of the most amplified receptors in GBM, PDGFRβ is only expressed in glioma stem cells and regulates stem cell marker expression levels [65]. According to Cancer Genome

Atlas (TCGA) [66], PDGFRα is significantly amplified (40%) and mutated (20%) in GBM particularly in the proneural subtype, although PDGFRβ is only mutated in 4% of GBMs with proneural subtypes.

3. PI3K/Akt/PTEN: PI3K/Akt pathway has a crucial role in regulating cell processes such as cell proliferation, growth, and survival. Particularly in GBM, the pathway remains constantly activated as a result of PTEN alterations or Akt amplification which leads to activation of mTOR, modulating cellular processes such as growth response. PI3K/Akt/PTEN and PI3K/Akt/mTOR are known as highly modified pathways in GBM which drive increased tumorigenicity of GBM.

Together, the above-mentioned aberrations in RTK signaling pathways significantly contribute to increasing the proliferative capacity of GBM.

P53: P53, the tumor suppressor with a significant role in tumor prevention, is the highest deregulated pathway in 84% of GBM patients. The components of the deregulated p53 pathway play critical role in GBM progression by causing cell invasion, proliferation, migration, cancer cell stemness, evasion of apoptosis and eventually tumor cell survival. The 2 regulators of the p53 pathway include MDM2 (amplificated in 10% of GBMs) and MDM4 (amplificated in 7% of GBMs) [61].

RB1: The main role for RB protein includes cell cycle control (suppression) specifically at S-phase which restricts cell division by preventing cell cycle progression from G1 phase to S phase. Therefore, mutations of the *RB* gene cause uncontrolled cell division which is similar to the effect of CDK4/CDK6 amplification or CDKN2A/CDKN2B mutation. However, these alterations do not occur simultaneously. Alteration of RB pathway

frequently happens in GBM and is present in 80% of GBMs, which results in increased tumor proliferation and decreased survival of tumor cells.

Altogether, these pathways form the core signalling networks that drive GBM tumor growth and exacerbation.

Following characterization of the GBM mutational landscape, effort was put into understanding the correlation between patients' clinical outcomes and these mutations for identification of targets with potential therapeutic benefit. In 2010, TCGA introduced a molecular classification for GBM which was defined based on identification of genomic drivers of GBM by sequencing 206 patient samples. Based on this study, GBMs were classified into four transcriptomic subtypes including Classical, Mesenchymal, Proneural and Neural.

The Classical subtype is characterized based on EGFR amplification or mutation and shows aberrant changes including amplification of Chr.7 and loss of Chr.10, inactivation of the RB pathway. Other pathways such as Sonic hedgehog and Notch signaling have high levels of expression in the classical subtype. It has been shown that patients diagnosed with GBM with classical subtype have a better response to therapy, which has resulted in significant reduction in mortality (median survival of 14.7) when patients were given chemotherapy and radiotherapy.

The Mesenchymal subtype is characterized by extensive inflammation, necrosis and upregulation of angiogenesis related genes such as *VEGF-A, VEGF-B, ANG1* and *ANG24* [67]. Moreover, deletion of tumor suppressor genes including *NF1*, *P53* and *PTEN* and high expression of genes in the NF-κB pathway and the TNF superfamily classifies tumors

of the mesenchymal subtype. The median survival for patients diagnosed with mesenchymal subtype is 11.5 months.

The Proneural subtype is characterized based on expression of neural stem cell genes such as *SOX2* and *OLIG2*, *PDGFRA* amplification, *TP53* mutation and frequent IDH1 mutation. Patients harboring GBM with proneural subtype are primarily younger and have better survival rates compared to other subtypes (17.0 months); however, no significant difference in response to chemotherapy and radiotherapy was seen in these patients [68].

The Neural subtype has a similar gene expression pattern to normal brain tissue. GBMs with expression of neuron markers such as GABRA1, SYT1, SLC12A5 and NEFL are classified as the Neural subtype [66] and are more responsive to the standard therapy including radiation and chemotherapy.

Later in 2013, Sottoriva *et al* [69] introduced characterization of spatial and temporal heterogeneity by genomic analysis of spatially distinct tumor fragments resected from 11 GBM patients. This study showed that there is an extensive intratumoral heterogeneity in a single tumor as tumor fragments from the same patient may be classified into different GBM subtypes. Using single cell transcriptome analysis performed by RNA-seq on 430 cells from five primary GBMs, Patel *et al* showed that these cells were highly variable in the expression of various transcriptional programs related to oncogenic signaling, proliferation, immune response and hypoxia as well as stemness-related expression states [70]. Moreover, Szerlip *et al* showed heterogeneous amplification of receptor tyrosine kinases (RTK), EGFR and PDGFRa within GBM cell subpopulations [71].

Most studies were focused on sequencing the bulk tumor; however, this approach might not be fully efficient in capturing the variable cells existing in the tumor that may drive a new tumor after therapy. In 2019 Neftel *et al*. performed a full-length scRNA-seq on 20 adult GBM and 8 pediatric GBM samples with the goal of identifying the transcriptional cellular states that define GBM. Moreover, they assessed various factors including genetic events, TME and tumor cell plasticity in modulating these states. This study led to identification of four different GBM cell states that dynamically populate each GBM. These four states contain features of normal neural cell populations as well as abnormal genetic events which were also identified by TCGA and include neural-progenitor cell (NPC)-like (CDK4 amplified), oligodendrocyte-progenitor cell (OPC)-like (PDFRA amplified), astrocyte cell (APC)-like (EGFR amplified) and mesenchymal cell (MES)-like (NF1 alterations). Although these cellular states stem from different genomic alterations, they showed that a genomic alteration at a clonal level does not exclusively drive a single cellular state, but rather favors the overall cellular composition of the tumor toward specific states. Moreover, this study suggested that particular cellular states may be more influenced by microenvironmental factors such as the presence of immune cell signatures in the MES-like state.

Lastly, using *in vivo* studies they showed the ability of cellular GBM subpopulations from a single state to give rise to tumors comprising all four cell states, indicating the plasticity of GBM cells and the equality of cell state capacity in initiating tumors [72].

These studies together inform not only the extensive genomic heterogeneity and complexity exists in GBM and causes tumor continuous evolution, but present heterogeneity as a

possible asset to evade therapy resistance. Consequently, this intra-tumoral heterogeneity (ITH) may then give rise to subclonal populations of cells with selectable traits that can respond to and escape any given stress, including therapy which drives ITH at the cellular level.

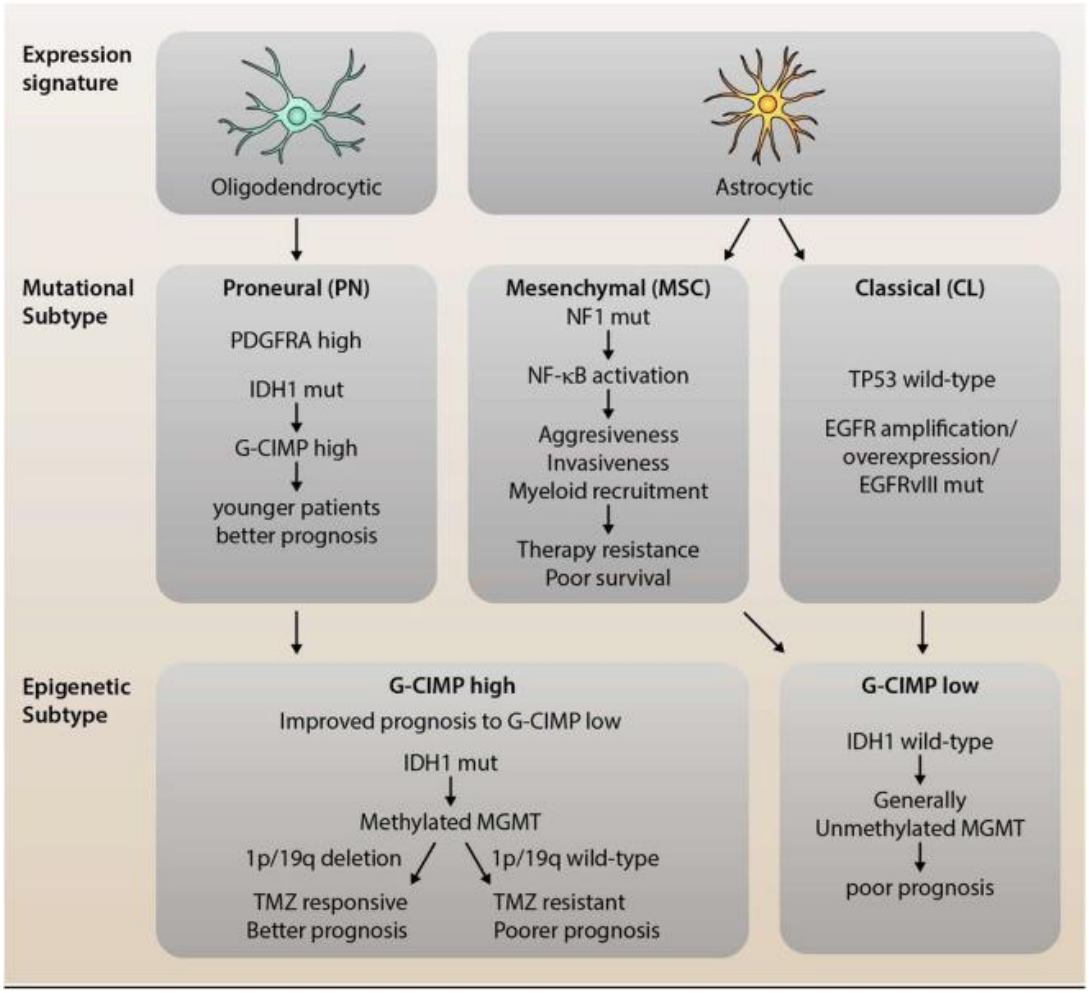

Figure 1.1. GBM Subtype Classifications. The mutational and epigenetic based analysis classified GBM into three main subtypes including the proneural (PN), mesenchymal (MSC), and classical (CL) subtype. This figure is adopted from DeCordova, S., *et al*. paper (*Front Immunol. 2020 Jul 17;11:1402. doi: 10.3389/fimmu.2020.01402*) [73].

1.2. Cancer Stem Cells (CSCs) in Glioblastoma

GBM cellular heterogeneity, which is associated with clonal evolution, can be explained by the existence of multiple cellular subpopulations of cancer cells that have acquired stem cell properties including self-renewal, multi-lineage differentiation and low but steady levels of unlimited proliferative capacity. This cell subpopulation is variably referred to in the literature as Brain Tumor Initiating Cells (BTICs) or Glioblastoma Initiating Cells (GICs) [74-77] based on *in vivo* functional definitions, or Brain Tumor Stem Cells (BTSCs) or Glioma Stem Cells (GSCs) based on *in vitro* stem cell assays. Poor patient survival has been shown to correlate with increased presence of these quiescent, pluripotent chemo- [78] and radio-resistant [7] BTICs [74] which also play a significant role in development of treatment resistance in GBM. In fact, due to low mitotic activity of GICs, treatment approaches that are directed against actively dividing cells are not fully effective. Thus, research efforts have been focused on understanding and targeting these treatment-resistant BTIC populations.

Particularly in brain tumors, BTICs were identified and purified as a small subpopulation of tumor that showed stem cell properties at both *in vitro* [76, 79, 80] and *in vivo* levels [74]. Also, it has been shown that GSCs have the ability of inducing tumors in immunocompromised mice, with a similar pattern of heterogeneity and complexity as the initial tumor which was a proof of the tumor-initiating property of BTICs [74, 81].

While GICs can rise from accumulation of somatic mutations in any of the cellular compartments in the neural lineages, a study performed by Lee *et al* showed that the GBM cell of origin is believed to be an astrocyte-like NSC with stem cell cardinal features

residing in the subventricular zone (SVZ) region of the brain that can migrate to the distant brain regions and generate the malignant disease phenotype of GBM [82].

1.2.1. Molecular markers of glioma stem cells (GSCs)

One of the major strategies for *in vitro* identification of GSCs from a mixed population of brain tumor cells is assessment of the expression of cell membrane antigens. So far, several GSC- specific markers have been identified. As such we can refer to CD133 (Prominin 1), CD44, CD15, L1CAM, GFAP and the other proteins including SOX2, OLIG2, NANOG, MYC, NESTIN and MUSASHI-1 [74, 83-85]. However, no single marker is universal for defining the GSC population [86]. CD133 is the first accepted GSC marker [76] and its expression is known to be associated with self-renewal; and reduction in its expression is seen during differentiation [87]. The other critical feature of $CD133^+$ cells is that they are capable of forming neurospheres and also initiate brain tumors in animal models [74]. Previous studies have shown that $CD133^+$ /$Ki\text{-}67^+$ cells as well as Nestin or HOX gene expression are considered as an adverse prognostic factor for GBM [88-90]. CXCR4 (CD184) is expressed predominantly in $CD133^+$ cells and is associated with increased expression of hypoxia-inducible factor (HIF-1-α) [91, 92]. MUSASHI-1 is another protein which acts as a regulator of cellular fate and translation [93]. It is important to note that all GBM cell subpopulations with stem cell properties are generally also tumorigenic in animal models and are able to adapt to different environmental modifications, implying that these Cancer Stem Cells (CSCs) do not represent a distinct clonal entity defined by specific cell-intrinsic functional properties and transcriptomic signatures, but rather a cellular state which is also determined by the influence of cell-extrinsic environmental factors.

CSC markers are heterogeneously expressed in GBM tumors. In fact, tumor cell subpopulations are capable of adjusting their phenotype, and the differences in the adaptation pace result in tumor growth at different rates. This phenotypic change, which is the result of cancer cell plasticity, has a direct impact on the design of therapeutic strategies. In fact, this transient state causes CSC therapeutic targeting to be only partially successful, as rapid phenotypic changes only allow for targeting a small subpopulation of cells. Moreover, different sensitivity rates of clonogenic GSCs to chemo and radiotherapy is another reason behind the failing of standard-of-care therapy to eliminate the tumor completely. Therefore, to have an effective therapeutic approach, these dynamic processes will need to be tackled, which can be possible by designing combinatorial therapeutic modalities that allows for targeting multiple CSC populations simultaneously and modulating their stemness [94].

1.2.2. The role of GSCs in glioblastoma therapy resistance

One of the main factors involved in GBM recurrence and treatment resistance to SoC therapy including chemotherapy and radiation, is the existence of GSCs as a small fraction of cells that survive and escape therapy. Two mechanisms of chemoresistance have been defined for GSCs which can be classified into intrinsic and extrinsic factors as have been elaborated in detail below.

1- Intrinsic factors: Molecular pathways and gene expression within GSCs are considered to be intrinsic factors [95]. From the intrinsic mechanisms, we can refer to activation of Hedgehog (Hh), Notch, Wnt and glioma associated oncogene 1 (GLI1) pathways in GSCs which along with insulin-like growth factor I (IGF-I)

[96] may promote GSC proliferation, invasion, and angiogenesis. The other intrinsic factor which plays a significant role in GSC chemoresistance is the presence of MGMT enzyme in GSCs [95]. Signaling pathways such as JNK and microenvironmental factors such as hypoxia can upregulate the MGMT expression and as a result cause chemoresistance [97, 98]. It has been shown that MGMT-positive GSCs require a significantly higher doses of TMZ to respond to therapy [99]. Another primary mechanism of GSC treatment resistance is increased expression of ATP-binding cassette (ABC) transporter which have the ability of mediating the efflux of cytotoxic chemotherapy agents and cause treatment resistance [100]. In fact, the regulation of ABCB1, ABCG2 and multidrug-resistant associated Protein1 (MRP1) in GCSs is under the effect of Notch, Hh, and Wnt signaling pathways, PTEN/PI3K/Akt pathway [101], CD133 expression and DNA dependent protein kinase (DNA-PK) through the PI3K/Akt-NF-κB pathway [102] which all results in chemoresistance. Emerging evidence indicate that Hh signaling pathway also causes chemoresistance in GSCs through regulating MGMT which is independent from MGMT promoter methylation status [103]. Besides, it has been demonstrated that these pathways cause overexpression of antiapoptotic proteins or downregulation of proapoptotic factors in GSCs [104]. It is also well stablished that Hh, Wnt and Notch pathways play a significant role in resistance to chemotherapeutics by modulating cell cycle, cell survival and proliferation and induction of ROS and Epithelial to Mesenchymal Transition (EMT) [105].

2- Extrinsic factors: From the extrinsic factors we can refer to TME components, cell-to-cell interactions, blood brain barrier functionality, endothelium and hypoxia [95] which can induce therapy resistance in GSCs through several processes such as increased angiogenesis and altered metabolism changes [106, 107]. Among the extrinsic factors, hypoxia is the most important environmental factor that causes chemoresistance in GSCs. Previous studies have shown increased numbers of GSCs in the core of the tumor where the intratumoral hypoxia was elevated [108]. In hypoxic conditions the GSCs remain in an undifferentiated state, which occurs under the influence of hypoxia-inducible factor-2α (HIF-2α) and several HIF-2α-induced genes [109, 110]. Hypoxic environments have been also proven to induce stemness genes including OCT4, NANOG, SOX2, KLF4, cMYC as well as CD133 and HIF (HIF1α and HIF2α). It has been indicated that majority of neurospheres in hypoxic condition are $CD133^{+}$. Moreover, hypoxia activates the Notch, Wnt, and Hedgehog (Hh) pathways which has a direct effect on maintaining the stemness of GSCs as well as chemoresistance. Previous studies have also indicated that hypoxia leads to increased GSC proliferation by activating various pathways such as NF-kB, PI3K/AKT, and STAT3 through which increase their chemo and radio resistance [111].

Another important mechanism involved in GBM chemoresistance is GSC plasticity. It has been shown that the niche factors including hypoxia and acidic environment and chemotherapy agents are able to induce stemness in non-GSCs [112]. This has been seen specifically in CD133- GSCs which are able to acquire CD133+

properties after chemotherapy [113]. Moreover, dedifferentiation of non-GSCs into GSCs following radiation is considered as another mechanism for GSCs treatment resistance [114].

To increase the efficacy of chemotherapy on GSCs, combination therapy comprising chemotherapy and immunotherapy has been used, which has shown enhanced efficacy of TMZ against GSCs through reducing GSC markers such as CD133 and nestin. This results in reduction in self-renewal and proliferation as well as abolishing clonogenicity and tumorigenicity of GSCs leading to increased tumor cell death [99, 115]. Moreover, another strategy used for targeting GSCs is the combination of TMZ with kinase inhibitors which also induced a decreased stemness and cell proliferation [116].

In addition to chemo-resistance, GSC radio-resistance has added another layer of challenge in GBM treatment resistance. Ionizing radiation causes DNA damage through various ways particularly by inducing DNA double strand breaks. One of the main survival mechanisms in CSCs after being exposed to radiation is cellular response to DNA damage through different mechanisms such as activation of DNA damage checkpoints or DNA repair mechanisms depending on the incurred injury which results in CSCs proliferation [117-119]. GSCs being exposed to radiation show higher levels of DNA repair-related genes including RAD51, BRCA1 and BRCA2 which results in reduced DNA damage [120, 121]. In addition, another key mechanism for DNA damage control in GSCs is replication stress (RS) which leads to stopping or reducing the speed of replication forks and results in inefficient DNA replication. The tyrosine kinase MET also plays a significant role in radio-

resistance of GSCs by activating AKT kinase and the downstream effectors of DNA repair as well as phosphorylation of p21 protein, which leads to anti-apoptosis [122].

It has been shown through various studies that $CD133^+$ GSCs have significantly higher resistance to radiation compared with $CD133^-$ glioma cells as the former population of cells are capable of repairing DNA damage through activating the DNA damage checkpoint [7]. Moreover, $CD133^+$ GSCs are more dominant in recurrent GBM tumors compared with primary tumors indicating that not only do they have the ability of surviving the radiation but also, they are highly proliferative [123, 124]. However, it is noteworthy that radiosensitivity is heterogeneous and is not only reliant on cell-intrinsic GSC characteristics but is a result of cellular interplay and is heavily under the influence of tumor microenvironment [87].

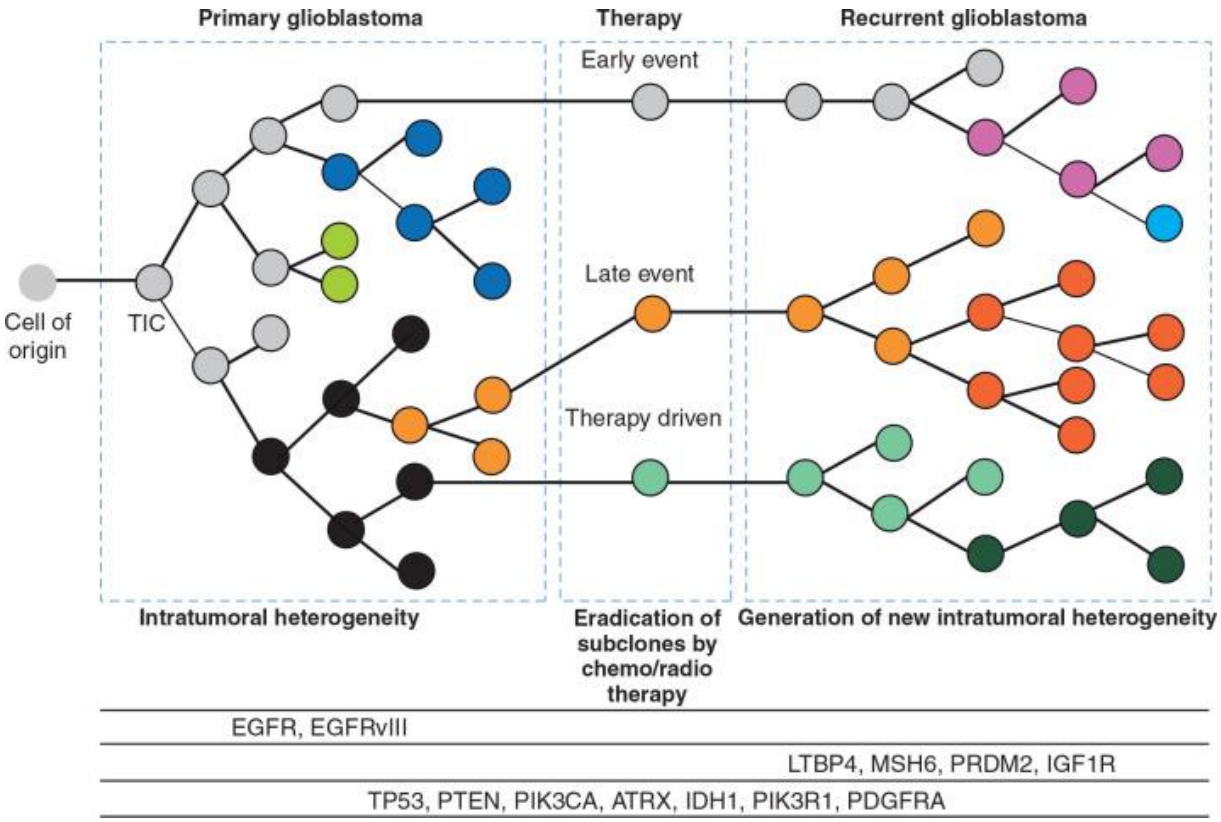

Figure 1.2. Cancer Stem Cell progression in GBM. Subclonal populations of GSCs in primary GBM have the ability of escaping therapy which results in generation of heterogeneous treatment-refractory, recurrent GBM. Therapeutic pressure causes selection of subclonal cell populations leading to generation of therapy-driven-resistant subclone which subsequently makes up recurrent GBM with different genetic, transcriptomic, and proteomic landscape compared to the primary counterpart. This figure is adopted from Qazi, M., *et al*. paper (*Ann Oncol. 2017 Jul 1;28(7):1448-1456. doi: 10.1093/annonc/mdx169.*) [125].

1.3. Tumor microenvironment in GBM

The tumor microenvironment (TME) is a critical regulator of GBM progression and therapy resistance in various ways. The TME consists of the non-cancerous cells as well as cancer cells, including immune cells, microglia/macrophages, fibroblasts, normal and reactive astrocytes, endothelial cells and vascular pericytes as well as proteins and non-protein biomolecules and cell products which all function together to aid in tumor progression. In fact, the unique cellular composition of TME contributes to making it highly immunosuppressive or "cold".

The TME can be divided into a non-immune compartment and an immune compartment:

1.3.1. Components of the TME's nonimmune compartment in GBM

The Blood-brain barrier (BBB) has a unique structure consisting of endothelial cells, pericytes and astrocytic foot processes [126, 127] which distinguishes the brain from other body organs. This happens as the BBB acts as a selective barrier between the brain and the systemic circulation which protects it from any toxic substances and infectious agents. It has been shown that the BBB obstructs the delivery of about 98% of molecules and therapeutics, as well as immune effector cells in certain conditions. However, the integrity and as a result the selective features of the BBB become disrupted in GBM, causing leakiness and makes it more permeable to therapies [126, 128, 129]. This phenomenon was observed in anti-CTLA-4 antibody trials in melanoma-to-brain metastases patients which resulted in clinical benefit. Interestingly it has been also shown that the molecular subtype of tumor has a direct effect on composition and integrity of the BBB [130] which may explain why some subtypes have better prognosis compared to the others. Moreover, the

BBB also allows the transmigration of metastasizing cancer cells from different sites of the body using various mechanisms such as junctional adhesion molecule proteolysis [131]. Altogether, all these studies have revealed that the properties of the BBB and its functionality are under the direct influence of various components of the brain TME.

GBM is a highly angiogenic tumor and vasculature have poor structural integrity and organization [132], resulting in leakiness. Leakiness itself leads to various phenomena including extensive hypoxia, necrosis, deregulated selectivity and edema which all cause tumor exacerbation [132]. Therefore, one of the significant efforts in advancing GBM therapy has been focused on targeting pro-angiogenic factors, which led to identification of antiangiogenic therapeutic modalities such as bevacizumab, sorafinib, sunitinib, etc. These therapeutics have shown limited success due mainly to their association with some unfavorable effects. For instance, addition of bevacizumab to SoC therapy for newly diagnosed GBM patients showed slight increase in patient progression-free survival; however, it caused other complications such as neutropenia, reduced cognitive function and hypertension. Despite these toxicities, bevacizumab has been approved as a combination therapy with SoC [10, 11]. Another effective method for targeting angiogenesis in GBM is vascular normalization which allows for controlling tumor-associated vasculature without affecting physiological angiogenesis. This results in reduction in hypoxia and improvement of drug delivery and perfusion; however, this therapeutic modality is still under investigation [133-135]. Limited understanding about the mechanism of vascularization in brain tumors makes designing effective anti-angiogenic therapies challenging. Previous studies have indicated that normal Neural Stem Cells (NSCs) have the ability to

differentiate into an endothelial-like phenotype which increases angiogenesis in the brain [136]. Moreover, it has been shown that GSCs have a transcriptional program that mimics endothelial cells [137]. Studies focused on GBM angiogenesis have also indicated that the perivascular niche is a glioma stem cell reservoir, and when endothelial cells secrete proangiogenic factors such as nitric oxide, they maintain BTIC populations which in turn causes tumor growth and resistance to radiation [138, 139]. Altogether, these studies show the critical effect of endothelial cells, NSCs and GSCs in tumor angiogenesis which should be targeted in the design of effective therapeutic modalities for GBM [140].

Astrocytes have a paradoxical role in the brain, in maintaining brain homeostasis but also aiding in tumor progression. In fact, they maintain brain homeostasis by providing structural support and by contributing into the maintenance of the BBB and wound healing processes [141, 142]. From the other side, they play a pro-tumorigenic role by secreting neurotrophic factors that result in GSC survival and proliferation [139]. Moreover, the growth factors and cytokines secreted by astrocytes in the reactive gliosis process, a mechanism of wound healing in the brain, have direct effect on tumor growth and cause resistance to therapy [143] and in some cases create a favorable condition for tumor invasion by secreting metalloproteinases [144].

Similar to astrocytes, neurons are also another brain-specific cell type which can aid tumor progression through various mechanisms. As such we can refer to secretion of mitogens such as neuron-derived neuroligin-3 (NLGN3) which causes an increased rate of tumor cell proliferation *via* activating PI3K signaling with resultant poor survival, particularly in patients harboring GBM [145, 146], and in some cases acts as an oncometabolite [147].

1.3.2. Tumor immune microenvironment (TIME) in GBM

The immune microenvironment of GBM consists of distinct immune cells that change under therapeutic pressure and can affect the clinical outcome [140]. Therefore, a detailed understanding of the GBM TIME is a crucial step towards improvement of therapeutic strategies against this tumor type [148]. Although the TIME in GBM contains various cells, it has been shown that immunosuppressive cells including immunoregulatory macrophages, T regulatory cells (Treg), myeloid-derived suppressor cells, and a distinct subset of dendritic cells (DCs) are the dominant subpopulations that cause tumor exacerbation. For a long time, the CNS was considered an immune-privileged site due to the lack of a lymphatic system and generation of a very weak immune response from the few antigen presenting cells in the brain, as well as brain antigens avoiding systemic immunological recognition [149]. However, based on recent studies the concept of immune privilege has changed and with the new definition, only brain parenchyma is considered an immune-privileged site [149, 150]. In inflammatory and cancerous conditions, BBB gets disrupted and loses its integrity which results in passing of various types of immune cells into the tumor niche. This phenomenon is heavily directed by the by tumor-secreted factors [151].

1.3.2.1. Tumor Associated Macrophages and Microglia (TAM)

Profiling the GBM immune landscape at both the genomic and proteomic levels has indicated that GBM tumor tissue is heavily enriched with a macrophage population that is predominantly polarized toward pro-tumorigenic and immunosuppressive phenotypes. The

healthy adult brain hosts only an immune population of microglia, which plays key roles in immune surveillance, brain development and CNS homeostasis by apoptotic cell removal, and is a critical component of the first line of defense [152]. However, the disrupted BBB in GBM allows passage of various types of immune cells into the tumor niche, including monocytes, which subsequently differentiate into macrophages in the TIME. Microglia, the resident macrophages of the CNS, are a population of cells that belong to innate immune system and arise during embryogenesis. They have limited capacity for self-renewal in brain tissue. In the GBM TIME, TAMs refer to both infiltrating bone marrow-derived macrophages and tissue-resident microglia [153, 154]. The lack of distinct markers for these two populations has made it challenging to distinguish between them; however, recently, transmembrane protein 119 (TMEM119) was accepted as a definite microglia marker and CD49D/ITGA4, as a marker specific marker for tumor infiltrating bone marrow- derived macrophages [155, 156].

Migration of macrophages to the tumor site is heavily under the influence of chemo-attractants secreted by GBM cells such as CCL2, CXCL12, CSF-1and SDF-1 [157, 158]. It has been shown that CCL2 inhibition leads to reduction of TAM infiltration and ultimately prolongs survival [159]. In addition to GBM cells, the GBM TIME microglia have the ability to secrete CCL2, thereby stimulating more microglia recruitment to the tumor [160]. CSF-1 overexpression in GBM not only results in higher infiltration of TAMs but also causes tumor invasion [161, 162]. Moreover, a recent study introduced osteopontin (OPN) as another important chemo-attractant for TAMs *via* integrin αvβ5 [163]. This was further proved by showing that αvβ5 deficiency leads to a direct CD8+ T cell cytotoxic

effect in the tumor site [163]. Periostin (POSTN) and OPN are other GSC-secreted chemokines that recruit M2-like TAMs to the tumor site [164]. TAMs also contribute to immunosuppression through secretion of anti-inflammatory cytokines such as TGF-β, IL-6 and IL-10 as well as MMP molecules such as MMP-2 and MMP-9 and growth factors including EGF and VEGF, which result in tumor growth by having an impact on angiogenesis, apoptosis and cell proliferation [165]. In fact, the secretion of MMP2 causes tumor invasion [166] and TGF-β1 causes Epithelial-to-Mesenchymal Transition (EMT) and, as a result, invasion of $CD133^+$ GSCs [167]. Another mechanism through which TAMs exert their immunosuppressive effect is through activating JAK2/STAT3 pathway [168], which results in decreased MHC class II and co-stimulatory molecules, CD40, CD86, CD80, resulting in poor induction of T-cell responses in the tumor [153, 169]. The secreted IL-10 by TAMs also reduces monocytic MHC class II expression and subsequently down-regulates IFN-γ and TNF-α production in GBM, preventing anti-tumor activity [170]. Microglia are known as one of the major sources of TGF-β in GBM [171]. TGF-β causes severe immunosuppression through different mechanisms including blocking T-cell proliferation and activation, inhibition of NK activation, reduction in IL-2 production, and increasing Tregs [172]. Moreover, it facilitates immune escape by inhibiting NKG2D on $CD8^+$ T cells and NK cells which subsequently leads to reduced cytotoxicity effects of T cells and NK cells against GBM cells [173].

GBM TIME macrophages are largely of the M2-like tumor-promoting phenotype, and thus present a potential therapeutic avenue to be exploited. While many publications have quickly classified TAMs as having an M2-like phenotype, this is in fact a gross

oversimplification of macrophage biology; a more apt description of TAM phenotypes is that they lay along a gradient, rather than a binary system. TAMs share both M1 and M2 characteristics, and often lie in between the two types, rather than being exclusively programmed towards one or the other. However, the main immunosuppression generated by TAMs in the GBM TIME is the effect of anti-tumor, or M2-like TAMs [154]. Transcriptional classifications of GBM indicated inter- and intra- tumoral heterogeneity for immune populations infiltrating GBM. The mesenchymal subtype has been shown to have a greater frequency of macrophage/microglia compared with proneural or classical subtypes which explains the reason behind the aggressiveness, therapy resistance and poor prognosis of the mesenchymal subtype [174, 175]. These findings make it evident that GBM can be considered to be a myeloid disease, and an effective therapy for GBM must also target TAMs.

1.3.2.2. Myeloid-Derived Suppressor Cells (MDSCs)

Myeloid-derived suppressor cells (MDSCs), identified as HLA-DR−CD11b^{+} CD14−CD33^{+} cells in humans, are the key components of the innate immune system, and are also one of the most abundant cells in the GBM TIME with a significant immune suppressive function against NK cells and cytotoxic T cells as well as paralyzing CD4 $^{+}$ T cell memory function. Preclinical studies have shown pharmacological targeting of MDSCs using Sunitinib as well as MDSC depletion led to increased amounts of CD3^{+} CD4^{+} T cells in the TIME [176-178]. In solid tumors, GSCs and neoplastic cells produce cell-intrinsic factors including CCL2, MIF, IL-10, TGF-β and IL-4Rα which results in recruitment of TAMs and MDSCs to the tumor site as well as activation of T reg cells and programing of

M2 macrophages. Together TAMs and MDSCs account for about 50% of the immune cells in GBM microenvironment which generated a dominant immunosuppressive environment by various mechanisms, such as producing TGF-β and PD-L1 in the tumor, causing tumor growth and poor prognosis in GBM patients [164, 179, 180]. Although, immunotherapeutic modalities alone have not shown much success in GBM, according to recent studies [180, 181], the combination of chemotherapy with immunotherapeutic modalities exclusively targeting MDSCs and TAMs results in reduction of GBM progression and treatment resistance.

1.3.2.3. Tumor-infiltrating lymphocytes (TILs)

TILs can be either pro-tumorigenic or anti-tumorigenic. Although T cells are the primary lymphoid cells in GBM TIME, they only make up less than 0.25% of tumors. TILs include $CD8^+$ cytotoxic T Lymphocytes (CTLs) and $CD4^+$ T helper cells, but CTLs have tumor clearance activities and compose less than a quarter of the TIL population in GBM TIME [182]. They are not generally capable of exerting their anti-tumorigenic and cytotoxic effects as they have an exhausted phenotype and impaired effector functions [183].

The exhausted T cells possess a particular transcriptional program that is phenotypically characterized by upregulation of several coinhibitory receptors, mainly immune checkpoints [184] including PD-1, CTLA-4, TIM-3, LAG-3, 2B4 and VISTA. The classical immune checkpoint (PD-1 and CTLA-4) inhibitors or blockades have been in clinical use as anticancer strategies aiming to improve T-cell function in tumor. However, they have shown limited success in GBM mainly due to upregulation of alternative immune checkpoints such as TIM-3 and LAG-3 [185], indicating that T-cell exhaustion plays a

significant role in negatively influencing therapeutic effects in GBM [186]. $CD4^+$ T helper cells in the GBM TIME are associated with poor survival as the majority of them are T regulatory cells and the rest have functionally exhausted phenotypes [187].

T regulatory cells, a subset of $CD4^+$ T cells, are another subpopulation of cells in the GBM TIME playing a critical role in immune suppression. Tregs originate from two different sources including thymus and periphery. The thymus induced T cells have high level of FoxP3 [188]; however, peripherally induced Tregs are characterized by low level of FoxP3 expression and IL-10 and TGF-β signaling are considered as key contributors in inducing the latter T reg category [189]. Tregs, particularly the thymus induced category, account for 25% of tumor infiltrating lymphocytes in GBM and are associated with poor prognosis as they dominate the tumor cytokine *milieu* toward immunosuppression and are characterized as $CD4^+$ $FOXP3^+$ $CD25^+$ cells [190-192]. Similar to MDSCs, Treg infiltration into tumor tissue occurs in response to chemokines secreted by tumor cells such as CCL22 and CCL2 [193, 194]. One dominant Treg immunosuppressive mechanism is through prevention of IL2 production which in turn results in impairing the function of infiltrating T cells [195].

1.3.3. Hypoxia niche in GBM

Extensive tissue hypoxia is a common feature of GBM. In addition to hypoxia in tumor tissue, it has also been shown that to a lesser extent that the hypoxic condition exists in non-neoplastic tissues. The level of oxygen (O2) concentration in non-neoplastic tissues is 2% to 9% whereas in atmospheric air it is 20.8% [196]. This is often a necessary condition for development and maintenance of normal somatic stem cells [197]. In addition to the effect

of hypoxia on normal stem cells, hypoxic conditions have a profound effect on enhancing the maintenance of GSCs and making this population of cells resistant to radiation. In fact, hypoxia reduces the generation of free radicals, which have antitumor effect, and through this mechanism blocks the effect of radiation on GSCs [198, 199]. It also causes chemo-resistance *via* upregulating the expression of the multi-drug resistance gene MDR1/ABCB1. Besides, it has been shown that hypoxia promotes cancer progression by inducing angiogenesis, cell growth, tumor cell invasion, genomic instability, immune evasion, immunomodulation and altering the metabolism of cancer cells [198, 200, 201]. Therefore, it is evident that the hypoxic niche is a critical component of the TME that needs to be targeted. However, as the hypoxic environment cannot be eradicated, therapeutic modalities have been designed in such a way that they are predominantly targeting the signaling responses generated in response to hypoxia [202-204].

The two main transcription factors first activated in response to hypoxia include Hypoxia-Inducible Factor 1 alpha (HIF1α) and Hypoxia-Inducible Factor 2 alpha (HIF2α). It has been shown that the destabilization of these two proteins in GBM results in reduction in tumor growth and loss of stemness as they both play critical roles in coordinating cellular processes such as proliferation, differentiation, metabolism, as well as development of immune T cells [205, 206].

The main metabolic alteration in tumor cells in response to hypoxia is the glycolytic switch, which is a shift from oxidative phosphorylation to glycolytic pathway [207, 208] and is a more efficient way of energy production for tumor cells in the absence of oxygen. This shift results in increased production of acidic metabolites and altered pH gradient [209]. In

physiological conditions, pH homeostasis is crucial for normal cellular functioning; however, in pathological conditions such as cancer, the acid/base balance gets disrupted due to overexpression of proteins which are involved in pH regulation and also through initiation of oncogenic metabolism which all results in extensive production of carbon dioxide, lactate and protons. This ultimately leads to pH dysregulation and acidification of tumor environment which influences the response to conventional therapy including chemotherapy and radiation and also the uptake of anticancer drugs. Moreover, it increases the activation of angiogenic factors and proteases, breaks down the extra cellular matrix (ECM), reduces cell-cell and cell-ECM adhesion and eventually causes tumor cell migration and invasion. This acidic environment is toxic for normal cells; however, the tumor cells are able to survive and proliferate by activating the molecular machinery that allows them to regulate their pH. This molecular machinery causes transmembrane inside-out and outside-in ion fluxes, which results in acidification of the extracellular space, as well as alkalization of the intracellular environment and ultimately tumor cell survival [198, 209].

Carbonic anhydrase IX (CA IX), a hypoxia inducible metalloenzyme, is an important component of this machinery and functions as a survival factor to protect tumor cells from hypoxia and acidosis by catalyzing the hydration of CO2, producing proton (H^+) and bicarbonate ($HCO3^-$) and transporting bicarbonate inside the cells. This mechanism increases the pH of the intracellular environment and makes the tumor cells resistant to acidosis [209]. Due to these functions, activation and over-expression of CA9 in cancer causes aggressive tumor behaviors and requires a targeted therapeutic strategy to overcome

this enzyme and ultimately balance the pH and metabolism of cancer cells. In fact, CA9 targeting is considered as an effective strategy for targeting the hypoxic niche.

All in all, GBM TME nonimmune components and the immune compartment together cause tumor progression and treatment resistance in various ways which explains why understanding of the GBM TME and TIME is essential for designing effective therapeutic strategies for treatment- resistant GBM.

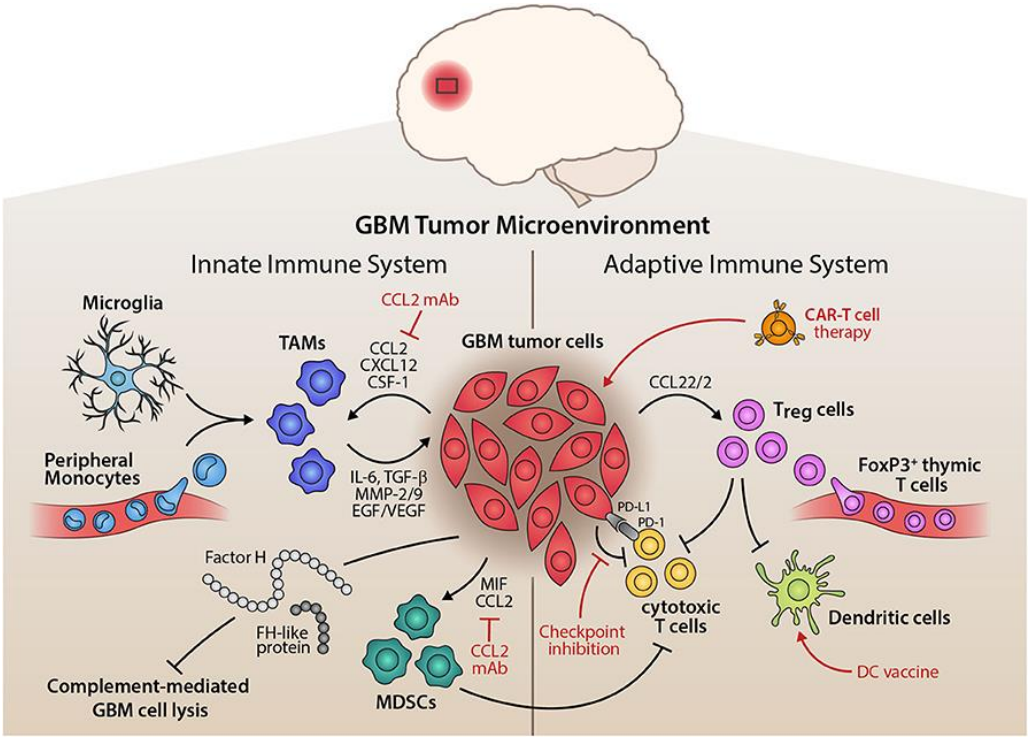

Figure 1.3. Heterogeneity of the GBM TIME. Within GBM tumors there is a distinct population of immune cells including immunoregulatory macrophages (tumor microglia and monocyte-derived macrophages), immunosuppressive Treg and dysfunctional T-cell populations, MDSCs. The genetic make-up of the cancer cells and GSCs, has a direct effect on immune composition of the tumor. Various therapeutic strategies have been used to block or neutralize immune cells or their products and function. This figure is adopted from DeCordova, S., *et al.* paper (*Front Immunol. 2020 Jul 17;11:1402. doi: 10.3389/fimmu.2020.01402*) [73].

1.4. Advances in immunotherapy for GBM

The current SoC therapy for GBM patients which includes surgical resection, radiation and chemotherapy has shown low therapeutic efficiency resulting in poor patient prognosis. For years the efforts have been focused on finding efficacious targeted therapies to overcome this challenge. As such, we can refer to various immunotherapeutic modalities including Bispecific T cell engagers (BiTEs), and Chimeric Antigen Receptor (CAR) T cells, Immune Checkpoint inhibitors (ICIs), vaccines, antibodies and oncolytic virotherapy which have shown promising results in both preclinical and clinical trials. However, having an integrated effort for designing a rational combination therapy consisting of both immunotherapy and SoC therapy is essential for having optimal personalized therapeutic strategies for GBM patients.

Cancer immunotherapy employs the host's immune system to recognize and eliminate cancer cells with minimal adverse effects and has shown efficacy in preventing tumor remission in some cases across multiple cancers including non-small cell lung cancer, renal cell carcinoma, melanoma, and non-Hodgkin lymphoma [210, 211]. GBM unresponsiveness to therapy is related to three major factors including immune privilege of the central nervous system, low immunogenicity and immunosuppressive TME. Immunotherapeutic modalities have shown efficacy in sensitizing tumor and TME and as a result better response to therapy [212].

1.4.1. Bispecific T cell Engagers (BiTEs)

BiTEs are fusion proteins consisting of two single-chain variable fragments (scFvs) of different antibodies linked by a small linker peptide, where one of the scFvs binds to T-

cells *via* the non-polymorphic CD3 epsilon subunit, and the other to a tumor cell *via* a tumor-specific antigen. The combination of these two specificities results in inducing targeted T cell-mediated killing of the recognized tumor cells. BiTEs are highly flexible and small in size (~55 kDa) which allows them to interact closely with the immune effector cells and the cancer cells and linking them together with high affinity. Given these features, BiTEs may prove to be more efficient in localizing to the CNS. The BiTE format has been evaluated against a variety of tumor-associated antigens, including CD19, CD20, EpCAM, EGFR, MUC-1, CEA, CD133, EphA2 and HER2. Moreover, they have shown specificity for GBM tumor cell surface antigens including CD133 [213] and EGFRvIII [214, 215] as well as tumor reduction/shrinkage and improved survival [215]. Although the efficacy of BiTEs has been confirmed across many cancers, it has been seen that a subset of patients does not respond to bispecific antibody-based immunotherapy in the long term due to having exhausted and non-functional T cells caused by upregulation of PD-1 and/or PD-L1 immune checkpoint proteins. Therefore, combining BiTEs with other immunotherapeutic modalities such as Immune Checkpoint Inhibitors (ICIs) would be of benefit as it allows for restoring T cell resistance and overcoming tumor immune escape. BiTEs are yet to be clinically translated for brain tumor patients; however, the technology represents a new hope for patients with difficult-to-treat cancers.

1.4.2. Chimeric Antigen Receptor (CAR) T cells

The first Adoptive Cell Transfer (ACT) using autologous lymphocytes for cancer therapy goes back to 1988 with patients diagnosed with metastatic melanoma [216]. Around the same time, genetically engineered T cell receptors (TCR) were investigated, which revealed

their ability in inducing robust T cell responses. This led to the emergence of chimeric antigen receptor (CAR) T-cell therapy particularly for cancers [217, 218]. CAR is a synthetic molecule which expresses an antigen recognition domain in a form of a single-chain variable fragment (scFv) or a ligand specific for one tumor associated antigens [219, 220] that is linked through a hinge and a spacer to the transmembrane and an intracellular signaling domain. The intracellular domain of the CAR varies depending on the CAR generation: the 1st generation CAR consists of CD3ζ activation domain, the 2nd or 3rd generation CAR consist of one or two co-stimulatory domain such as 4-1BB, CD28, or OX40. Amongst these 3 different CAR generations the second and third generation CAR-T cells have shown better proliferation and effector function when compared to the first-generation CAR [221]. Further genetic modification led to 4th generation CARs that have the ability of releasing transgenic proteins of interest, such as cytokines. This allows for enhancement of CAR-T cell functionality by improving the expansion and survival rate of CAR-T cells [222]. The design of CAR-T allows for targeting specific tumor cells independent of MHC expression which is a great strategy for overcoming a tumor's immune escape mechanisms and resistance to T cell immunity [223]. Although a single-antigen targeting CAR T-cell therapy for GBM has shown clinical benefit, due to the high level of heterogeneity and plasticity of GBM, full targeting of tumor cell populations has not yet been achieved. This results in failing of single antigen-targeting CAR-T cells in entirely eradicating brain tumors [224]. However, designing CARs that can target multiple TAAs has produced different versions including bi-specific, trivalent, and tandem CARs, which are being explored for targeting brain tumors [225].

CD19-CAR was the first FDA-approved CAR-T cell therapy used for treating patients diagnosed with refractory B cell acute lymphoblastic leukemia (ALL) which resulted in complete remission rate with durability, and minimal residual disease less than 0.01% when given to a cohort of 63 children and young adults with either relapsed or refractory ALL [226]. For GBM, CAR T cell therapy has shown promising results in clinical practice particularly for targeting a few tumor associated antigens overexpressed in tumor cells including IL13Rα2 [227], EGFRvIII [228], HER2 [229] and EphA2 [230]. Other newly developed targets include ganglioside 2 (GD2) [231, 232], B7-H3 [233] and chlorotoxin [234] CD70 [235] and CD133 [236]. Although these targets have been showing promising results at the preclinical stage, clinical trials have shown some limitations such as partial antitumor response mainly due to limited T cell persistence. Moreover, another concern with CAR-T cell therapy is the toxicity that is associated with it. Cytokine release syndrome (CRS) has been the major reported cytotoxicity associated with CAR-T cell therapy and is determined by rapid cytokine release including IFNγ, IL-2, IL-6, IL-10 resulting in T cell activation and expansion. However, this effect has been modulated with the use of FDA-approved anti-IL-6 antibody which causes a rapid reversal of severe CRS syndromes [237]. Therefore, similar to other immunotherapeutic modalities combining CAR-T cell therapy with other therapeutics is the next step for improving CAR-T cell therapy [238].

1.4.3. Immune Checkpoint Inhibitors (ICI)

T cells have a crucial role in generating antitumor responses. The process of effector T cell production against cancerous cells is complex and regulated by a series of activation and inhibition signals [239]. Inhibiting signals prevent the uncontrolled inflammatory response

as well as overactivation of the immune system generating a balance for eliminating tumor cells while preventing autoimmune responses [240]. Immune checkpoint receptors are T-cell surface expressed molecules such as cytotoxic T lymphocyte-associated antigen-4 (CTLA-4) and programmed cell death protein-1 (PD-1), which have the ability of generating negative regulatory signals throughout the T-cell activation process thereby preventing over-activation [241]. Modulating immune checkpoint signals has been used as a therapeutic strategy to improve antitumor immune response as it leads to restoring T-cell function. CTLA-4 is known as the early-stage immune activation molecule and PD-1 has a significant role in the effector phase of the immune response [242]. CTLA-4 negatively regulates the initiation and activation of T cells and the interaction of PD-1 with its ligand PD-L1 or PD-L2 leads to inhibition of T-cell signals transduction and cytokine production resulting in T cells reduction [241]. CTLA-4 and PD-1 are expressed in many tumor cells including GBM; however, inhibiting PD-1 or PD-L1 function can restore cell function. For this purpose, ICIs have been employed to stimulate immune response in the immunosuppressed GBM TME and are mainly divided into two categories of immune checkpoint inhibitor monotherapy and combination therapy. Combination therapy is when ICIs is given to the patients in combination with other therapeutic regimes such as chemotherapy, radiosurgery, or other immunotherapeutic modalities. Although ICIs for GBM are still at the early stage, currently, few ICIs have been approved for clinical use including Ipilumumab which is a monoclonal antibody against CTLA-4, Nivolumab, pembrolizumab, and Cemiplimab which are monoclonal antibodies against PD-1 and atezolizumab, Devaru, and Avelumab which are monoclonal antibodies against PD-L1. It

has been shown that administration of Nivolumab increases chemokines and immune cells infiltration; however, it hasn't shown significant survival benefit in patients with recurrent GBM [36].

Although only few GBM ICI clinical trials have shown successful effect on patients, research towards identifying new ICIs as well as immune checkpoints is ongoing [243, 244].

Currently clinical trials have been mainly focused on exploring combination therapy between various immunotherapeutic modalities including immune checkpoint therapies, vaccine therapy and CAR-T cells as well establishing a synergy between immunotherapy and current SoC. Moreover, due to the complexity of the antitumor immune response and the huge heterogeneity in GBM, combining tumor gene analysis and immune characteristic analysis for biomarker development would allow for better predicting the therapy effect. This would also allow for reducing or delaying drug resistance and shifting GBM treatment towards a personalized and patient-specific manner.

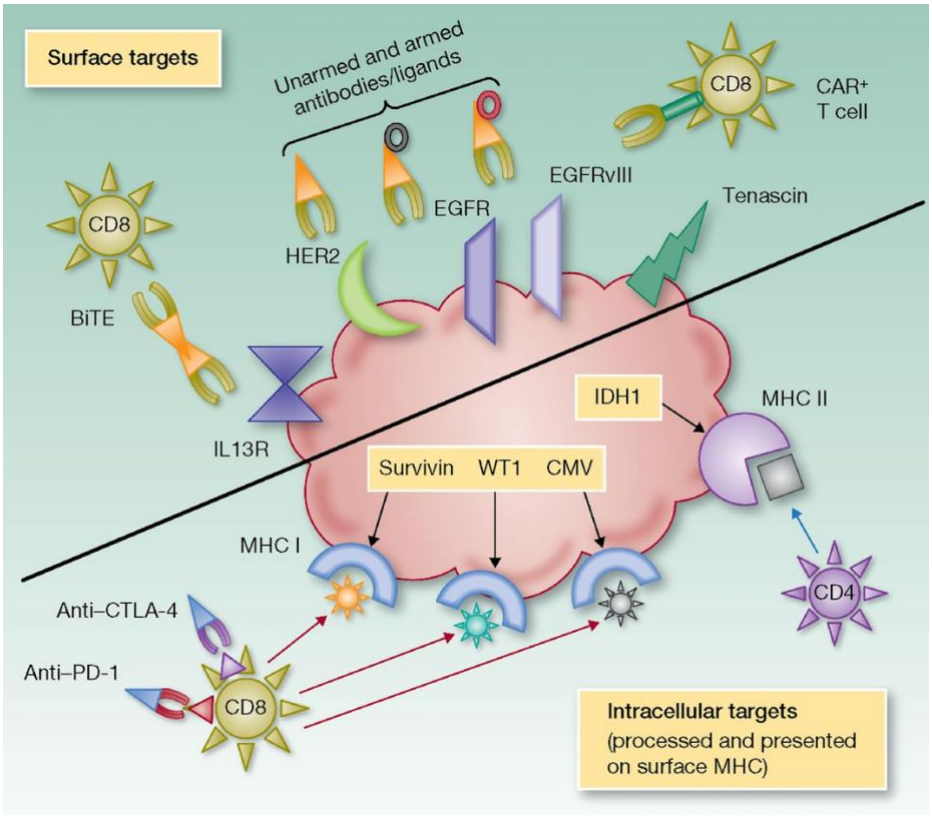

Figure 1.4. Immunotherapeutic targeting of GBM associated antigens. Immunotherapeutic modalities targeting antigens, receptors or ligands include BiTEs, which has the ability of bringing T cells in to close proximity of tumor cell, CAR-T cells with surface-antigen specificity targeting tumor cells via recognition of specific tumor associated antigen and immune checkpoint inhibitors targeting CTLA-4 and PD-1 and PD-L1 resulting in T cell stimulation and subsequently activation. This figure is adopted from Fecci, P.E., *et al*. paper. (*Clin Cancer Res. 2014 Nov 15;20(22):5620-9. doi: 10.1158/1078-0432.CCR-14-0832*) [245].

1.5. Summary of Intent

GBM is a dynamic disease, and its genetic and molecular landscape is constantly evolving. This, together with emergence of various subpopulations of cells results in formation of an extensive cellular and genetic intratumoral heterogeneity in a single GBM tumor [71, 246, 247]. In addition, the mutations caused by therapy itself also have a significant effect on tumor evolution [248]. Ultimately, the result of evolutionary dynamics of tumor progression is that the genetic landscape of a primary tumor is completely different when compared to the recurrent one which results in therapy failure and patient relapse. Due to lack of biological characterization of the distinct genomic and cellular landscape of GBM recurrence, as well as our poor understanding of the tumor immune microenvironment (TIME) and its evolution through disease progression, not only has SoC been partially effective in eradicating the tumor, but also clinical trials have not shown significant survival advantages for GBM patients. Therefore, **we hypothesize that the concerted characterization of the rGBM and its cognate TIME utilizing an integrative multi-omics analysis paradigm would allow for identification of therapy resistance targets for designing effective and appropriate targeted therapies for GBM to reach sustainable tumor remission.**

In **chapter 2** of this thesis, we were focused on identification of GBM BTIC cell surface markers specific to treatment-refractory GBM. RNA-sequencing analysis was performed on GBM BTICs that underwent *in vitro* chemotherapy protocol [249]. *In vitro* chemotherapy model represents therapy-induced selection pressure on the treatment-naïve

GBM BTICs as is present in GBM patients. Specifically, in our study, this model was designed to profile the evolution of primary treatment-naïve GBM BTICs through chemo-therapy and to study GBM BTICs chemo-resistance. It also enabled us to identify a chemo-resistant gene signature of GBM BITCs which ultimately leads to tumor recurrence. The differential gene expression analysis by microarray followed by network analysis of TMZ vs control treated samples indicated higher level of hypoxia signature for TMZ treated cells. CA9 was one of the overexpressed hypoxia related gene in TMZ resistant cells compared to controls [249] indicating that CA9 plays a significant role in treatment resistance and thereby recurrence, underscoring that CA9 is a potential therapeutic target in GBM.

In spite of using multi model therapy for treating GBM, tumor re-growth and patient relapse is inevitable. Therefore, there is an urgent need for exploring and developing new effective therapeutic strategies. In the past few years, Immunotherapy has emerged as more effective treatment strategy for patients with cancer which simultaneously harnesses the immune system and redirects the immune response specifically towards targeting cancer cells [250]. The aim of this project is to develop novel immunotherapeutic strategies using Dual Antigen T cell Engager (DATE), to target the identified novel tumor associated markers.

We hypothesize that targeting hypoxia niche via targeting $CA9^{+}$ GBM BTICs using CA9 specific Dual Antigen T cell Engager (DATE) would be an effective therapeutic strategy for GBM patients by eliminating the treatment refractory GBM BTICs. This therapeutic modality was also tested against another clear cell Renal Cell Carcinoma (ccRCC) as another solid tumor with high level of CA9 expression. To conduct this project our aims included:

Aim 1: To evaluate the efficacy of CA9 specific DATE on patient-derived GBMs and RCCs *in vitro*.

Aim 2: To perform pre-clinical testing of DATE in xenografted mice bearing patient-derived GBM and RCC tumors.

This work resulted in building a new immunotherapeutic against treatment resistant cancer targets, and preclinical testing in patient-derived xenograft models of treatment-resistant GBM and RCC. In the next step, which is beyond the scope of this thesis, this preclinically validated immunotherapeutic modality will ultimately be translated into early clinical development, generating targeted therapies and hope for future GBM patients.

In **chapter 3** we took advantage of multi-omics profiling technologies particularly advanced proteomics techniques for detailed characterization of the evolution of the GBM molecular signatures from primary to the recurrent state, which allows for better understanding of the molecular pathogenesis of the disease and ultimately identification of new biomarkers. Biomarkers play an important role in the clinical management of cancer patients. A number of potential diagnostics, prognostic, and predictive biomarkers which are frequently tested in routine clinical practice for GBM patients includes *IDH* mutations, 1p19q deletion, MGMT promoter methylation, and *EGFRvIII* amplification [251]. However, none of the given biomarkers provide a complete picture of the GBM evolution. Besides, although genome and transcriptome have been well elucidated in pGBM, GBM proteome and its relation to up-stream genomic alterations are poorly documented [252, 253]. Importantly, no studies have been performed on matched primary and recurrent tissues, using comprehensive proteomics. This has led to identification of the drivers of

malignant transformations only at the early stage of the disease (primary tumor) but does not reveal how the tumor evolves throughout the course of therapy and disease progression. Moreover, while these studies have been technically impressive, but they often lack tissue annotation, patient follow-up, clinical expertise and the capacity to drive novel discoveries to potential therapeutic interventions.

Therefore, identifying the pattern of evolution from primary tumor to recurrent tumor in a more comprehensive way is needed for efficient early diagnosis and clinical assessment of GBM. This ultimately results in discovery of new biomarkers which allows for selective molecular targeted therapies and development of more effective personalized therapeutic approaches.

Due to the important role of immune system in GBM prognosis, identification of the evolutionary pattern of tumor immune landscape using primary and recurrent patient samples is crucial. In fact, patient samples are the only resources that allow us to study the tumor immune response and immune system's function in a proper way. The reason behind this is that the final immune response to the tumor is shaped by a multifactorial and complex interaction between the tumor, the host/microenvironment and the immune system. Studying all these factors as a complete network is not possible in other models. For instance, although patient-derived xenograft model (PDX) allows to recapitulate the histopathological features of parental GBM and study the tumor itself but due to the lack of immune system it doesn't give us the opportunity of studying the tumor, the immune system and the tumor microenvironment as a network. Therefore, using patient primary and recurrent GBM matched pair samples also allows for better understanding the GBM

immunosuppressive microenvironment and intrinsic properties of tumor which causes tumor poor immunogenicity and uncontrolled proliferation of tumor cells as well as increased tumor burden throughout the disease progression [254, 255].

We hypothesized that proteomic analysis on a large number of patient primary and recurrent GBM

matched pairs would allow us to study tumor evolution from primary to the recurrent stage and to generate detailed molecular profiles of pGBM and rGBM and its cognate immune niche as a critical factor involved in patient's prognosis. This novel study would be an effective strategy to fully understand the biology underlying GBM evolution and to identify the drivers of malignant transformations and therapy resistance. The result of this work will lead to identification of new GBM biomarkers which will eventually improve GBM diagnosis and results in efficient targeted therapy. Moreover, we also generated detailed molecular profiles of rGBM which increased our understanding of the aberrant pathways specific to rGBM for biomarker development and therapeutic intervention, using advanced proteomics technologies. We identified a dramatic difference between pGBM and rGBM with rGBM being associated with severe immunosuppression. This allowed us to identify novel, rational targets and to validate predictive biomarkers across larger pGBM-rGBM patient cohorts for this treatment refractory disease. In the future, projects built based on newly identified targets will be used for the development of rational combinatorial therapeutic approaches for targeting both tumor and TIME simultaneously.

Altogether, this thesis has been focused on studying primary GBMs with the goal of characterizing rGBM and its cognate TME using an integrated multi-omics platform

particularly proteomics and combinatorial indexing RNA sequencing analysis for identification of novel treatment resistant targets for rGBM and designing rational immunotherapeutic approaches for the treatment of therapy-resistant GBM.

Chapter 2: Immunotherapeutic targeting of Carbonic Anhydrase 9 (CA9) in treatment refractory Glioblastoma using Dual Antigen T cell Engagers (DATEs)

Abstract

Glioblastoma (GBM) is the most common malignant primary adult brain tumor, characterized by extensive cellular and genetic heterogeneity. Even with surgery, chemotherapy with temozolomide (TMZ), and radiation, tumor re-growth and patient relapse are inevitable. This poor patient survival is correlated with increased presence of chemo- and radio-resistance brain tumor-initiating cells (BTICs). Tumor hypoxic microenvironment is considered as one of the main factors that can promote stem cell maintenance and therapeutic resistance. We observed that expression of Carbonic Anhydrase 9 (CA9), a hypoxia and acidic stress induced enzyme, was increased in treatment resistant BTICs. We also observed that $CA9^+$ GBM BTICs have increased self-renewal and proliferation properties when compared to $CA9^-$ cells. This indicates that CA9 plays an important role in treatment resistance and thereby recurrence, underscoring that CA9 is a potential therapeutic target in GBM.

To target $CA9^+$ GBM BTICs, we constructed CA9 DATEs, which consist of two arms for CA9 and T-cells CD3 antigen recognition. The dual specificity of DATEs for CD3 of T cells and CA9 on GBM cells were confirmed using flow cytometry. We observed that in the co-culture of T cells and GBM cells, $CA9^{high}$ GBM cells were killed in the presence of CA9 DATEs, validating their specificity to target $CA9^+$ BTICs. Incubating T cells with CA9 DATEs and GBMs resulted in increased surface expression of T-cell activation markers CD69 and CD25 in both, $CD4^+$ and $CD8^+$ T cells. Moreover, activated T cells

showed higher release of pro-inflammatory cytokines including TNF-α and IFN-γ. The *in vivo* preclinical studies also indicated that the treatment of GBM tumor-bearing mice with CA9-specific DATEs yielded extended survival in mice and significant reductions in brain tumor burden. Additionally, we preclinically tested the efficacy of CA9 DATE against clear cell Renal Cell Carcinoma (ccRCC) as another solid tumor, which showed a potent anti-tumor effect for this immunotherapeutic modality at both *in vitro* and *in vivo* level.

This rigorously obtained data suggest that DATE-mediated cytotoxicity against treatment-resistant and evasive $CA9^{+}$ tumor cells could provide a novel therapeutic strategy for patients with solid tumors.

Introduction

Glioblastoma (GBM), a highly aggressive astrocytic tumor (WHO grade IV), is the most common primary malignant brain tumor in adults [1, 256]. Despite aggressive multi-modal treatment, including maximal safe surgical resection, chemotherapy with the alkylating agent temozolomide (TMZ) and radiotherapy, tumor re-growth and patient relapse occurs within 7-9 months post-diagnosis [257, 258]. The average survival in GBM patients is only 12-14 months [19, 259-262] with an abysmal two-year survival rate of 16.9% and only 5.5% of patients surviving at five years and 2.9% at ten years [258], underscoring the urgent need for novel therapeutic approaches. Treatment failure and disease relapse are attributed to extensive cellular and genetic heterogeneity existing not only between patients but also within a single tumor through space and time [71, 72, 246, 247]. This cellular heterogeneity, which is associated with clonal evolution, can be explained by the existence of multiple cellular subpopulations of cancer cells, called brain tumor initiating cells (BTICs), which have acquired stem cell properties including self-renewal, proliferation and multi-lineage differentiation [74-77]. Increased presence of chemo- [263] and radio-resistant [7] BTICs [74] plays a significant role in development of GBM treatment resistance and eventually tumor recurrence. Therefore, development of novel therapeutic modalities for targeting BTIC populations is a crucial step for the GBM field.

Components of the tumor microenvironment play key roles in BTIC maintenance. A dominant microenvironmental factor of solid tumors including GBM is hypoxia [264]. Intratumoral hypoxia has a significant effect on BTIC maintenance by supporting critical stem cell features including self-renewal, multipotency, and tumorigenicity and make this

population of cells resistant to radiation [197, 198]. In addition, hypoxia promotes cancer progression by inducing angiogenesis, cell growth, tumor cell invasion, genomic instability and immunomodulation, and by altering the metabolism of cancer cells and tumor stroma [198, 200, 201, 207, 208]. Therefore, targeting the hypoxic niche would be a necessary step towards decreasing BTIC survival and chemo-resistance in GBM patients. One of the main metabolic alterations in tumor cells in response to hypoxia is glycolytic switch as a more efficient way of energy production for tumor cells in the absence of oxygen. This shift results in increased production of acidic metabolites and altered pH gradient [200, 209]. Although the pH dysregulation and subsequently acidification of the tumor environment is toxic for normal cells, tumor cells can survive and proliferate by activating their molecular machinery. This molecular machinery causes transmembrane inside-out and outside-in ion fluxes, which results in acidification of extracellular space, as well as alkalization of intracellular environment and ultimately tumor cell survival [198, 209]. One of the most critical components of this machinery which functions as a survival factor to protect tumor cells from hypoxia and acidosis is Carbonic Anhydrase 9 (CA9). CA9 is a hypoxia inducible metalloenzyme which catalyzes the reversible hydration of CO_2 and produces proton (H^+) and bicarbonate ($HCO3^-$) through which makes the tumor cells resistant to acidosis [207, 209, 265, 266]. Due to these functions, activation and over-expression of CA9 in cancer causes aggressive tumor behavior and warrants a targeted therapeutic strategy to overcome the adverse effect of this enzyme and ultimately balance the pH and metabolism of cells. CA9 is highly overexpressed in many types of solid tumors including GBM [267, 268], clear cell Renal Cell Carcinoma (ccRCC) [269, 270] and many others but

has no expression in most normal tissues with the exception of gastrointestinal tract, gallbladder, and pancreatic ducts [271, 272]. It has been shown that elevation of CA9 expression is positively correlated with poor patient prognosis [273]. The major current targeted therapy against CA9 in solid tumors has been focused on using small molecule inhibitors [274, 275] and monoclonal antibodies such as G250 [276-278]; however, majority of these therapeutic modalities are fully effective when combined with other therapeutic agents. To overcome this issue and direct the therapeutic approach towards using a potent single therapeutic agent, we designed a T cell-based therapy that employs a Dual Antigen T-cell engager (DATE) / Bi-specific T cell engager (BiTE) antibody as a promising alternate strategy, which allows for targeting the cancer stem cells and activating and redirecting immune cells against tumor cells simultaneously.

DATEs are fusion proteins consisting of two single-chain variable fragments (scFvs) of different antibodies flexibly held together by a short nonimmunogenic peptide linker, where one of the scFvs binds to T-cells via the non-polymorphic CD3 epsilon subunit, and the other to a tumor cell *via* a tumor-specific antigen [279]. DATEs exhibiting specificity for the GBM tumor cell surface antigen CD133 [213]/EGFRvIII [214, 215] and for T-cell receptor CD3 have also been shown to induce anti-tumorigenic activity in xenograft tumor models. Importantly, preclinical evaluation of EGFRvIII-specific BiTEs (Bispecific T cell engagers)/DATEs delivered intravenously showed tumor reduction/shrinkage, extending survival in mice with well-established EGFRvIII-expressing GBM [215]. Given their low molecular weight, DATEs may prove to be more efficient in localizing to the central nervous system (CNS) and this particular feature allows for maximal membrane proximity

between the T cell and the cancer cell necessary for the immune response [280-283]. However, DATEs are yet to be clinically translated for many solid tumors such as GBM and ccRCC. Therefore, the current study focuses on designing CD3xCA9 specific DATEs and performing preclinical evaluation of their efficacy against human GBM and ccRCC. This technology represents a new hope for patients with hard-to-treat cancers for which CA9 and its functionality warrant targeting.

Materials & Methods

Human GBM and ccRCC sample collection

Human GBM brain tumors (Table S1) and patient-derived RCC cell lines (Table S2) were obtained from consenting patients, as approved by the Hamilton Health Sciences/McMaster Health Sciences Research Ethics Board and the Princess Margaret Cancer Centre, Toronto, respectively.

Culture conditions for isolating and propagating the GBM and RCC tumor cells

Human brain tumor tissue was processed as previously described [74, 76, 284]. Briefly, samples were dissociated in PBS (ThermoFisher, Cat#10010049) containing 0.2 Wünsch unit/mL Liberase Blendzyme 3 (Millipore Sigma, Cat#5401119001) and incubated on a shaker at 37 °C for 15 mins. The dissociated tissue was then filtered through a 70 μm cell strainer (Falcon, Cat#08-771-2) and collected by centrifugation at 1200 rpm for 5 min. Red blood cells were lysed using ammonium chloride solution (STEMCELL Technologies, Cat#07850). GBM cells were resuspended in NeuroCult complete (NCC) media, a chemically defined serum-free neural stem cell medium (STEMCELL Technologies, Cat#05751), supplemented with human recombinant epidermal growth factor (hrEGF) (20ng/mL: STEMCELL Technologies, Cat#78006), basic fibroblast growth factor (bFGF) (10ng/mL; STEMCELL Technologies Cat#78006), heparin (2 mg/mL 0.2% Heparin Sodium Salt in PBS; STEMCELL technologies, Cat#07980), antibiotic-antimycotic (1X; Wisent, Cat# 450-115-EL), and plated on ultra-low attachment plates (Corning, Cat#431110) and cultured as neurospheres. GBM BTICs Neurospheres were propagated

by minimally-culturing (< 20 passages) human GBM samples and plating them on polyornithine- laminin coated plates for adherent growth. Adherent cells were replated in low-binding plates and cultured as tumorspheres, which were maintained as spheres upon serial passaging *in vitro*. These cells retained their self-renewal potential and were capable of *in vivo* tumor formation.

The human RCC cell lines were generated by sorting CA9-positive cells from patient tumor specimens as previously described [285]. The RCC cell lines and their derived overexpression or knockout cell lines were grown in Iscove's Modified Dulbecco's Medium (IMDM) (ThermoFisher, Cat#12440053) supplemented with 10% fetal bovine serum (FBS, Thermo Fisher, Waltham) and 1% penicillin/streptomycin (ThermoFisher, Cat#15140122) at 37°C in 5% CO_2. The murine cortical adenocarcinoma renal cell carcinoma cell line, Renca, was purchased from the American Type Culture Collection (ATCC). Renca and its derived overexpression cell lines were grown in Roswell Park Memorial Institute medium (RPMI 1640) (ThermoFisher, Cat#11875101) supplemented with 10% FBS and 1% penicillin/streptomycin at 37°C in 5% CO2.

Engineering and production of CA9 DATEs

The complementarity-determining region (CDR) sequences of previously selected CA9-binders (generated by Dr. Sunandan Banerjee) were sub-cloned into the pSCSTa antibody expression vectors designed in-house, containing the OKT3-anti-CD3 single-chain variable fragment (scFv). The CDR-containing light and heavy chain variable regions of the F library phage-mids were amplified using polymerase chain reaction (RCR) and restriction enzyme-digested to ligate with the pSCSTa backbone vectors. Both light- and heavy-chain

pSCSTa expression vectors were then transfected into Expi293™ cells using the PEIpro® transfection reagents (Polyplus, New York) following the manufacturer's instruction. The transfected Expi293™ cells were cultured in the Expi293™ expression medium (Thermo Fisher, Waltham) and incubated at 37°C, 5% CO2 on a shaker. Five days post-transfection, the supernatant was harvested, and the antibody products were extracted by incubating with protein A resin and purified by affinity chromatography (Bio-Rad Laboratories, Hercules). The antibodies were exchanged into PBS buffer using Amicon® Pro Purification tubes. The protein concentrations were measured using NanoDrop. The protein purity was verified using SDS-PAGE followed by Coomasie Blue staining.

Flow cytometry analysis

GBM tumorspheres were dissociated using 0.2 Wünsch unit/mL Liberase Blendzyme 3 (Millipore Sigma, Cat#5401119001) plus 10 μL DNase (Worthington Biochemical, Cat#LK003170) and adherent cultures were dissociated using dissociation enzyme TrypL E (ThermoFisher, Cat#12605028). The single cells were resuspended in PBS+2 mM EDTA (Invitrogen, Cat# AM9260G). Cells were then stained with APC conjugated mouse monoclonal human Carbonic Anhydrase 9 antibody (1:10) (R&D, Cat#FAB2188A) or a matched isotype control and CA9 DATEs followed by goat anti human APC-Fab IgG (1:2000, Jackson ImmunoResearch, Cat#109-136-170) and incubated for 15 min at room temperature. T cells were stained with CA9 DATEs (15min RT) followed by goat anti human APC-Fab IgG (1:2000, Jackson ImmunoResearch, Cat#109-136-170), anti-CD25 (Miltenyi Biotech, Cat#130-113-283) and anti-CD69 (BD Bioscienecs, Cat#555533). Samples were run on a MoFlo XDP Cell Sorter (Beckman Coulter). Dead cells were

excluded using the viability dye 7AAD (1:10; Beckman Coulter, Cat#A07704). Compensation was performed using mouse IgG CompBeads (BD Biosciences, Cat#552843). Samples were run on a MoFlo XDP Cell Sorter (Beckman Coulter) to assess the level of CA9 surface expression.

Secondary sphere formation assay (Self-renewal assay)

Tumorspheres were dissociated using 10 μL Liberase Blendzyme3 (0.2 Wunsch unit/mL) plus 10 μL of DNase in 1 mL PBS for 5 minutes at 37°C and adherent cultures were dissociated using dissociation enzyme TrypL E. $CA9^+$ and $CA9^-$ sorted GBM BTICs were plated at 200 cells per well in 200 μL of NCC media in a 96-well plate. Cultures were left undisturbed at 37°C, 5% CO2. The number of secondary spheres per well was counted at day 3 to 7 every day and used to estimate the mean number of spheres per 2,000 cells.

Cell proliferation assay

Upon tumor culture dissociation, single cells were sorted into $CA9^+$ and $CA9^-$ population and 1,000 single cells were plated in 180 μL NCC per well in quadruplicate in a 96-well plate and incubated for five days. 20 microliters of Presto Blue (ThermoFisher, Cat#A13262), a fluorescent cell viability (metabolism) indicator, was added to each well approximately 4 hours prior to the readout time point. Fluorescence was measured using a FLUOstar Omega Fluorescence 556 Microplate reader (BMG LABTECH) at excitation and emission wavelengths of 544 nm and 590 nm, respectively. Readings were analyzed using Omega analysis software.

Cell growth in hypoxic condition

$CA9^{lo}$ expressing GBM BTICs were cultured in both hypoxic and normoxic conditions. In hypoxic condition, cells were incubated in hypoxia chamber (1% O_2) and in normoxic condition they were incubated in normoxia (21% O_2) for a total of 5 days. After 5 days cultures were dissociated, and single cells were resuspended in PBS + 2 mM EDTA. Cells were then stained with mouse monoclonal human Carbonic Anhydrase 9 antibody (1:10) (R&D, Cat#AF2344-SP) and run on the LSRII flow cytometer (BD) to assess the effect of hypoxia on CA9 expression on GBM BTICs.

PBMC isolation and T cell purification and expansion

Peripheral blood mononuclear cells (PBMCs) from consenting healthy blood donors were obtained using SepMate ™ (STEMCELL technologies, Cat#85450) or Ficoll-Paque PLUS (GE Healthcare). This study was approved by the McMaster Health Sciences Research and the University of Toronto Ethics Board for GBM and RCC projects, respectively. 1×10^5 cells in XSFM media (Irvine Scientific, Cat#91141) were activated with anti-CD3/CD28 beads at a 1:1 ratio (Dynabeads, Life Technologies) in a 96-well round bottom plate with 100U/mL rhIL-2 (Peprotech, Cat#200-02). T cell cultures were expanded into fresh media (XSFM media supplemented with 100U/mL rhIL-2) as required for a period of 12–15 days prior to experimentation.

Binding assay

The specificity of CA9 DATE for GBM cells, RCC cells and T cells were tested using flow cytometry analysis. $CA9^{hi}$ GBMs, $CA9^{-}$ GBMs, RCCs and T cells (isolated form human

PBMCs for GBM study and Jurkat cells for RCC study) were resuspended in PBS plus 2 mM EDTA and were stained with CA9 DATEs followed by the secondary antibody, goat anti -human APC-Fab IgG (1:2000, Jackson ImmunoResearch, Cat#109-136-170) staining. GBM and RCC cells were incubated for 15 minutes at room temperature and for 20 minutes on ice, respectively followed by 15 minutes incubation at room temperature for the secondary antibody staining. Dead cells were excluded using the viability dye 7AAD (1:10; Beckman Coulter, Cat#A07704) and samples were run on MoFlo XDP Cell Sorter (Beckman Coulter) to assess the level CA9 DATE binding to each of the above-mentioned lines.

T cell activation assays

In GBM models, GBM cells and T cells were co-incubated at a 1:1 ratio for 24 hours with (1μg) or without CA9 DATEs. The $CD3^+$ (BD Pharmingen, Cat#563423) T cells and sub population of T cells including $CD4^+$ (BD Pharmingen, Cat#555347) and $CD8^+$ T (BD Horizon, Cat#562428) cells were analyzed for activation markers CD25 (Miltenyi Biotech, Cat#130-113-283) and CD69 (BD Pharmingen, Cat#555533) by Flow cytometry. Supernatants were collected and stored at -80°C for cytokines release analysis by enzyme-linked immunosorbent assay (ELISA). In RCC model, RCC243 and RCC243 CA9-KO cells were plated at 200,000 cells/well in 6 well plates the night prior to treatment. Human $CD3^+$ T cells at an E:T ratio of 5:1 were added to the wells along with (1 nM) or without CA9 DATEs and incubated at 37°C in 5% CO_2 for 48 hours. The T cells were collected and stained for BV785 anti-human CD3 (BioLegend, Cat#317330), BV605 anti-human CD4 (BioLegend, Cat#317438), PE-anti-human CD8 (BioLegend, Cat#300908), and PE-

CF594-anti-CD25 (BD Biosciences, Cat#562403) antibodies. Supernatants were collected and stored at -80°C for cytokines release analysis by enzyme-linked immunosorbent assay (ELISA).

Enzyme Linked Immunosorbent Assay (ELISA)

The concentration of TNF-α and IFN-γ were quantitated in the supernatant collected from the T cell activation assay (the T cell and GBM co-culture +/- CA9 DATE) using commercially available human TNF-α DuoSet ELISA kit (R & D Systems, Cat#DY210-05) and IFN-γ DuoSet ELISA kit (R & D Systems, Cat#DY285B-05) respectively. The sensitivity limits of TNF-α and IFN-γ assay were 15.60 pg/ml and 9.38 pg/ml, respectively. The experiment was performed in duplicates and the OD was measured at 450 nm using the FLUOstar Omega Fluorescence 556 Microplate reader (BMG LABTECH). The IFN-γ concentration in RCC model was quantified using the eBioscience Ready-SET-Go human IFN-γ ELISA kit (ThermoFisher, Cat#88-7386-88).

Cytotoxicity assay

GBM model: Luciferase-expressing GBM cells ($CA9^{hi}$ GBM BTICs) and HEK cells at a concentration of 25,000 cells/well were plated in 96–well plates in triplicates. T cells at different effector-to-target (E:T) ratios (0:1, 0:0.25, 0.5:1, 0.75:1, 1:1, 2:1) were added to each well in the presence (1nM) and absence of CA9 DATE. The cultures were then incubated at 37^{o}C for 18 hours. The next day 150 μg/mL D-firefly luciferin potassium salt was added to each well and the BLI was measured with a luminometer (Omega) as relative luminescence units (RLU). Target cells incubated without effector cells were used to

measure spontaneous death RLU. The readings from triplicates were averaged and percent lysis was calculated with the following equation:

% Specific lysis =100X (spontaneous death RLU – test RLU)/ (spontaneous death RLU – maximal killing RLU).

RCC model: The RCC243 and RCC243 CA9-KO target cells were plated at 25,000 cells/well in triplicates in 96 well plate the night prior to treatment. The next morning, purified human $CD3^+$ T cells were added at an E:T ratio of 5:1, along with 4256, 4261, and anti-CD3/BCMA control antibody at 1 nM concentration in standard complete IMDM media supplemented with 100 µM beta-mercaptoethanol (Sigma-Aldrich, Cat# M3148-25ML) to reduce T cell oxidative stress. The assays were incubated for 40-48 hours at 37°C, 5% CO 2 before the microscopic images were documented and bioluminescence signals were measured. Working concentration (7.5 mg/mL) of firefly luciferin (R&D systems, Cat#800-LN-05M) was added to the washed wells and read immediately with a spectrophotometer (BioTek plate reader).

In vivo intracranial injections, histological analysis of xenograft tumors and survival studies

Animal studies were performed according to guidelines under Animal Use Protocols of McMaster University Central Animal Facility. In GBM model, GBM cells (10^6 BT935 and 200,000 BT241) were intracranially injected into right frontal lobes of 6- to 8- week old immunocompromised NSG mice for tumor formation as previously described [286]. Briefly, mice were anaesthetized using 2.5% Isoflurane (gas anaesthesia). Using a 15-blade scalpel a 1.5 cm vertical midline incision was made on top of the skull. A small burr hole

was then made (2-3 mm anterior to the coronal suture, 3 mm lateral to midline) using a drill held perpendicular to the skull. A Hamilton syringe (Hamilton, Cat#7635-01) was used to inject 10μL of cell suspension (GBM cells suspended in 10 mL PBS) into the frontal lobe. The syringe was inserted through the burr hole to a 5 mm depth. The incision was closed using interrupted stitches and sutures were sealed with a tissue adhesive. After the half-maximal tumor engraftment which was confirmed by MRI imaging (6 weeks post-surgery for BT935 and 10 days post-surgery for BT241) mice were randomly assigned into control or treatment groups and CA9 DATE treatment started as described in Supplementary Figure 4. All animals received 4 doses of therapy within a 2-weeks' time frame. The animals which were assigned to the treatment group were intracranially injected with 50 μg CA9 DATE + 10^6 T cells and received only 50 μg CA9 DATE top up each once a week for 2 weeks. Mice in the control group received the same therapy regimen as treatment group; however, the CA9 DATE was replaced with CA9 DATE control. For tumor volume evaluation, animals were perfused with 10% formalin one week after the last treatment and the collected brains were sliced at 2mm thickness using brain-slicing matrix for paraffin embedding and H&E staining. Images were captured using an Aperio Slide Scanner and analyzed using ImageScope v11.1.2.760 (Aperio) and imageJ software. For survival studies, all the mice were kept until they reached endpoint and number of days of survival were noted *for Kaplan Meier* Analysis.

In RCC model 5 x 10^6 RCC243 VHL mutant were subcutaneously injected into the right flank of 8- to 10- week old immunocompromised NSG mice for tumor formation. After the half-maximal tumor engraftment (4 weeks post-engraftment) mice were randomly assigned

into control or treatment groups and CA9 DATE treatment started as described in Supplementary Figure 4. All animals received 12 doses of therapy within a 6-weeks' time frame. The animals which were assigned to the treatment group were intratumorally injected with 50 μg CA9 DATE + 2 x10^6 T cells (isolated from the freshly thawed PBMC of healthy donors) once a week and only 50 μg CA9 DATE for the second treatment in the week. Mice in the control group received the same therapy regimen as treatment group; however, the CA9 DATE was replaced with CA9 DATE control. Tumor size was measured using a ruler calibrator after each treatment. To study the effect of CA9 DATE treatment on tumor volume, tumors were collected one week after the last treatment and the tumor size was measured using a ruler calibrator. For survival studies, all the mice were kept until they reached endpoint and the number of days for survival were noted for *Kaplan Meier* Analysis. The endpoint criteria were defined as 20% weight loss and 1.0 cm x 1.0 cm tumor volume.

Statistical Analysis

Biological replicates from at least three patient samples were compiled for each experiment, unless otherwise specified in figure legends. Respective data represent mean±SEM, n values are listed in figure legends. *Student's t-test* analyses, 2-way *ANOVA* analysis were performed using GraphPad Prism 6. $P<0.05$ was considered significant.

Results

CA9 is a safe target for GBM immunotherapy

To evaluate the potential utility of CA9 as a safe and suitable therapeutic target, we performed CA9 *in silico* validation using GlioVis database to assess the level of CA9 expression in GBM vs normal tissue. This *in silico* analysis indicated a significant upregulation of CA9 in GBM tissue compared to normal tissues (**Figure 1.A.**). In addition, using flow cytometry analysis we determined the level of CA9 expression and its localization in our patient derived GBM BTIC lines as well as also normal brain cell lines (Normal Human Astrocyte [NHA] and Neural Stem Cells [NSC]). This analysis indicated no/very low level of CA9 expression on brain normal cells (NHAs and NSCs), implying a reduced risk of off-target cytotoxicity (**Figure 1.B.**). Flow cytometry characterization of patient-derived GBM BTIC lines indicated extracellular/surface expression for CA9, making it a suitable target for immunotherapeutic modalities. We next investigated the effect of CA9 expression on GBM patient survival advantage using our brain tumor tissue bank, composed of patient-derived GBM tumor samples with variable expression of CA9, which revealed a positive correlation between CA9 expression and poor patient survival (**Figure 1. C.** and **Table S1**). In addition, data from Gliovis database confirmed that the patients with $CA9^{hi}$ GBM have lower survival advantage.

The TCGA glioma database shows higher expression of CA9 in GBM (grade IV glioma) compared to low-grade glioma (**Figure S1A**). Notably, this *in silico* analysis revealed a significantly higher expression of CA9 in the most aggressive GBM subtype

(mesenchymal) (**Figure S1B**). CA9 expression was also significantly higher in all subtypes of GBM compared to normal tissue (**Figure S1C**). Collectively, our data introduced CA9 as a suitable target for GBM. We showed GBM particularly at mesenchymal state has high CA9 expression (**Figure S1**) which is associated with poor survival (TCGA and in-house) (**Figure 1.B.** and **1.C.**). Moreover, due to CA9 localization (surface expression) and its low abundance in normal tissue (**Figure 1.A.** and **1.B.**) CA9 is considered as a suitable and safe target for immunotherapy.

Hypoxia induces CA9 expression on GBM BTICs which leads to increased stem-like properties

As mentioned previously, Carbonic Anhydrase 9 (CA9) is a transmembrane hypoxia-inducible enzyme, which is actively involved in catalyzing the reversible hydration of carbon dioxide and thus drives cancer progression [287].

To investigate the effect of hypoxia on CA9 expression in our GBM BTIC lines, $CA9^{lo}$ expressing GBM BTICs were cultured side by side in hypoxic (1% O2) and normoxic condition. Cell surface characterization by flow cytometry analysis indicated that cells cultured in hypoxic conditions had significant elevation of CA9 expression compared to cells which were cultured in normoxic condition (**Figure 1.D.**). This experiment confirmed that hypoxia can induce CA9 expression on GBM BTICs, as has been observed in other solid tumors.

There is accumulating evidence about the effect of tumor microenvironment, particularly hypoxia, on BTIC maintenance and treatment resistance [109, 288]. It has also been shown that hypoxia can induce a stem-like phenotype in non-stem-like cancer cells (promoting

cell growth and self-renewal) [288]. To particularly assess the effect of CA9 on GBM BTIC stem-like properties including self-renewal and proliferation, secondary sphere formation and proliferation assays were performed. For this purpose, each GBM BTIC line was sorted into $CA9^{+}$and $CA9^{-}$ fractions using flow cytometry and plated for self-renewal and proliferation assays. The result of this study indicated marked reduction in clonogenicity of $CA9^{-}$ cell populations compared to $CA9^{+}$ cell populations as measured by the secondary sphere formation assay (**Figure 1.E.**). Moreover, in 2 out of 3 GBM BTIC lines, the $CA9^{+}$ cell population had significantly higher levels of proliferative capacity compared to $CA9^{-}$ cell fractions (**Figure 1.F.**). Altogether, these data revealed that CA9 has the ability of driving stem-like properties in GBM BTICs which may then allow for cancer progression.

Generation of CA9-specific Dual Antigen T cell Engager (DATE) and testing its dual specificity for CA9 and CD3 on T cells

CA9 validation using GBM BTICs confirmed that CA9 is a potential therapeutic target in GBM. In addition, CA9 expression is known for its significant role in cancer progression across multiple solid tumors such as RCC, by causing tumor growth and metastasis [272, 289, 290]. Therefore, to target CA9, specifically in $CA9^{+}$ GBM BTICs and RCC cells, we generated Bispecific T Cell Engagers (BiTEs) also called Dual Antigen T cell Engagers (DATEs), which allows for bridging cancer cells to T cells by binding to Tumor Associate Antigen expressed on tumor cell surface and CD3ε of T cells. CA9-specific DATEs were engineered by fusing the antigen-binding portion (Fab) of the anti-CA9 to the antigen-binding region of mitogenic anti CD3ε clone (scFv OKT3) with a short flexible amino acid linker [291].

To test the dual specificity of the purified DATEs for CD3 of T cells and CA9 on GBM BTICs and RCC cells, binding assay was performed using flow cytometry analysis. For this purpose, the $CA9^{hi}$ GBM BTIC expressing line (BT241), $CA9^{lo}$ GBM BTIC expressing line (BT667) and T cells were stained with increasing concentration of CA9 DATE. This experiment indicated that the binding kinetic of CA9 DATE to $CA9^{hi}$ GBM BTICs (**Figure 2.A.**) and CD3 of T cells (**Figure 2.B.**) increased as we increased the DATE concentration. However, the binding assay on $CA9^{lo}$ GBM BTICs indicated no binding of DATEs to these GBM BTICs (**Figure 2.A.**) confirming that the constructed DATEs effectively recognize both CD3 and CA9-expressing GBM cells. This feature enables DATEs to bind to T cells and GBM BTICs simultaneously and bring them into close proximity to each other, which facilitates GBM cell recognition and eventually GBM cell lysis by T cells. In addition, the same method was used for confirming the CA9 DATE's dual specificity for $CA9^{+}$ RCC lines and CD3-expressing human Jurkat cells. For this purpose, patient derived RCC243 and RCC243 CA9 KO as well as WT and human CA9 overexpressed murine cortical adenocarcinoma renal cell carcinoma cell line (Renca), were stained with varying concentration of CA9 DATE (**Figure S2A**). CA9 binding was only observed in CA9-expressing lines and no binding was seen in RCC243 CA9 KO and Renca WT, as $CA9^{-}$ lines, indicating that CA9 DATE specifically binds to the target cells in an antigen (CA9) restricted manner (**Figure S2B** and **S2C**). Followed by confirming Jurkat cells' high CD3 expression (**Figure S2D**), these cells were also stained with increasing concentration of CA9 DATEs which also indicated increased binding kinetic to these cells (**Figure S2E**). Together, our results confirmed antigen specificity and high affinity binding of CA9

DATEs to the tumor cells and T cells, which can then lead to selective killing of tumor cells.

CA9 DATE activates T cells in the co-culture of tumor cells and T cells leading to tumor cell lysis

The main mechanism of action for the CA9 DATE upon binding to T cells and tumor cells is T cell activation and subsequently tumor cell lysis. Upon confirming the antigen specificity of CA9 DATE for both T cells and tumor cells (GBM BTICs and RCC cells), we aimed to assess the efficacy of CA9 DATE by further investigating their ability in activating and re-directing human T-cells against antigen-expressing tumor cells. For this purpose, T cells were co-cultured with GBM BTICs in the presence and absence of DATEs. T-cell activation evaluation by extracellular staining of only T cells, showed elevated expression of CD25 (late activation marker) and CD69 (early activation marker) only in the presence of CA9 DATEs (**Figure 3.A.**) with $CD8^+$ T cells as the main activated subset (**Figure 3.B.**) in GBM models. T-cell activation was associated with the elevation of pro-inflammatory cytokines secretion including TNFα and IFNγ (**Figure 3.C.**). In addition, to further investigate the effect of CA9 DATE in other solid tumors, we studied the effect of CA9 DATE on T cell activation in a RCC model. This study also involved adding CA9 DATE to the co-culture of T cells and CA9-expressing RCC cells, which caused increased levels of CD25 expression particularly in $CD8^+$ T cell populations (**Figure S3A**). Moreover, drastic T cell IFN-γ production was observed only in the presence of $CA9^+$ RCC cells and the CA9 DATEs, an indicator of effective functionality of T cells (**Figure S3B**).

These results demonstrated that the CA9 DATE has the ability to activate T cells in a strictly antigen-dependent manner.

We next assessed the efficacy and potency of CA9 DATE-directed T-cell cytotoxicity in tumor cells (GBM BTICs and RCC cells). To find the concentration at which the CA9 DATE has optimal cytotoxicity on GBM BTICs, different concentrations of DATEs ranging from 0 nM to 200 nM were added to co-cultured GBM BTICs and T cells. Even the lowest concentration of CA9 DATE (0.05 nM) invoked a potent cytolytic effect on GBM BTICs (**Figure S3E**). Ultimately, 1 nM was chosen as the best concentration for performing cytotoxicity assays.

A bioluminescence-based cytotoxicity assay was used to assess the redirected lysis of GBM cells by CA9 DATEs. The dose-dependent killing of firefly luciferase^{+} GBM cells was observed in cultures with CA9 DATEs, whereas no killing was observed in the control group with no DATEs and in HEK cells, indicating the specific cytolytic effect of CA9 DATE for CA9-expressing GBM BTICs (**Figure 3.D**.). This potent activity of CA9 DATEs against CA9^{hi} GBM cells was observed at greatly reduced concentration (1nM) as well as at E:T ratios as low as 0.25:1. In addition, microscopic examination confirmed that co-incubation of T cells (suspension) and GBM BTICs (adherent) in the presence of CA9 DATEs leads to GBM BTICs lysis. In contrast to wells without DATEs, the co-cultures with CA9 DATEs showed detachment of target GBM cells that formed rosettes, indicating clumps of dying cells (**Figure 3.E.**). Moreover, the same potent cytolytic effect was observed when CA9 DATE was added into the co-culture of T cells and RCC cells. This experiment was also performed across a panel of patient-derived RCC cell lines as well as

CA9 KO (RCC243 CA9-KO) and CA9 overexpressed (Renca) lines which indicated the potent effect of CA9 DATE in lysing target cells in an antigen-dependent manner (**Figure S3C and S3D**). Altogether, our data from 2 different solid tumor models across multiple patient derived lines, strongly confirmed that CA9 DATE can activate T cells and redirect them against tumor cells, causing tumor cell lysis.

CA9 DATE inhibits GBM and RCC tumor growth in orthotopic xenograft models

The antitumorigenic effect of CA9 DATE *in vivo* was assessed using two different early passage patient-derived GBM cell lines enriched for BTIC populations (BT935 and BT 241). CA9 DATEs and isolated T cells from freshly thawed human PBMCs were co-injected intracranially into immunocompromised NSG mice previously engrafted with GBM BTICs as CA9 DATEs did not cross-react to murine CA9 and CD3ε (**Schematic Figure 4.A.** and **4.B.**). The result of this study indicated that in contrast to mice treated with control DATE and T cells, the mice treated with CA9 DATE and T cells had significantly reduced tumor size following treatment (**Figure 5.A.**). Mice receiving control DATE and T cells demonstrated rapid tumor growth; however, in the treatment arm, mice survived longer (**Figure 5.B.**). In addition, the anti-tumorigenic activity of CA9 DATE was tested in ccRCC model. RCC243 VHL mutant lines sorted for $CA9^{+}$ cell population were injected into the flank of immunocompromised NSG mice. Upon tumor formation, mice were co-injected with DATEs and isolated T cells from freshly thawed human PBMCs intratumorally (**Schematic Figure 4.C.**). In this model we also observed that the mice treated with CA9 DATE and T cells had significantly reduced tumor size (**Figure 5.C.**) and

increase in survival, (**Figure 5.D.**) opposite to what was seen in mice that received control DATE and T cells. The *in vivo* preclinical testing of CA9 DATE in both patient-derived GBM and RCC models confirmed the efficacy of this novel immunotherapeutic modality against solid tumors with high levels of CA9 expression.

Discussion

The data presented in this study indicated that DATEs, as a novel targeted immunotherapeutic approach against CA9, have a potent antitumor effect in 2 different solid tumors including GBM and RCC.

CA9, a cell membrane expressed protein, is overexpressed in many solid tumors in response to hypoxia as a result of a glycolytic switch. The pH dysregulation and acidification of the tumor environment occurring following this metabolic alteration and as a result of CA9 expression and activation, have direct influence on response to conventional therapy including chemotherapy and radiation, as well as the uptake of anticancer drugs through various mechanisms [292]. This explains why patients with high CA9 expression have worse survival outcomes as indicated by our study on GBM patient samples. In addition to the critical role of CA9 in tumor exacerbation and treatment resistance, there are numerous other factors that make CA9 an attractive therapeutic target for solid tumors particularly for GBM and RCC. CA9 localization on the cell surface makes it targetable using immunotherapeutic modalities as well as its exclusive expression in tumor tissue (on both GBM and RCC tumors) and absence in normal tissue (both brain and kidney) which reduces the risk of off-target toxicity. Moreover, the critical role of CA9 in tumor progression and metastasis by regulating pH in a favorable manner for tumor cell survival, and in facilitating tumor invasion, migration and eventually metastasis [293], makes it a suitable therapeutic target for solid tumors. In several studies it has been shown that genetic silencing of CA9 in preclinical solid tumor models such as breast cancer [294] and colorectal cancer [295] leads to reduction of tumor growth and metastasis [209]. These

proof-of-principle data indicate that inhibition of CA9 has great therapeutic potential for solid tumors. However, the majority of the existing therapeutic modalities against CA9 are only effective when used in combination with other therapeutic agents. The CA9 inhibitor, SLC-0111, only provides a therapeutic benefit for GBM when combined with TMZ [274]. In another study it was shown that targeting CA9 in renal cell carcinoma and other malignancies with high levels of CA9 expression is more effective when the small molecule-drug conjugate against CA9 was combined with a clinical stage fusion protein L19-IL2. The *in vivo* preclinical testing of this combinatorial therapy indicated that durable complete responses were only observed when combination treatment was administered, while the antibody-cytokine fusion and the small-molecule drug conjugate alone were only partially effective [296]. Moreover, it has been shown that G250 (Girentuximab), a well-known antibody-based therapeutic modality for CA9 targeted therapy, has stronger enhancement and maintenance of antibody-dependent cellular cytotoxicity and a potent and sustained immune effector activity when combined with IL-2 [277]. Previous studies have indicated therapeutic monoclonal antibodies have several major limitations in their mode of action, including redundancy of molecular pathways leading to tumor cell survival, failure to irreversibly mitigate the microenvironment, activation of inhibitory receptors and competition with circulating IgG [297]. To dramatically improve the potency of TAA-targeted Ab therapy, a powerful new drug class, called BiTEs/DATEs, has been developed [298, 299]. Blinatumomab (Amgen's Blincyto®), the first drug in this class, was approved for use to treat acute lymphoblastic leukemia (ALL) and targets CD19, a cell surface protein expressed on normal and malignant B-cell lymphoblasts [300]. The low pM to fM DATE

concentrations required to elicit remission in humans have made it highly effective at inducing objective and lasting rates of remission [301]. DATEs act as a tumor-specific immune stimulus that decorates the tumor cell and specifically engages the patient's own circulating T cells. T cell engagement triggers an antigen-like stimulation signal within the recruited T cell, driving immune targeting or destruction of the antigen-expressing tumor cell. DATEs can exert their antitumor activity in a more efficient way due to their unique features, which allow for targeting tumor cells without need for antigen processing, peptide presentation by MHC I or the presence of co-stimulatory factors [279, 281, 302]. Furthermore, DATEs can induce serial lysis of cancer cells by T cells after they have been activated, without the prerequisite of MHC class I presentation of the TAA [298]. In a side-by-side study comparing the potency of an anti-CD19 Ab with an anti-CD19/CD3BiTE, the BiTE molecule had far superior activity with respect to redirected tumor cell lysis compared to the single target Ab [303]. These observations therefore warrant the continued development of immune enhanced targeted therapies for solid tumors. Due to the critical role of CA9 in GBM and RCC treatment resistance and disease progression, we designed and engineered CA9-specific DATEs and tested their antitumor effect in these tumor models for the first time. Our data strongly supports the potency and efficacy of CA9 DATEs against GBM and RCC tumors. We believe this antibody- based targeted therapy offers an advance in designing effective therapeutic approaches for patients with CA9 high tumors, allowing for targeting a marker of treatment resistance and stimulation of immune system simultaneously.

A

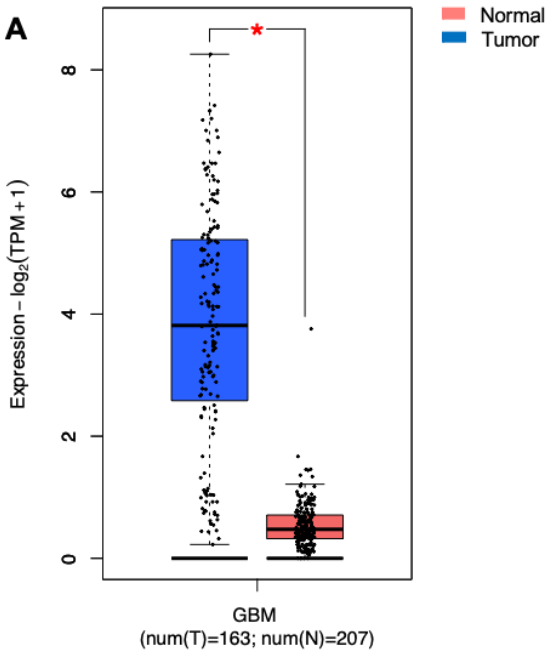

B

Cells	Percentage of CA9 expression
BT428	69.76%
BT 935	66.80%
BT241	66.17%
MBT212	48.37%
GBM08	36.68%
BT618	13.58%
MBT225	12.64
BT594	11.81%
BT 458	0.56%
BT667	0.37%
BT799	0.15%
Normal Stem Cells (NSCs)	0.99%
Normal Human Astrocytes (NHA)	2.12%

C

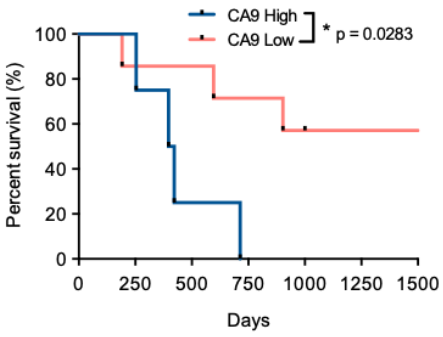

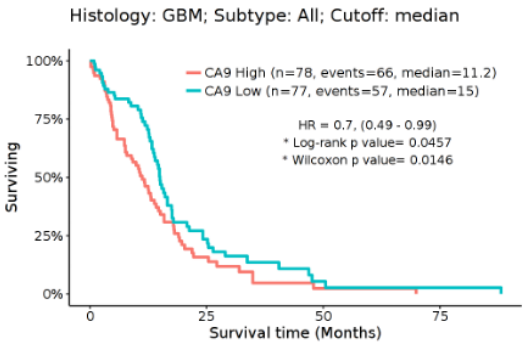

D

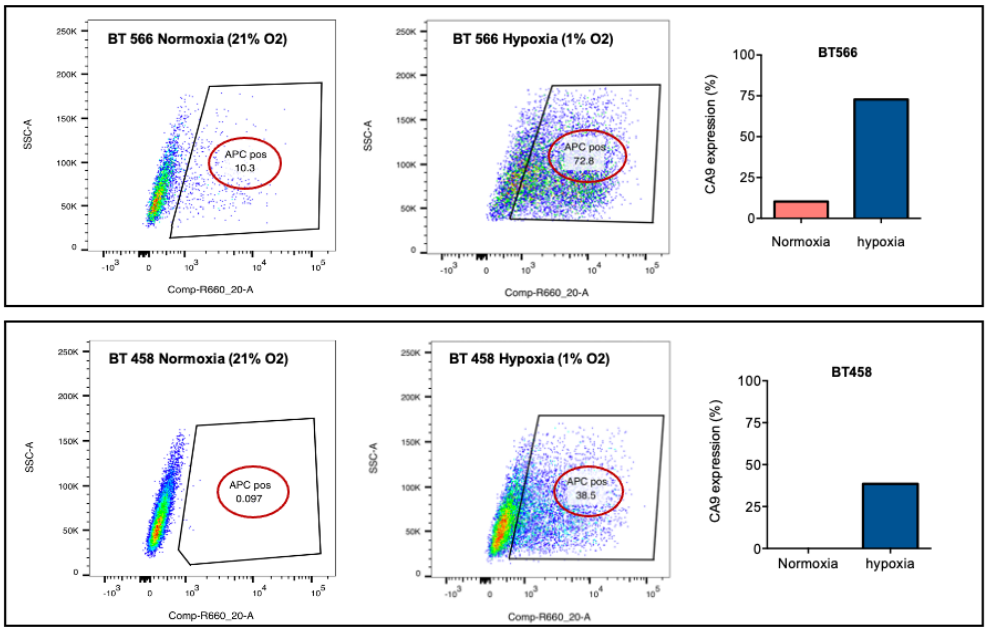

E. Self-renewal

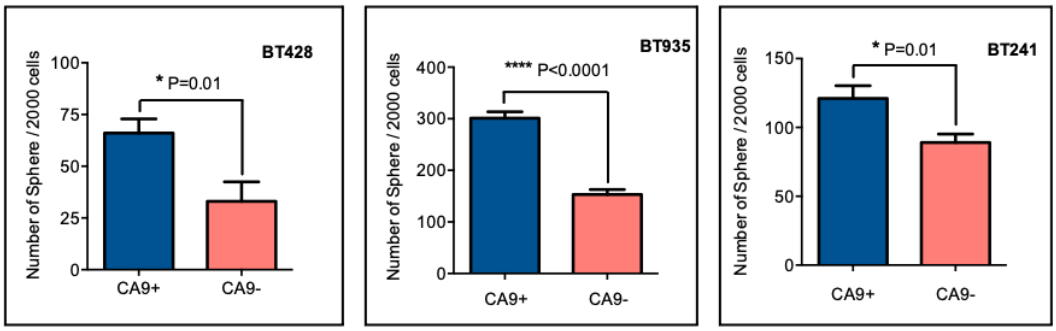

F. Proliferation

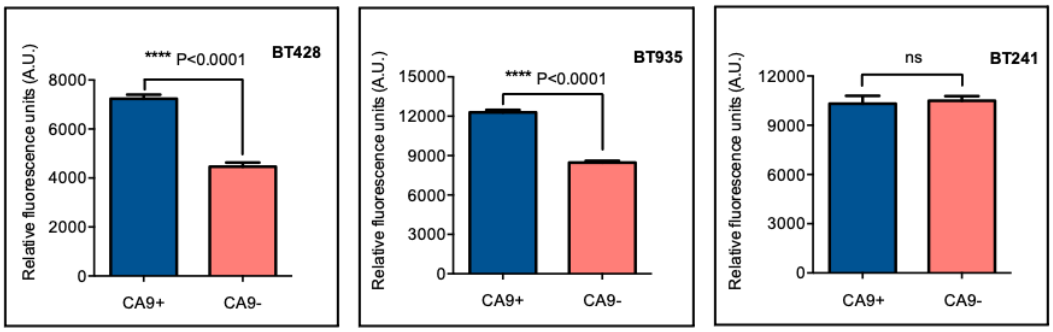

Figure 1. CA9 as a therapeutic target in GBM. A) Transcriptomic dataset shows significant upregulation of CA9 in GBM samples (n=163) when compared to non-tumor (n=207) (GEPIA2) (P value: * < 0.05). **B)** Characterisation of surface CA9 expression of GBM samples along with normal stem cells (NSCs) and normal human astrocytes (NHAs) by flow cytometry reveals varying expression of CA9 in GBM lines, but low levels in normal cells. **C)** (Left panel) GBM samples (n=11) were grouped into either $CA9^{low}$ (red, n=5) or $CA9^{high}$ (blue, n=4) expression based on a flow cytometric median of 20%. Log-rank (Mantel-Cox Test) analysis demonstrated a significant survival benefit for $CA9^{low}$ tumors with a median survival of 33 and 13.5 months for $CA9^{low}$ and $CA9^{high}$ tumors, respectively (P value: * =0.0283). (Right panel) Survival data from the TCGA dataset for *CA9* ^{high} (n=78) transcript expression of GBM samples illustrating a significant increase in survival when compared to *CA9* ^{low} (n=77) samples (HR: 0.7 (0.62-116); Logrank p value: 0.0146) **D)** CA9 surface expression was evaluated after cells were cultured in normoxia (21% O_2) or hypoxia (1% O_2) for 5 days; and the results indicated a dramatic increase in CA9 expression on both GBM BTIC lines upon exposure to hypoxia. **E)** Significant increase of self-renewal capacity as measured by secondary sphere formation assay and **F)** proliferative potential as measured by PrestoBlue proliferation assay is seen in $CA9^{+}$ when compared to $CA9^{-}$ cells. (P value: **** < 0.0001, * 0.01, ns: non-significant) (mean±SEM, two-tailed t-test).

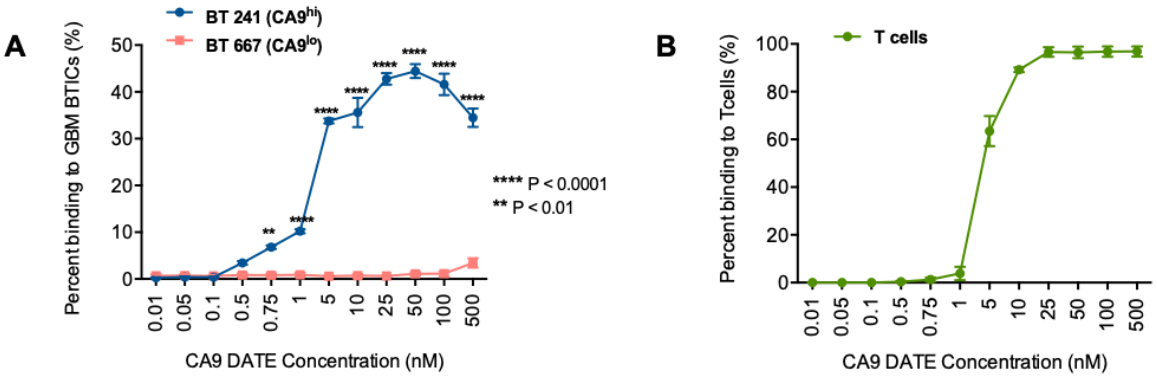

Figure 2. Generation and assessment of human anti-CA9 Dual specific T cell engagers (DATEs). A) Dual specificity of CA9 DATEs on $CA9^{hi}$ GBM BTIC (BT241), $CA9^{lo}$ GBM BTIC (BT667) and **B)** human PBMC-derived T cells by flow cytometry. (P value: **<0.01, **** <0.0001) (2-way RM AVOVA).

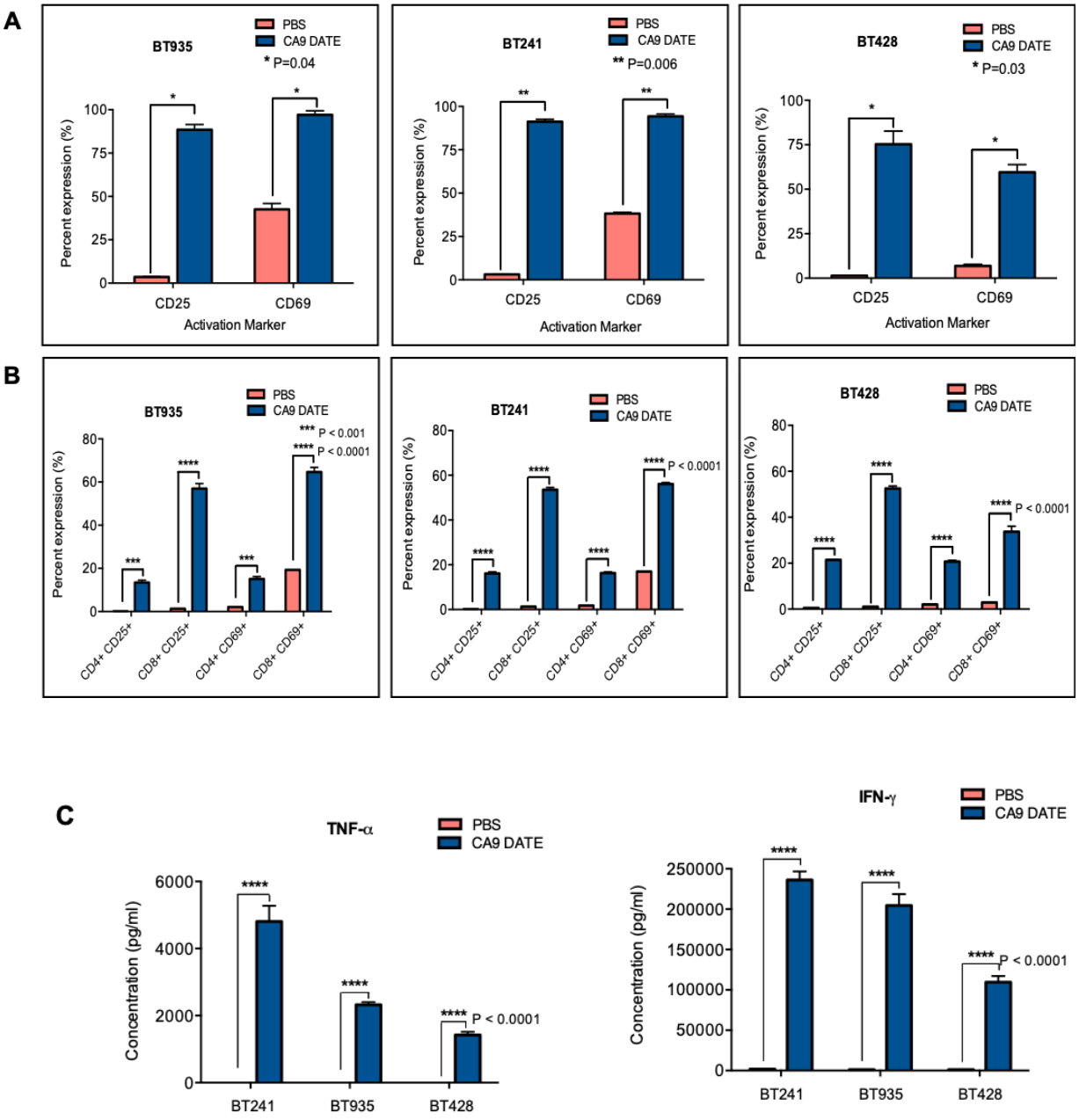
A
BT935
PBS
CA9 DATE
* P=0.04
Percent expression (%)
CD25
CD69
Activation Marker
BT241
** P=0.006
BT428
* P=0.03
B
BT935
*** P < 0.001
**** P < 0.0001
CD4+ CD25+
CD8+ CD25+
CD4+ CD69+
CD8+ CD69+
BT241
BT428
C
TNF-α
Concentration (pg/ml)
BT241
BT935
BT428
IFN-γ

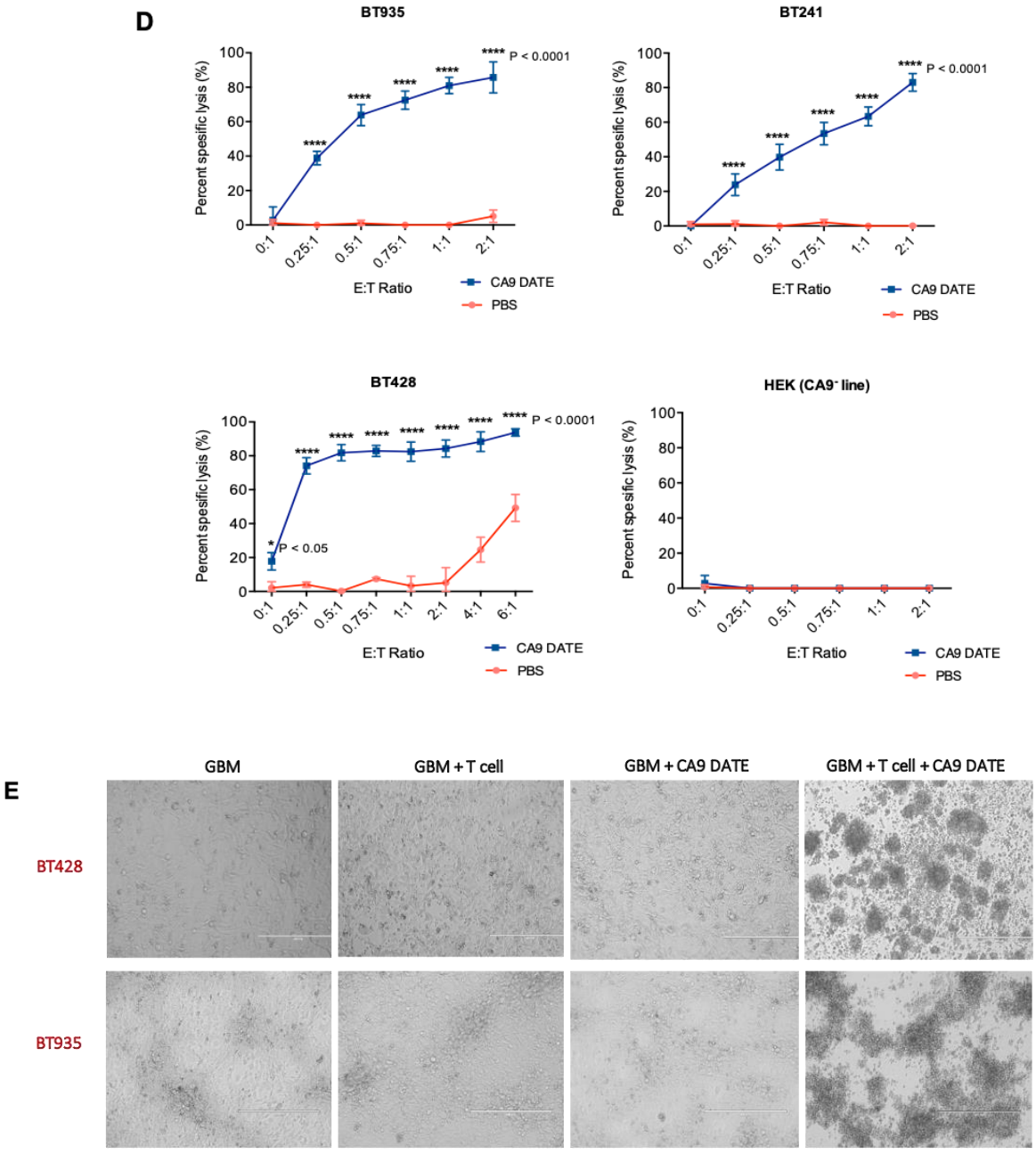

Figure 3. Therapeutic targeting of CA9^{hi} GBM BTICs using CA9 DATEs. A) Addition of CA9 DATE (1µg/mL) to the co-culture of CA9^{hi} GBM BTICs (BT241, BT935, BT428) and T cells (E:T ratio, 1:1) (overnight incubation) caused T cells activation as confirmed

by increased expression of CD25 and CD69 by flow cytometry analysis (n=2). (P value: *= 0.04, **= 0.006) (2 way ANOVA) **B)** $CD8^+$ T cells were the main subset of activated T cells. (P value: ***< 0.001, **** < 0.0001) (2 way ANOVA) **C)** Enzyme-linked immunosorbent assay (ELISA) shows elevated secretion IFN-γ and TNF-α cytokines in supernatant collected from co-cultures of T cells and GBM BTICs treated with CA9 DATEs. (n=2) (P value: **** < 0.0001) **D)** DATEs significantly induced cytotoxicity of $CA9^{hi}$ GBM BTICs (BT241, BT935, BT428) but not $CA9^-$ cells (HEK) when co-cultured with T cells and DATEs (1nM) for 16 hours at different E:T ratios. (n=3) (P value: *< 0.05, **** < 0.0001) (2 way ANOVA). **E)** Micrographs of GBM BTICs and T-cell co-culture with and without DATEs. $CA9^{hi}$ GBM BTIC lines (BT 935 and BT 428) were incubated with either T cells (E:T ratio, 1:2) or CA9 DATE alone or with both. GBM BTIC lysis were observed only in the presence of both T cells and CA9 DATEs (Scale bar: 400 μm).

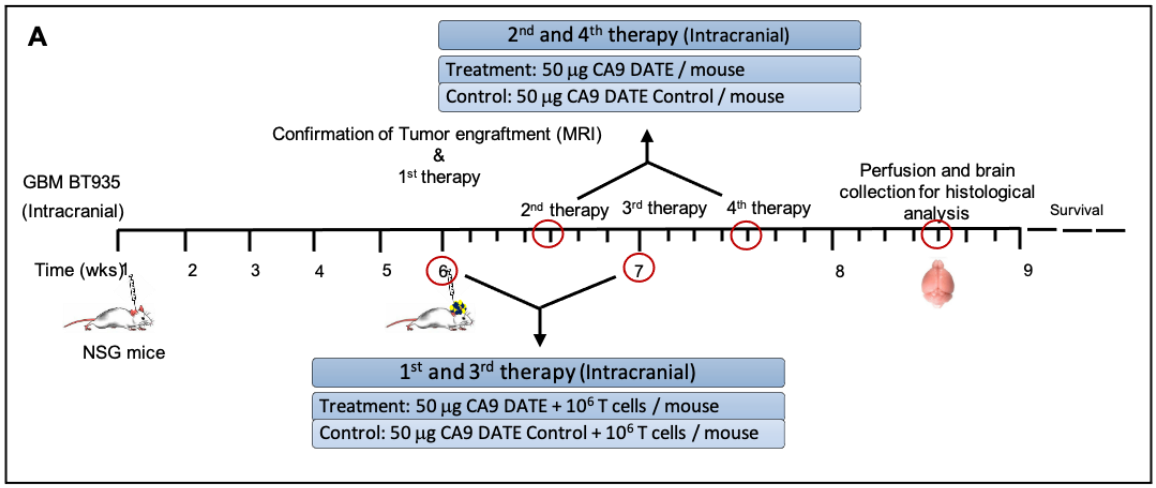
A
2nd and 4th therapy (Intracranial)
Treatment: 50 µg CA9 DATE / mouse
Control: 50 µg CA9 DATE Control / mouse
Confirmation of Tumor engraftment (MRI)
&
1st therapy
GBM BT935
(Intracranial)
2nd therapy
3rd therapy
4th therapy
Perfusion and brain collection for histological analysis
Survival
Time (wks) 1 2 3 4 5 6 7 8 9
NSG mice
1st and 3rd therapy (Intracranial)
Treatment: 50 µg CA9 DATE + 10^6 T cells / mouse
Control: 50 µg CA9 DATE Control + 10^6 T cells / mouse

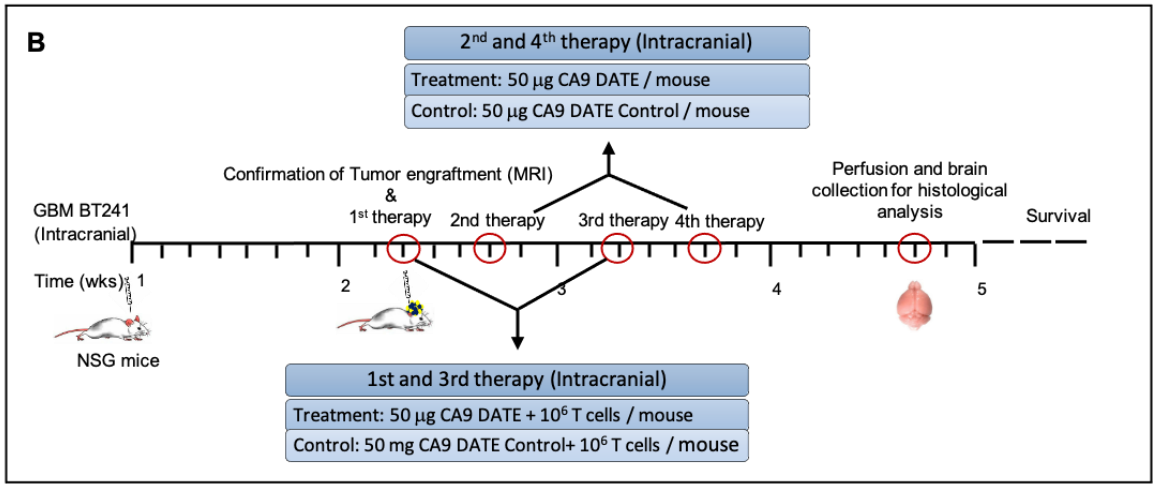
B
2nd and 4th therapy (Intracranial)
Treatment: 50 µg CA9 DATE / mouse
Control: 50 µg CA9 DATE Control / mouse
Confirmation of Tumor engraftment (MRI)
&
1st therapy
GBM BT241
(Intracranial)
2nd therapy
3rd therapy
4th therapy
Perfusion and brain collection for histological analysis
Survival
Time (wks) 1 2 3 4 5
NSG mice
1st and 3rd therapy (Intracranial)
Treatment: 50 µg CA9 DATE + 10^6 T cells / mouse
Control: 50 mg CA9 DATE Control+ 10^6 T cells / mouse

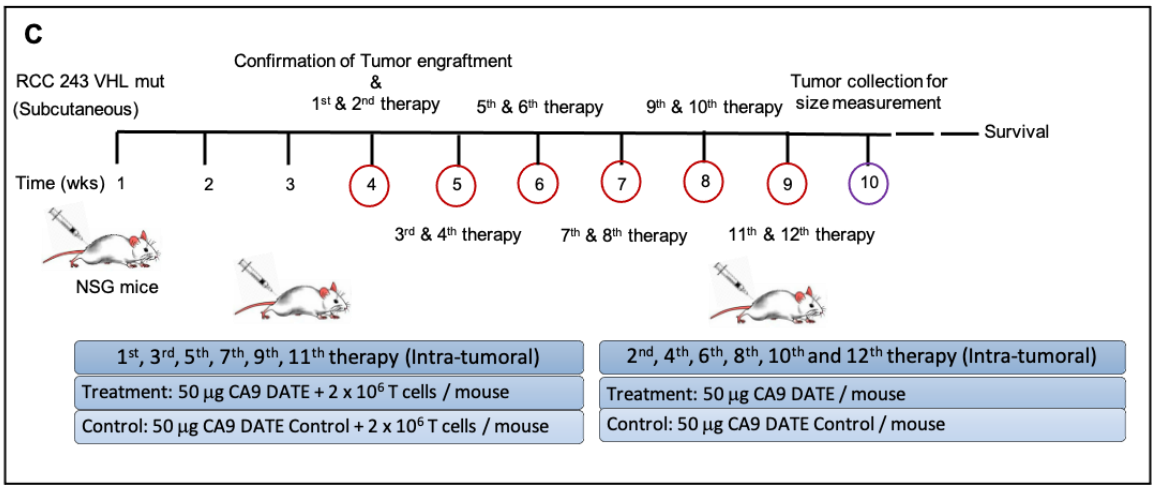
C
RCC 243 VHL mut
(Subcutaneous)
Confirmation of Tumor engraftment
&
1st & 2nd therapy
5th & 6th therapy
9th & 10th therapy
Tumor collection for size measurement
Survival
Time (wks) 1 2 3 4 5 6 7 8 9 10
3rd & 4th therapy
7th & 8th therapy
11th & 12th therapy
NSG mice
1st, 3rd, 5th, 7th, 9th, 11th therapy (Intra-tumoral)
Treatment: 50 µg CA9 DATE + 2 x 10^6 T cells / mouse
Control: 50 µg CA9 DATE Control + 2 x 10^6 T cells / mouse
2nd, 4th, 6th, 8th, 10th and 12th therapy (Intra-tumoral)
Treatment: 50 µg CA9 DATE / mouse
Control: 50 µg CA9 DATE Control / mouse

Figure. 4. The schematic of *in vivo* preclinical testing of CA9xCD3 DATE antitumor activity using patient derived xenograft models. A and **B)** Intracranial engraftment of human CA9^{hi} GBM BTICs (BT935 and BT241) for generating GBM model and the detail of treatment regimen. **C)** Subcutaneous implantation of human CA9^{+} RCC 243 VHL mut cells for generating RCC model and the detailed treatment plan.

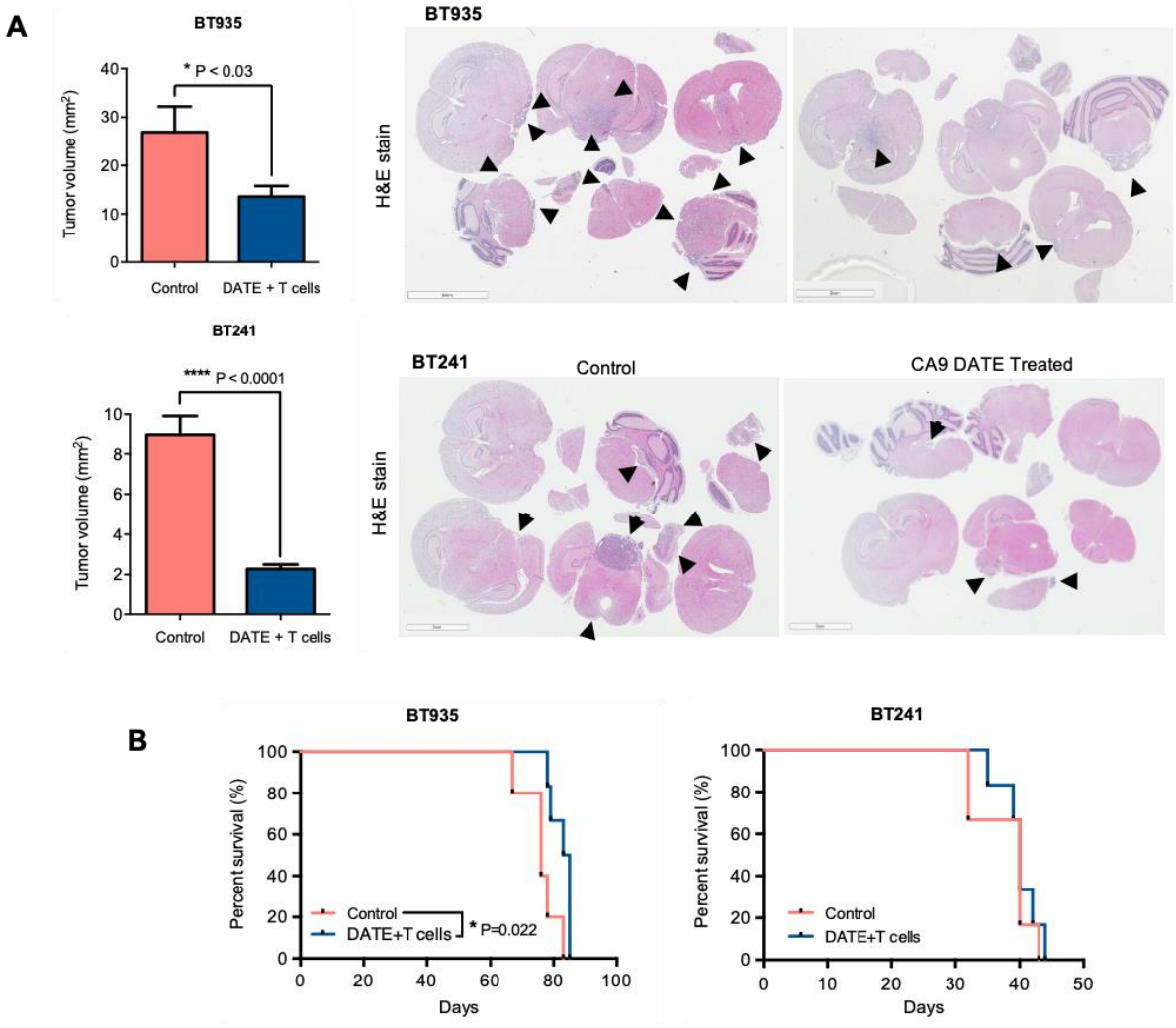

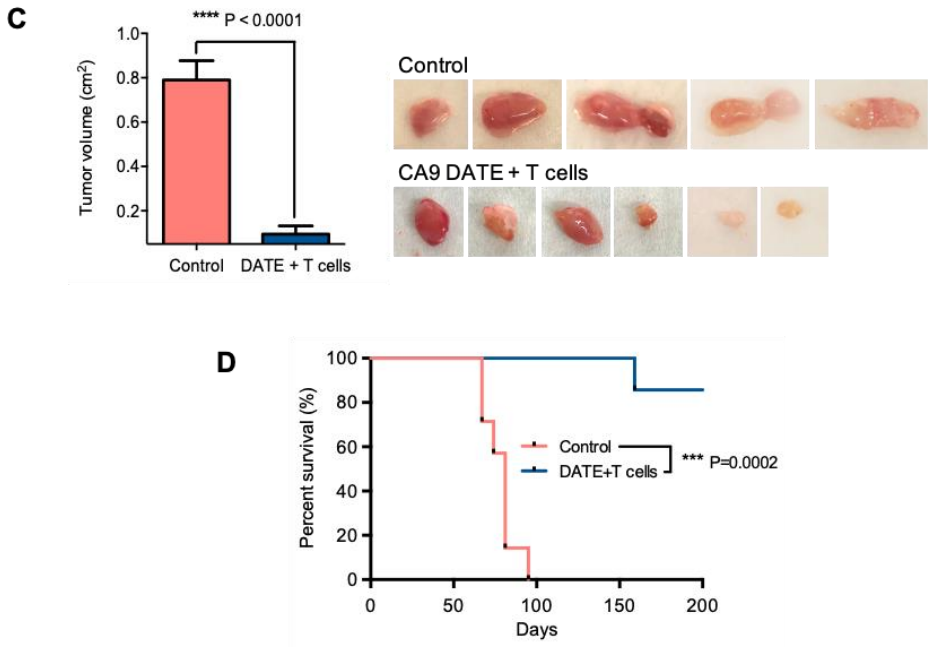

Figure 5. CA9 DATE mediated antitumor response in xenografted immunocompromised mice. A) NSG mice were intracranially implanted with human CA9^{hi} GBM BTICs (BT935 and BT241). Upon successful engraftment, mice were intracranially treated with 1x10^6 T cells isolated from human PBMCs either with CA9 DATE or CA9 DATE control (50µg) for a total of four doses over two weeks. Mouse xenografts generated after CA9 DATE treatment had less tumor burden (n=6) (P value: * < 0.03, **** < 0.0001) (mean±SEM, two-tailed t-test) and **B)** maintained a significant survival advantage over control mice (n=6). (P value: * < 0.03) (Log-rank Mantel-Cox Test) **C)** NSG mice were subcutaneously implanted with human CA9$^+$ RCC 243 VHL mut cells. Upon successful engraftment and having a palpable tumor, mice were intratumorally treated with 2x10^6 T cells isolated from human PBMCs either with CA9 DATE or CA9 DATE control (50µg) for a total of 12 doses over 6 weeks. Mouse xenografts generated after CA9 DATE treatment had less tumor burden (n=6) (P value: **** < 0.0001)

(mean±SEM, two-tailed t-test) and **D)** maintained a significant survival advantage over control mice (n=7) (P value: *** < 0.0004) (Log-rank Mantel-Cox Test)

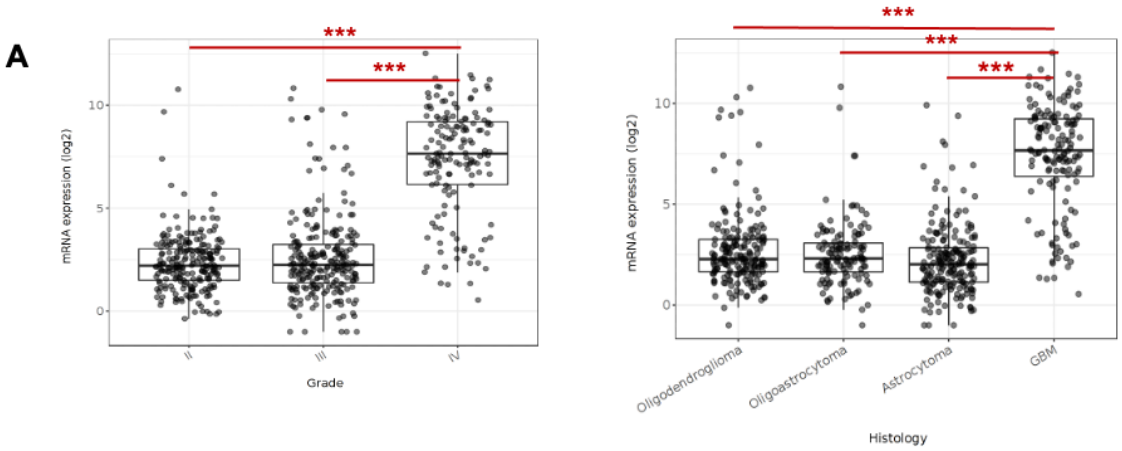
A
***
***
mRNA expression (log2)
10
5
0
II
III
IV
Grade
***
***
***
mRNA expression (log2)
10
5
0
Oligodendroglioma
Oligoastrocytoma
Astrocytoma
GBM
Histology

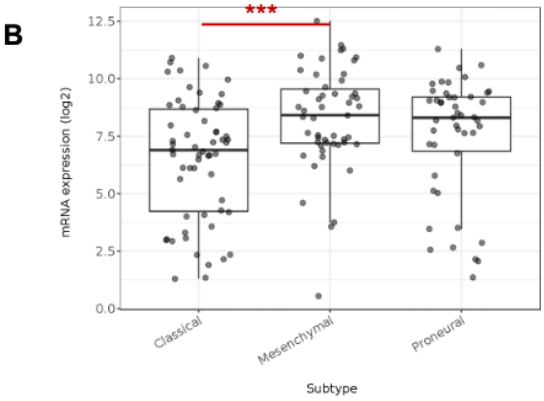
B
***
mRNA expression (log2)
12.5
10.0
7.5
5.0
2.5
0.0
Classical
Mesenchymal
Proneural
Subtype

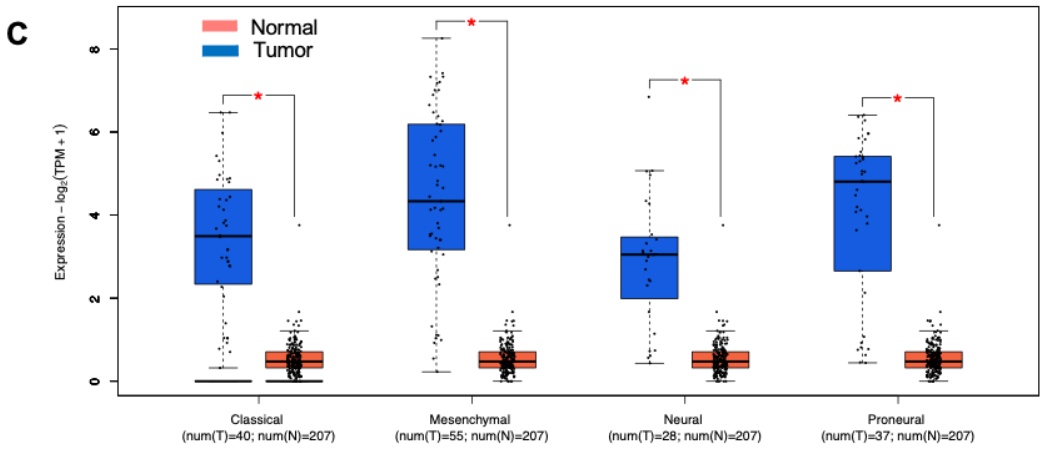
C
Normal
Tumor
Expression – log2(TPM + 1)
8
6
4
2
0
Classical
(num(T)=40; num(N)=207)
Mesenchymal
(num(T)=55; num(N)=207)
Neural
(num(T)=28; num(N)=207)
Proneural
(num(T)=37; num(N)=207)

Supplementary Figure. 1. CA9 expression in glioblastoma. A) CA9 has higher expression in GBM (grade IV) (n=150) compared with low-grade gliomas (II and III) (n=226 and 244 respectively), oligodendroglioma (OG) (n=191), and astrocytoma (Astro) (n=194) at the transcriptomics level according to the GlioVis database (TGCA) (P value: *** < 0.001). **B)** CA9 has higher expression in mesenchymal (Mes) subtype (n=51) compared to proneural (PN) (n=46) and classical (Cla) (n=59) of GBM (GlioVis-TCGA) (P value: *** < 0.001). **C)** and CA9 expression is higher in each subtype compared to normal tissue (PEGIA2). (P value * < 0.05, ***, P < 0.001).

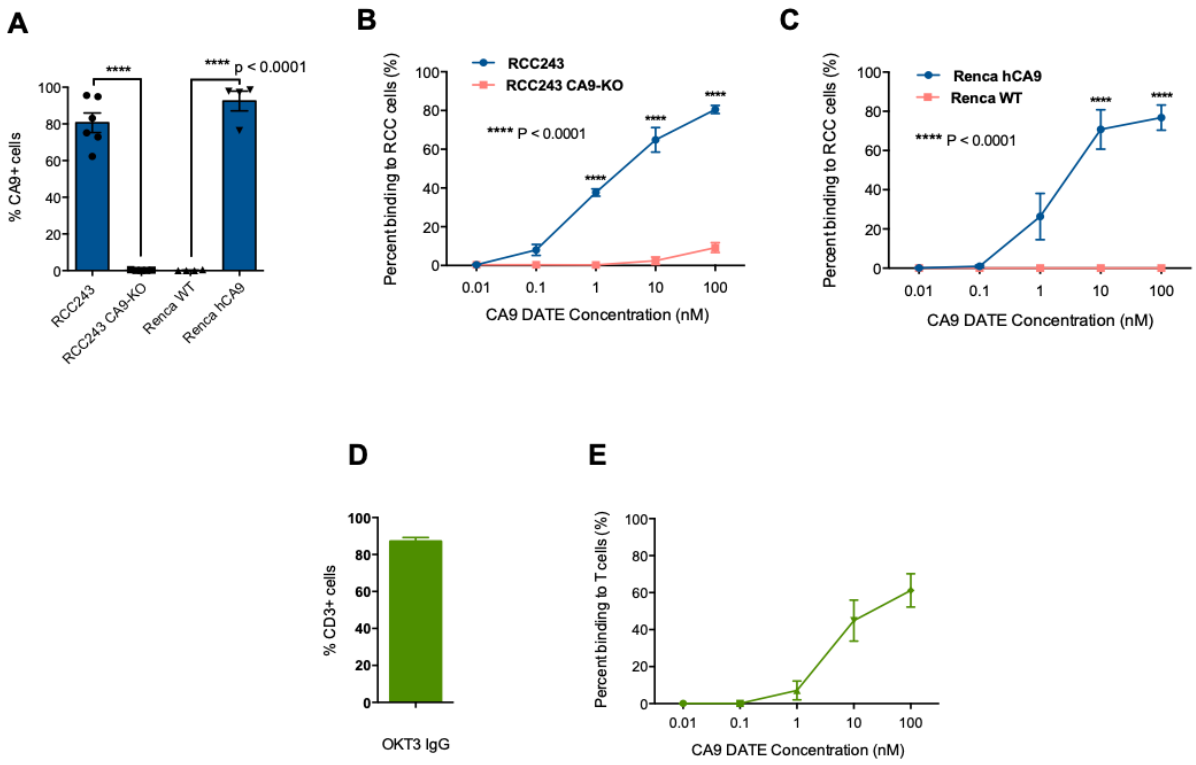

Supplementary Figure. 2. Dual specificity testing of CA9 DATEs in Renal Cell Carcinoma (RCC) models and Jurkat cells. A) CA9 expression level on RCC243, RCC243 CA9-KO, Renca and Renca hCA9 cells. **B)** Increasing concentrations of CA9 DATE binding to RCC243 vs RCC243 CA9-KO, **C)** Renca hCA9 vs Renca WT cells and **E)** CD3 expressing Jurkat cells were measured using flow cytometry. Error bars: mean ± SEM. **D)** okt3 expression level on Jurkat cells

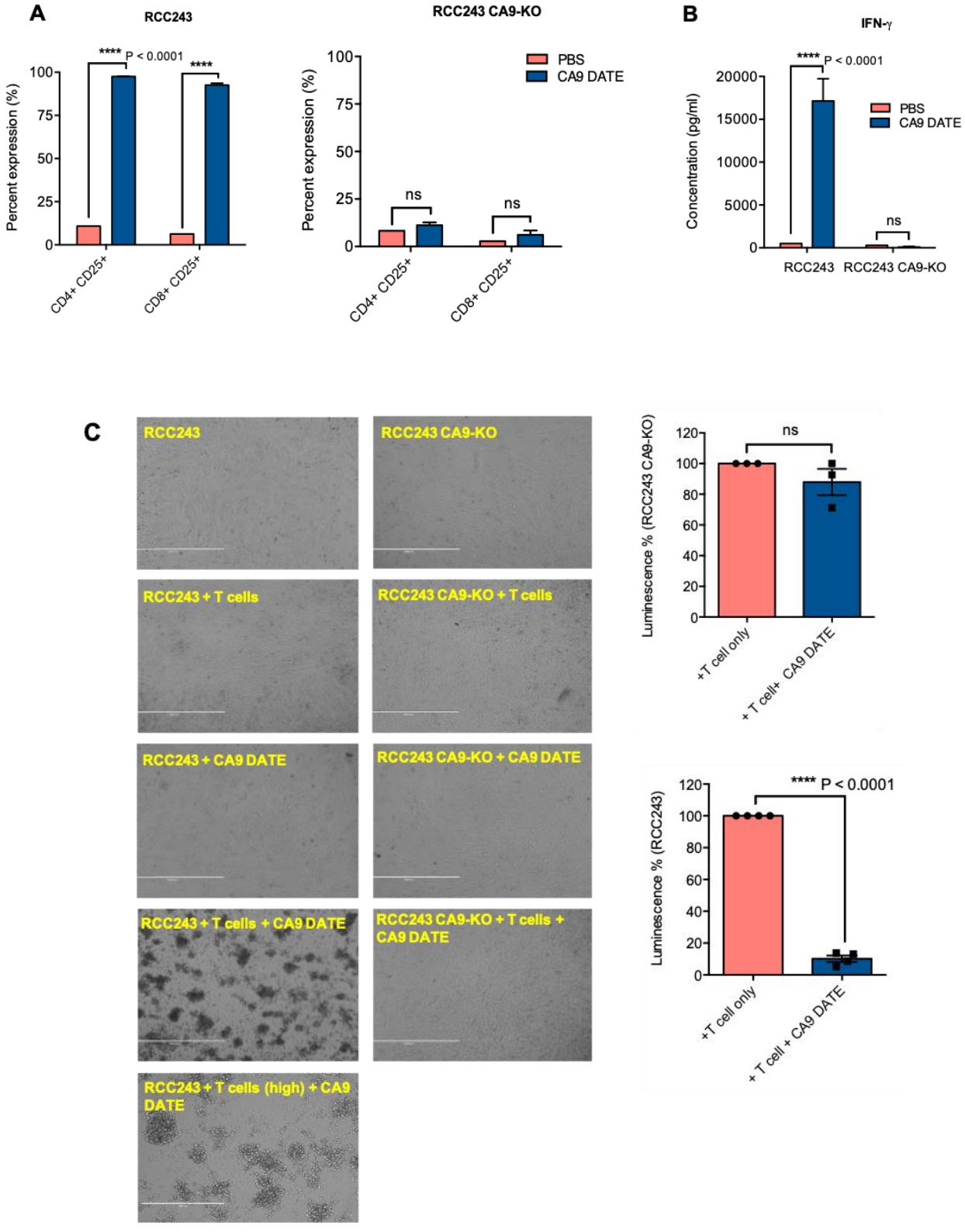
A
RCC243
RCC243 CA9-KO
Percent expression (%)
**** P < 0.0001
****
ns
CD4+ CD25+
CD8+ CD25+
PBS
CA9 DATE
B
IFN-γ
Concentration (pg/ml)
RCC243
RCC243 CA9-KO
C
RCC243
RCC243 CA9-KO
RCC243 + T cells
RCC243 CA9-KO + T cells
RCC243 + CA9 DATE
RCC243 CA9-KO + CA9 DATE
RCC243 + T cells + CA9 DATE
RCC243 CA9-KO + T cells + CA9 DATE
RCC243 + T cells (high) + CA9 DATE
Luminescence % (RCC243 CA9-KO)
+T cell only
+ T cell+ CA9 DATE
Luminescence % (RCC243)
+ T cell + CA9 DATE

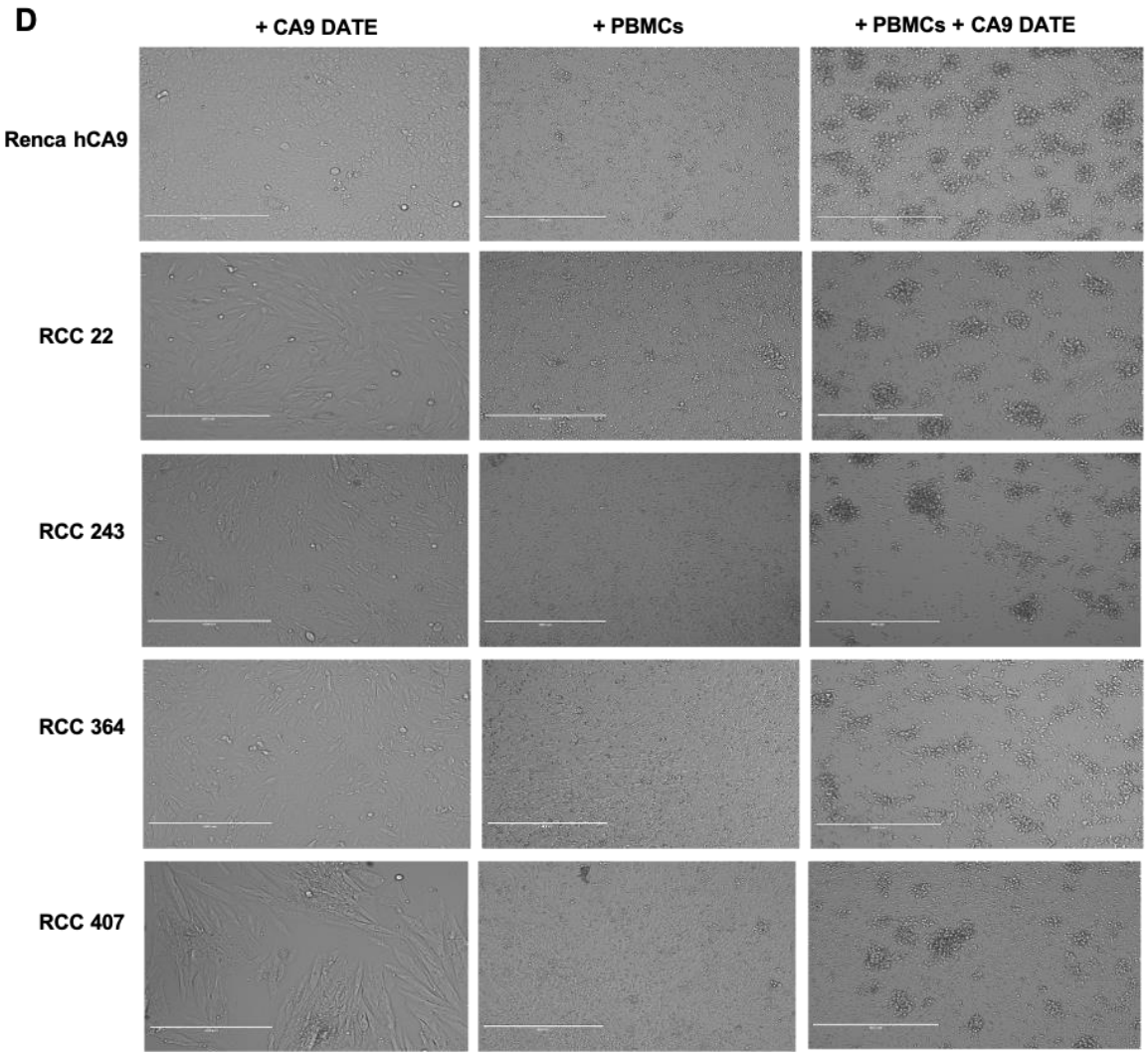
D
+ CA9 DATE
+ PBMCs
+ PBMCs + CA9 DATE
Renca hCA9
RCC 22
RCC 243
RCC 364
RCC 407

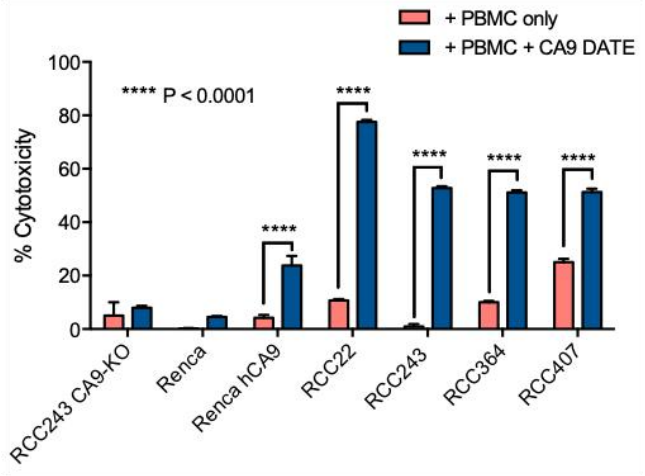
+ PBMC only
+ PBMC + CA9 DATE
**** P < 0.0001
% Cytotoxicity
100
80
60
40
20
0
****
RCC243 CA9-KO
Renca
Renca hCA9
RCC22
RCC243
RCC364
RCC407

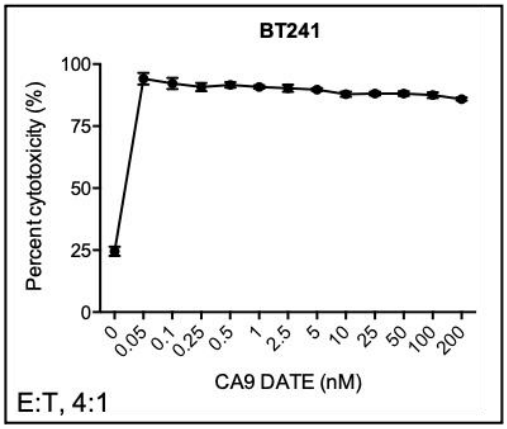
E
BT241
Percent cytotoxicity (%)
100
75
50
25
0
0
0.05
0.1
0.25
0.5
1
2.5
5
10
25
50
100
200
CA9 DATE (nM)
E:T, 4:1

Supplementary Figure. 3. Assessing the efficacy of CA9 DATE in therapeutic targeting of CA9 expressing RCC lines. A) Addition of CA9 DATEs (1 nM) to the co-culture of human CD3+ T cells with CA9 expressing target cells (Luciferase-expressing RCC 243 cell lines and the CA9 knockout counterpart [CA9-KO]) for 48 hours at the E:T ratio, 1:5 resulted in a significant elevation of CD25 expression on both CD4 + and CD8 + T cells population confirmed by flow cytometry analysis. (n=4) (P value: **** < 0.0001) (2 way ANOVA) **B)** Enzyme-linked immunosorbent assay (ELISA) indicated increased secretion of Interferon-gamma (IFN-γ) by T cells only in the presence of CA9 DATE and CA9 expression on target cells. (P value: **** < 0.0001) (2 way ANOVA) **C)** CA9 DATE (1 nM) induced potent cytolysis in antigen expressing target cells when co-cultured with human $CD3^+$ T cells at an E:T ratio of 5:1 for 48 hours quantified by luminescence assay. Phase contrast images of the *in vitro* cytotoxicity assay confirmed potent cytolytic effect of CA9 DATE on CA9 antigen expression. (n=4) (Scale bar: 1000 μm). **D)** CA9 DATE effectively induced target lysis across a panel of kidney cancer cell lines when co-cultured with CD3+ T cells at E:T ratio of 10:1 (*In vitro* cytotoxicity assay setup as described earlier). lactate dehydrogenase (LDH) release assay on the supernatant indicated a drastic increase in target cell cytotoxicity in the presence of CA9 DATE and CA9 antigen expression. The phase contrast images of light microscope confirmed the cytolytic effect of CA9 DATE on CA9 expressing RCC lines (n=2). (P value: **** < 0.0001) (2 way ANOVA) **E)** Dose response study performed on BT 241, $CA9^{hi}$ GBM BTIC, identified 1 nM as the optimal dose for GBM cytotoxicity assay.

Specimen ID	Age/Gender	Diagnosis	CA9 expression in GBM cells (%)	Survival time from diagnosis (months)
BT 935	53/F	P-GBM	66.80	8.3
BT 458	81/M	P-GBM	0.56	N/A
BT 428	63/F	P-GBM	69.76	13.8
BT 667	47/M	P-GBM	0.37	29.6
BT 566	55/F	R-GBM	0.33	N/A
BT 241	68/F	R-GBM	66.17	23.4
BT618	67/F	R-GBM	13.58	N/A
BT972	53/M	R-GBM	44.12	N/A
BT799	77/F	P-GBM	0.15	6.2

Table 1. GBM patient demographics. Related to Figures 1, 2, 3, 4, 5, S3: GBM patient samples analyzed

Specimen ID	Gender	Age at diagnosis	Age at surgery	Diagnosis	CA9 expression (%)
RCC 22	F	66.8	67.6	RCC	_
RCC 162	_	_	_	RCC	61.80
RCC 243	_	_	_	RCC	80.50
RCC 323	M	57.9	57.10	RCC	48.70
RCC 364	M	45.7	45.9	RCC	_
RCC 407	M	62.7	62.9	RCC	_

Table 2. RCC patient demographics. Related to Figures S2, S3, 4, 5

Chapter 3: The proteomic landscape of Glioblastoma recurrence reveals novel and targetable immunoregulatory drivers

Abstract

Glioblastoma (GBM) is characterized by extensive cellular and genetic heterogeneity. Its initial presentation as primary disease (pGBM) has been subject to exhaustive molecular and cellular profiling. By contrast, our understanding of how GBM evolves to evade the selective pressure of therapy is starkly limited, with little profiling of recurrent GBM (rGBM), which is refractory to most treatments used for pGBM. We therefore quantified the transcriptome and proteome of 134 patient-derived pGBM and rGBM samples, including 40 matched pGBM-rGBM pairs. Distinct gene-expression profiles are activated in pGBM *vs.* rGBM, and these clearly differentiate short-term from long-term survivors. GBM subtypes evolve towards a mesenchymal state at recurrence, consistent with the increasingly invasive and aggressive biological activity of rGBM. We identified immune regulatory/suppressive genes as important drivers of rGBM and in particular 2-5-oligoadenylate synthase 2 (OAS2) as an essential and functional driver of rGBM *via* immune suppression. Our data identifies a new class of therapeutic targets that emerge from the adaptive response of pGBM to therapy, emerging specifically in recurrent disease. These may provide new therapeutic opportunities not present at primary GBM diagnosis.

Introduction

Glioblastoma (GBM) is the most commonly diagnosed and lethal primary malignant brain tumor in adults and constitutes ~60% of all neuroepithelial tumors [1]. Despite aggressive multimodal treatment, including surgical resection followed by radiotherapy and chemotherapy, GBM remains incurable. Almost all patients experience relapse 7-9 months post-diagnosis and median survival has remained around 15 months for the past decade [9]. Cellular and molecular characterization of treatment-naïve primary GBM (pGBM) has revealed extensive inter- and intra-tumoral heterogeneity caused by multiple types of molecular dysregulation [69, 72, 248, 304]. Most molecular landscape studies of GBM have focused on pGBM, with comparably little focus on the molecular features of GBM that recurs after initial treatment (rGBM). Recent studies suggest that GBM evolves significantly in response to therapy and that rGBM represents a distinct biological entity [70, 305]. For example, an evolutionary analysis of 21 paired primary and locally-recurrent GBM specimens found that overall mutation burden was not changed in rGBM, but that additional driver mutations were frequently acquired [306]. New driver mutations were not only acquired in rGBM, but pGBM clones harbouring specific drivers could also be preferentially lost. For example, focal EGFR amplifications were detected in ~95% of pGBM and either reverted or the underlying clone went extinct in 27% of rGBM. It is thus clear that GBM evolves significantly in response to therapy, making it refractory to first-line therapies, but the key signaling pathways involved remain largely unclear.

To fill this gap in our understanding of rGBM, we characterize how GBMs evolved and adapted their signaling in response to conventional therapy with longitudinal proteome

analysis of 134 tissue samples from patients with recurrent GBM. Using this resource, we identified new therapeutic targets specifically activated at GBM recurrence, many of which regulate processes related to maintenance of an immunosuppressive niche. Our data implies that GBM treatment resistance may evolve not only due to escape of cancer stem cell populations, but also an altered tumor immune microenvironment (TIME) in response to selective pressures of therapy.

Materials & Methods

Patient samples and clinical data

Human GBM patient samples and fetal brain samples were collected from the Hamilton Health Sciences (Juravinski Cancer Centre and Hamilton General Hospital) from consenting patients as approved by the Hamilton Health Sciences (HHS) /McMaster Health Sciences research ethics board (REB #07-366 and REB# 08-005) and at University Health Network (REB #19-6350). Electronic health record software including Citrix, Meditech and MOSAIQ databases were used to search the Hamilton Health Sciences records (2001-2016) to collect primary-recurrent GBM matched-pair Formalin-fixed paraffin-embedded (FFPE) samples and patient's clinicopathological information.

Sample preparation for Tissue Microarray (TMA) construction, proteomics and NanoString analysis

The hematoxylin and eosin (H&E)-stained slides associated with each FFPE block were used to mark the area of interest (tumor tissue and normal tissue adjacent to the tumor) by neuropathologist Dr. Cynthia Hawkins, University of Toronto. The marked FFPE blocks were then used for constructing Tissue Microarrays (TMA) and collecting tissue punches for proteomics and NanoString analysis. Briefly, three tissue cores from each donor block were acquired in circular spots form (1 mm in diameter) using a tissue microarray automated machine (3DHISTECH TMA Master, Quorum Technologies) and were placed in an empty paraffin block. In addition to sampling for constructing TMA blocks, 3 - 4

more tissue cores (1.5 mm in diameter) from each block were collected for proteomics and NanoString analysis.

FFPE tissue sample preparation for Mass Spectrometry (MS) analysis

GBM FFPE tissue cores (1.5 mm) were deparaffinized twice using 500 µL of xylene (Sigma, Cat# 534056) with continuous end-to-end rotation for 5 minutes at room temperature. The samples were centrifuged at 14,000-g for 5 minutes and the supernatant was discarded. The tissue cores were rehydrated using sequential stepwise gradient treatment with 100%, 90%, 70% and 50% ethanol followed with water as the final step, with 5 minutes of end-to-end rotation for each step. The rehydrated tissue cores were lysed in 100 µL of 50% (v/v) 2,2,2-Trifluoroethanol (Sigma, Cat# 96924) with 300 mM Tris (pH 8) and sonicated using 5 cycles of pulse sonication 10 seconds each. The protein lysates were heated at 95°C for 2 hours for decrosslinking of the proteins. Two pmol of Suc2 (yeast invertase, Sigma, Cat# I4504) was added as digestion control. The disulphide bonds were reduced using 5 mM dithiothreitol for 30 minutes at 60 °C, the reduced disulphide bridges were alkylated with 25 mM iodoacetamide for 30 minutes at room temperature in the dark. The samples were diluted 1:5 with 100 mM ammonium bicarbonate (pH 8.0) and 2 mM CaCl2 was added. The proteins were digested overnight with 2 µg of trypsin/Lys-C enzyme mix (Promega, Cat# V5072) at 37 °C. The reaction was quenched with addition of formic acid and the peptides were desalted by C18-based solid phase extraction, then lyophilized in a SpeedVac vacuum concentrator. The peptides were solubilized in mass spectrometer-grade 0.1% formic acid in water and the peptide concentration determined with NanoDrop Lite (at 280 nm).

MS sample processing and data analysis

Prior to data acquisition, synthetic iRT peptides (Biognosys, Cat#Ki-3002) were spiked into each sample at a ratio of 1:10. LC-MS/MS data was acquired using an Easy nLC 1000 (Thermo) nano-flow liquid chromatography system with a 50 cm EasySpray ES803 column (Thermo) coupled to a Orbitrap Fusion tandem mass spectrometer (Thermo). Peptides were separated by reverse phase chromatography using a 4-hour non-linear chromatographic gradient of 4-48% buffer B (0.1% FA in ACN) at a flow rate of 250 nL/minute. Mass spectrometry data was acquired in positive-ion data-dependent mode. MS1 data was acquired at a resolution of 240,000 in the orbitrap with maximum injection time (maxIT) of 1000 ms and 40s dynamic exclusion, while MS2 data was acquired in the ion trap at 'Normal' scan rate, maxIT of 10 ms. HCD fragmentation was done at a normalized collision energy of 31%. The raw files were searched in MaxQuant (version 1.6.2.3) [307] using a UniProt protein sequence database containing human protein sequences from Uniprot (complete human proteome; Released 2019-09) merged with, Suc2 (yeast) protein sequences from Uniprot, and iRT synthetic peptide sequences (Biognosis). Searches were performed with a maximum of two missed cleavages, and carbamidomethylation of cysteine as a fixed modification. The oxidation at methionine, acetylation (N-term), arginine and lysine methylation was set as variable modifications. The FDR for the target-decoy search was set to 1% for protein and peptide level. Intensity-based absolute quantification (iBAQ), label-free quantitation (LFQ), and match between runs (matching and alignment time windows set as 2 and 20 minutes, respectively) were enabled. The proteinGroups.txt file was used for subsequent analysis. Proteins matching decoy and

contaminant sequences were removed, and proteins identified with two or more unique peptides were carried forward. LFQ intensities were used for protein quantitation [308]. For proteins with missing LFQ values, median-adjusted iBAQ values were used as replacement [309]. The missing data was imputed using the normal distribution where the missing values were imputed from the lower half of the Gaussian distribution (width = 0.3, downshift = 1.8). Differentially expressed proteins among the GBM pairs were identified using paired sample Mann-Whitney U-test with multiple test correction using FDR. Pathway enrichment analysis was performed using Gene Set Enrichment Analysis (GSEA) or g:profiler (https://biit.cs.ut.ee/gprofiler). Pre-rank mode was used to perform GSEA using hallmark gene set from molecular signature database (MSigDB) with the following parameters, number of permutations = 1000, where FDR < 0.25 was considered significant. The g:Profiler searches were performed using a list of all the proteins detected as background, with ordered query based on significance. The FDR threshold was set to 0.05 and the gene ontology biological process database was used to perform the searches. Visualization was done using Cytoscape (v3.7.2) (Enrichment Map app).

Proteomic subtype identification

Consensus clustering of the proteomics data was performed using the R package ConsensusClusterPlus v1.52.0 [310] using the proteins (n = 1,595) detected in all matched primary and recurrence pairs (n = 83 samples; 40 pairs) with protein clusters (k) varying from 2 to 20. Hierarchical clustering was performed using Euclidean distance and Ward linkage, with 80% gene resampling and 80% item resampling with 1,000 iterations. Clustering of samples and proteins was performed separately. The optimal cluster number

(k = 5) was chosen based on the delta area, which is the relative change in the area under the CDF curve comparing k and k-1.

Comparison to CPTAC proteomics

For the Clinical Proteomic Tumor Analysis Consortium GBM (CPTAC-GBM) data, the processed TMT protein abundance table and its associated clinical data were downloaded from the CPTAC data portal (https://cptac-data-portal.georgetown.edu/study-summary/S057). The experimental procedure and quantification were described in the original report [311]. To eliminate samples that were potentially mislabelled or swapped, the Pearson's correlation was calculated between all samples and samples with a correlation above 90% were removed (n = 2). Proteins missing in more than 90% of the samples were excluded from the analysis. We performed a Student's t-test for each protein comparing tumor and normal tissue adjacent to the tumor (NAT). The Benjamini-Hochberg test was performed to correct for multiple-testing. Spearman's correlation was calculated between the log2 fold change of NAT and pGBM samples in each cohort. Venn diagrams of the overlapping proteins were created using the R package VennDiagram [312]; (v1.6.20). Centroids were created in the Hamilton Health Sciences (HHS) dataset using the median abundance per protein in each of the five proteomic subtypes. CPTAC proteomic profiles were correlated to each centroid and samples were classified based on the highest positive Spearman's correlation.

Comparison of pGBM proteomics with TCGA RNA abundance

Level 3 TCGA RNA-Sequencing data was downloaded from the Genomic Data Commons Data Portal and only primary samples were kept. The median abundance per protein was used to calculate the Spearman's correlation.

NanoString analysis

RNA was extracted from FFPE tissue cores using the Qiagen Allprep DNA/RNA FFPE kit per manufacturer's protocol. 300 ng of total RNA of each sample were analyzed by NanoString gene expression assay using a custom codeset profiling four housekeeping genes and 30 classifier genes (one probe per gene) corresponding to the classical (CL), mesenchymal (MES), proneural (PN), and neural (NL) subtypes (**Supplementary Table 1**). Raw counts were background subtracted then normalized using the geometric mean of the samples analyzed using NanoString nSolver (nSolver Analysis Software: https://hdmzstaging.nanostring.com/products/analysis-software/nsolver). After removal of outlier probe values, data from 83 samples from 52 patients was classified using non-negative matrix factorization (NMF) into up to four groups. NMF was run with 200 iterations at ranks k = 2 to k = 7, approximating at each rank (1) metagenes representing the expression pattern of discriminatory genes, and (2) the weights of each metagene per sample. Rank k = 4 was the most parsimonious solution yielding clusters with a high cophenetic correlation coefficient, and separation of subtyping genes among metagenes. Metagene 2 includes both PN and NL classifier genes and was thereafter used to represent both groups. Metagene 3 corresponds to the CL subtype. The MES classifier genes were

split between metagenes 1 and 4, potentially indicating two MES subtypes. Samples were assigned to subtypes via hard clustering using the maximum weights of each metagene. To account for the presence of multiple metagene contributions in each sample, weights were converted to percentages. Using these values, significant changes in subtype composition between paired primary-recurrence samples were identified using a paired t-test and corrected using the Benjamini-Hochberg procedure.

Time to event analysis

Patients were split in quartiles based on time to death or time to recurrence and then classified into three groups: short- (1st quartile), intermediate- (2nd and 3rd quartiles) and long-term survivors (4th quartile). Mann-Whitney U-tests were performed per protein between the lowest and highest quartile. Cox proportional hazards models were fit using protein abundance as a continuous measure with the R package survival (v2.40-3). P values were corrected for multiple-testing using FDR.

Cell culture

The cells used in this study were patient-derived GBM lines. To isolate and propagate Brain Tumor Initiating Cells (BTICs), human brain tumor tissues were processed upon surgical resection according to the previously described protocol [74, 76, 284]. Briefly, tumor specimens were dissociated in enzymatic solution consisting of PBS (ThermoFisher, Cat#10010049) and 0.2 Wünsch unit/mL Liberase Blendzyme 3 (Millipore Sigma, Cat#5401119001) and incubated on a shaker at 37 °C for 15 minutes. The dissociated tissue was then filtered through a 70 μm cell strainer (Falcon, Cat#08-771-2) and collected by

centrifugation at 1200 rpm for 5 minutes. Ammonium chloride solution (STEMCELL Technologies, Cat#07850) was used for lysing the red blood cells. BTICs were cultured in NeuroCult complete (NCC) media, a chemically defined serum-free neural stem cell medium (STEMCELL Technologies, Cat#05751), complemented with human recombinant epidermal growth factor (hrEGF) (20ng/mL: STEMCELL Technologies, Cat#78006), basic fibroblast growth factor (bFGF) (10ng/mL; STEMCELL Technologies Cat#78006), heparin (2 mg/mL 0.2% Heparin Sodium Salt in PBS; STEMCELL technologies, Cat#07980), antibiotic-antimycotic (1X; Wisent, Cat# 450-115-EL). GBM BTICs were plated on ultra-low attachment plates (Corning, Cat#431110), cultured as neurospheres and propagated by minimally-culturing (< 20 passages) human GBM samples and plating them on polyornithine-laminin coated plates for adherent growth. After enough expansion, adherent cells were replated in low-binding plates and cultured as tumorspheres. These cells were maintained as spheres upon serial passaging *in vitro* and retained their self-renewal potential and were capable of *in vivo* tumor formation.

Cloning of OAS2 KO lentivectors and Generation of lentiviruses

Guide RNAs (gRNAs) targeting AAVS1 (5'-GGGGCCACTAGGGACAGGAT-3') and OAS2 (A: 5'-TATGGCCACTCCCTGCACCA-3', B: 5'- AGGGCATACGGAGACAGCGA-3', C: 5'- ACTGGCATTTGTCTTATCCA-3') were obtained from TKOv3 [313] and cloned into a single-gRNA lentiCRISPRv2 construct (Addgene 52961). Sequences were verified using Sanger sequencing and each construct was packaged independently into lentivirus using second-generation packaging constructs. Briefly, sixteen hours prior to transfection, HEK293T cells were seeded into tissue-culture

treated T75 cm^2 flasks at a density of 10 million cells per flask using high-glucose DMEM with 2 mM L-glutamine and 1 mM sodium pyruvate (ThermoFisher, Cat#: 11995065), supplemented with 1% non-essential amino acid solution (ThermoFisher, Cat#: 11140050) and 10% fetal bovine serum (Gibco, Cat#: 12483020). The following day, the HEK293T media was replaced with viral harvesting media which is HEK culture media that is supplemented with 10 mM HEPES (ThermoFisher, Cat#: 15630080) and 1 mM sodium butyrate (Sigma-Aldrich, Cat#: 303410). Next, 15 µg of transfer plasmid (lentiCRISPRv2, AAVS1, OAS2-Knockout (KO) 1/A, OAS2-KO2/B and OAS2-KO3/C), 7.2 µg of psPAX2 (Addgene), and 4.8 µg of pMD2.G (Addgene) were mixed with polyethylenimin (PEI; Sigma-Aldrich, Cat#: 408719) at a 1:3 ratio (m:v) in 1.3 mL of Opti-MEM. After complexing for 15 minutes at room temperature, the PEI/DNA mixture was transferred to the HEK293T-containing flasks in dropwise fashion. Viral supernatants were collected 24 and 48 hours after transfection and then concentrated using ultracentrifugation (25,000 RPM for 2 hours at 4 °C) before being snap frozen and stored at -80 °C.

Lentiviral transduction of GBM cells

One million tumor cells (BT972 or BT241 or BT618) were plated in cell-repellent dishes (Greiner Bio, Cat#662970) and infected with lentivirus containing single-gRNA lentiCRISPRv2 constructs targeting AAVS1 or OAS2 (three gRNAs). Twenty-four hours post-infection, virus-containing media was replaced with fresh NCC media containing puromycin (1-2 µg/mL) (ThermoFisher, Cat#A1113803) for 48-72 hours.

Cell proliferation assay

Upon confirmation of OAS2 knockout by Western blotting analysis, OAS2 KO and AAVS1 transduced cells were dissociated, and 1,000 single cells were plated in 180 μL NCC per well in pentaplicate in a 96-well plate (Greiner Bio, Cat#655970) and incubated for three days. 20 μLs of Presto Blue (ThermoFisher, Cat#A13262), a fluorescent cell viability (metabolism) indicator, was added to each well two hours prior to the readout time point. FLUOstar Omega Fluorescence 556 Microplate reader (BMG LABTECH) was used to measure the fluorescence signal at excitation and emission wavelengths of 544 nm and 590 nm, respectively. Readings were analyzed using Omega analysis software.

Secondary sphere formation assay

After confirming OAS2 knockout by western blotting, tumorspheres were dissociated using enzymatic digestion solution containing 10 μL Liberase Blendzyme3 (0.2 Wunsch unit/mL) plus 10 μL of DNase in 1 mL PBS for 5 minutes at 37°C. Single cell GBM BTICs were plated at 200 cells per well in 200 μL of NCC media in a 96-well plate (Greiner Bio, Cat#655970). Cultures were left untouched at 37°C, 5% CO2. The number of secondary spheres per well was counted everyday from day three to seven and used to estimate the mean number of spheres per 2,000 cells.

Immunohistochemistry (IHC)

OAS2, CD3 and CD163 IHC was performed on TMA consisting of patient's GBM samples on the Leica Bond RX (Leica Biosystems). Antigen retrieval was performed in Epitope Retrieval Buffer (ER2) (Leica, Cat#AR9640-Leica) for 20 minutes at 100°C. Antibodies

were diluted in Powervision IHC Super Blocker (Leica, Cat#PV6122) and stained for 15 minutes as follows: rabbit monoclonal CD3 1:150 (abcam, Cat#ab16669), rabbit monoclonal CD163 1:1000 (abcam, Cat#182422) and mouse monoclonal OAS2 1:800 (Origene, Cat#CF802824). For the mouse antibodies, a post primary antibody contained in the detection kit was applied before a polymer/HRP reagent. For rabbit antibodies, only the polymer reagent was applied. Both the post primary and polymer reagents were incubated for 8 minutes each. Slides were treated to a peroxidase block, developed with DAB and counterstained with hematoxylin all contained in the Leica Bond Polymer Refine Detection Kit (Leica, Cat#DS9800). Slides were then coverslipped with Permount. The digitization of the immunohistochemically stained TMA histology slides was performed using the Olympus® VS120 Slide Scanner. The cellular data was acquired through the HALO® Image Analysis Platform by Indica Labs. The quantitative tissue analysis was performed using HALO® Multiplex IHC module in combination with HALO® TMA module. This technology allowed us to detect and quantify the total number of OAS2+, CD3+ and CD163+ cells present in each tissue core of the TMA as well as the percentage of those cells that contain sufficient chromogenic IHC stain to be considered positive for the protein of interest.

Western blotting

Total protein was isolated from GBM BTICs and brain normal cells (Neural Stem Cells and Normal Human Astrocytes) with 1X RIPA buffer. Denatured proteins resolved on a 4–15% Mini-PROTEAN® TGX Stain-Free™ precast polyacrylamide gel, 1.5 mm, 10-well (Bio-Rad Cat#4568084) using 10x Tris/Glycine/SDS running buffer (Bio-Rad,

Cat#1610732). Thereafter, resolved proteins were transferred onto polyvinylidene difluoride (PVDF) membranes, and membranes blocked in ODYSSEY buffer (LI-COR, Cat# 927-60001) diluted in TBS (1:1) for 30 minutes at room temperature. Following blocking, the membranes were incubated with primary antibodies (1:300 Mouse anti human monoclonal OAS2, [Origene, Cat#CF802824]) or GAPDH (1:2000 Mouse anti human monoclonal antibody, [abcam, Cat#ab8245]) as a loading control at 4°C overnight. Following primary antibody overnight incubation, membranes were thoroughly washed in 1X TBS-T for 3 x 5 minutes before subsequent incubation with HRP-conjugated secondary antibody (Goat Anti-Mouse IgG (H + L)-HRP Conjugate [Bio-Rad, Cat#1706516]) for one hour at room temperature. Band visualization was performed using Clarity™ Western ECL Substrate, (Bio-Rad, Cat#1705060). Data acquisition and protein detection was done using Chemidoc. Immunoblots were quantified and normalized to the loading control using ImageJ (1.52K) software.

In vivo experiments: intracranial injections, histological analysis for tumor size measurement and survival studies

All animal studies were conducted according to McMaster University Animal Research Ethics Board approved protocols. Intracranial transplantation of GBM BTICs was performed as previously described [286]. 100,000 BT972 AAVS1 or 100,000 BT972 OAS2 KO cells were injected into the right frontal lobes of 6- to 8-week old immunocompromised NSG mice. Briefly, mice were anaesthetized using Isoflurane gas (5% induction, 2.5% maintenance). A 1.5 cm vertical midline incision was made on top of the skull using a 15-blade scalpel and a small burr hole was then generated 2-3 mm anterior

to the coronal suture, 3 mm lateral to midline by a drill held perpendicular to the skull. Tumor cells which were suspended in 10 μL PBS, were injected into the frontal lobe using Hamilton syringe (Hamilton, Cat#7635-01) while it was inserted through the burr hole to a 5 mm depth. The incision was closed using interrupted stitches and sutures (Ethicon, Cat#J493G) and were sealed with a tissue adhesive (3M Vetabond, Cat#70200742529). The tumor formation and progression were tracked by MRI imaging. All mice were sacrificed at endpoint, brains were collected, formalin-fixed, and paraffin-embedded for H&E staining to assess the tumor burden. Images were captured using an Aperio Slide Scanner and analyzed using ImageScope v11.1.2.760 (Aperio) and imageJ (1.52K) software. The number of days of survival were also recorded for survival analysis.

Statistical Analyses

All experiments were performed in duplicates or triplicates. Applicable data were analyzed and represented using GraphPad Prism 6 software or within the R statistical environment (v3.6.0). Data are presented as means ± S.E.M. Unpaired Student's t-tests were used for statistical analysis of two groups and one-way analysis of variance with Tukey/Newman–Keuls test was used for statistical analysis of more than two groups with a p-value < 0.05 deemed as statistically significant. Visualization in R was performed using the BoutrosLab Plotting General package [314]; (v6.0.2) and ggplot2 (3.2.1).

Data availability

All mass spectrometry raw data has been deposited to the Mass Spectrometry Interactive Virtual Environment (MassIVE) with the following MassiVE ID: MSV000087947 and

FTP link: ftp://massive.ucsd.edu/MSV000087947/. Data will be made public after acceptance of the manuscript.

Results

Primary and Recurrent GBM have distinct transcriptomic and protein landscapes

To identify potential neoplastic drivers generated throughout the course of therapy, we assembled a cohort of 143 GBMs: 45 pGBM-rGBM matched pairs, 9 unmatched pGBM, 24 unmatched rGBM, and 20 normal adjacent tissue (NAT) specimens. FFPE punches were collected for proteomic and NanoString mRNA analysis from these 143 samples. In addition, three cores from each block were used to construct a tissue microarray (TMA). Detailed clinico-pathological information was collected for each patient (**Figure 1A**; **Table 1**).

Proteomic profiling was performed on 134 of these 143 specimens using an optimized and validated mass spectrometry workflow [315] (**Figure 1A**). Proteomic profiling was performed on 134 of these 143 specimens using previously established mass spectrometry workflow[27] (**Figure 1A**). Using label free quantification, 6,977 distinct protein groups were detected, of which 2,515 were identified in at least 95% of samples (**Figure 1B**, **Supplementary Figure 1A**). The well-known drivers IDH1, EGFR and PTPN11 were detected in all samples (**Figure 1B**). The proteomic landscape of our pGBM samples (n = 51) were well-correlated to the pGBM transcriptome landscape in TCGA (n = 166; ρ = 0.58, $P < 2.2 \times 10^{-16}$; **Supplementary Figure 1B**). There was a similar correlation between the mean rGBM protein abundance and mean pGBM RNA abundance ($\rho = 0.56$, $P < 2.2 \times 10^{-16}$; **Supplementary Figure 1C**) (n = 28). To identify the proteomic subtypes of GBM across disease states, we performed consensus clustering on 40 matched pGBM-rGBM pairs (n = 84) using 1,595 proteins detected in all matched pairs. We identified five sample

subtypes, which we term S1 through S5 and five protein subtypes, which we termed P1 through P5 (**Figure 1C**). Proteomic subtypes differed by age at treatment (P = 0.02; one-way ANOVA), with the median in P5 (63.6 years) being older and P1 or P2 being the youngest (54.9 years). Subtypes were independent of sex (P = 0.21), and tumor classification (primary *vs*. recurrence; P = 0.21; Pearson's X^2 Test). Matched pGBM-rGBM tumors were not preferentially classified in the same subtype; subtype concordance was 27.5% (11/40; **Figure 1D**), reflecting wide-spread rewiring of signaling pathways during the response to therapy. pGBM tumors assigned in the P2 subtype usually reclassified to the P1 subtype at recurrence (83%; 5/6). The P1 subtype was enriched in leucocyte related immune pathways, P2 in transmembrane transport and ion transport, P3 in mRNA metabolic processing and RNA splicing, P4 in immune related pathways such as complement activation, humoral immune response and adaptive immunity and P5 subtype in protein conjugation, cell cycle and metabolic processes.

To validate the subtypes, we created a centroid-based single-sample subtype-classifier. This classifier was used to subtype a set of 99 publicly available pGBM proteomes (**Supplementary Figure 1D**). P1 and P3 were present in similar proportions between the two datasets, while a higher proportion of samples were classified as P2 in the current (HHS) dataset and a higher proportion of samples were classified as P4 and P5 in the CPTAC dataset (**Supplementary Figure 1E**; P = 1.27 x 10-3; Pearson's X^2 test). Although these two proteomics datasets were created using different technologies (TMT *vs*. LC-MS/MS) the same subtypes are visible suggesting true biological patterns.

To quantify the relationship of proteomics subtypes with transcriptomic ones, we defined RNA subtypes for 22 paired pGBM and rGBM samples (**Supplementary Figure 1F**). As in the proteome, it was common for rGBM to transition to different transcriptional subtypes than their pGBM counterparts (13/22 paired samples; **Figure 1E**). Transcriptomic and proteomic subtypes were associated with one another ($P = 0.03$; Pearson's X^2 test). For example, 10/14 tumors with the proneural/neural transcriptomic signature were classified as the proteomic subtype P3, while tumors with the mesenchymal transcriptomic subtype were preferentially classified into the P1, P2 and P4 proteomic subtypes (**Supplementary Figure 1G**).

pGBM patients were split into three groups based on quartiles of overall survival time (OS): short-term (1st quartile; n = 13; median = 7.9 months), intermediate-term (2nd and 3rd quartile; n = 25; median = 15.7 months) and long-term (4th quartile; n = 13; median = 23.1 months). pGBM tumors from the long-term survivor group had 32 proteins with higher abundance than in short-term survivors and 72 with lower abundance ($P < 0.05$, $|\log_2 FC| > 1$), Mann-Whitney U-test; **Figure 2A**). No hits survived FDR adjustment for multiple hypothesis testing, reflecting the limited statistical power of this cohort. Gene Set Enrichment Analysis (GSEA) was performed using the hallmark gene sets [314], and identified various pathways upregulated in the short-term survivors including hypoxia, PI3k AKT MTOR pathways and immune regulatory pathways such as IL6_JAK_STAT3 and Interferon alpha pathway (**Figure 2B**).

Next, we identified proteins whose abundance was associated with OS by fitting Cox proportional hazards models using pGBM proteomics abundance per protein. One protein

was significantly associated with overall survival after multiple testing correction, GK2 (Glycerol Kinase 2) which plays a critical role in regulation of glycerol uptake and metabolism (Q = 0.10, hazard ratio = 2.6; Cox Proportional Hazards model; **Figure 2C**). Overall survival time does not capture quality-of-life, which in GBM can be critically influenced by impaired neurological status. We therefore also split patients into quantiles based on the quartiles of relapse-free survival time (RFS) and performed similar statistical analyses. We identified 43 proteins preferentially abundant in tumors with long times to relapse and 346 preferentially abundant in tumors with short times to relapse ($P < 0.05$, $\log_2FC > 2$, Mann-Whitney U-test).

Adjacent normal tissue has distinct proteome compared to pGBM

A recent study in 99 pGBM tumors included proteomics from 10 normal samples from the reference GTEx dataset [316]. While the methods used to quantify proteins differed between both studies, there was a high overlap in the proteins observed (**Supplementary Figure 2A**). Comparison of the proteomics profile between NAT (n = 17) and pGBM samples identified 1,065 proteins that were significantly differentially abundant ($Q < 0.05$, $|\log_2FC| > 2$; **Figure 3A**). GSEA revealed that neuron activity related pathways were upregulated in NAT, whereas mRNA processing, DNA repair and immune related pathways were enriched in pGBM (**Figure 3B**). A similar analysis in the CPTAC cohort, comparing normal brain tissue and pGBM samples, showed similar effect sizes in the overlapping detected proteins ($\rho = 0.79$, $P < 2.2 \times 10^{-16}$; **Supplementary Figure 2B**).

Proteomic profiling of pGBM and rGBM matched samples revealed rGBM is associated with immunosuppression

Next, we asked what signaling pathways were changed during the evolutionary response of pGBMs to the selective pressure of treatment. We performed differential abundance analysis with 40 pGBM-rGBM matched pairs and identified 132 proteins significantly differing ($Q < 0.1$, $|\log_2 FC| > 1$, Mann-Whitney U-test; **Figure 3C**). The rGBM proteome was enriched in proteins associated with interferon alpha and gamma (broad inflammatory response), epithelial to mesenchymal transition, TNF-a signaling, fatty acid metabolism, hypoxia and oxidative phosphorylation pathways to be mainly upregulated in the rGBM proteome (**Figure 3D**).

To identify the top potentially targetable hits enriched at in rGBM, we prioritized these 132 candidates based on magnitude of differential abundance, low abundance in normal tissue (*in silico* validation and proteomic analysis of brain normal cells including Normal Human Astrocytes [NHAs] and Neural Stem Cells [NSCs]), a known role in immunosuppression. This resulted in identification of 2-5-oligoadenylate synthase 2 (*OAS2*) as the top candidate. *OAS2* plays a crucial role in regulating immunosuppression and has been previously implicated in rGBM [317, 318] (**Supplementary Figure 3A)**. In addition, Periostin (POSTN), previously described in literature [164] as a tumor associated macrophage (TAM) marker, was also enriched in the rGBM cohort, further validating the upregulation of immune related proteins in rGBMs.

To further characterize OAS2 across a broader cohort of GBM patients, we assessed its abundance in pGBM-rGBM intact tissues. We observed a significant upregulation in OAS2 expression on tumor-intact tissues, particularly on endothelial cells and foamy macrophages, as assessed by immunohistochemical analysis on 45 pGBM-rGBM matched

and, 9 pGBM and 24 rGBM unmatched tissues (**Figure 4A, Supplementary Figure 3B)**, as well as in an independent pGBM-rGBM cohort of 20 further patient matched pairs (**Supplementary Figure 3C**). Moreover, there was a significant increase in OAS2 protein abundance in rGBM compared to pGBM in purely enriched patient-derived BTICs while no/very low levels were observed in brain normal cells (Neural Stem Cells [NSCs] and Normal Human Astrocytes [NHAs]) (**Figure 4B**). The role of OAS2 in GBM pathogenesis has not yet been investigated, although we demonstrate its expression both within rGBM cells (specifically BTICs) and in cells comprising the rGBM tumor immune microenvironment. Therefore, our next step was focused on further validating the role of OAS2 in rGBM tumorigenesis.

OAS2 is an essential driver of treatment-resistant cell populations in rGBM

To specifically investigate the effect of OAS2 on GBM BTIC stem-like properties including self-renewal and proliferative capacity, secondary sphere formation and proliferation assays were performed. Upon knocking out (KO) OAS2 in OAS2-high rGBM lines, we observed a marked reduction in clonogenicity, and proliferative capacity of OAS2 KO cells (constructs A, B and C) compared to OAS2 control cells (AAVS1) as measured by the secondary sphere formation and proliferation assays, respectively (**Figure 4C, Supplementary Figure 3D**). This indicated that OAS2 has the ability to drive stem-like properties in GBM BTICs which in turn fuels cancer progression. In a parallel study by our team, we conducted genome-wide CRISPR-Cas9 gene knockout screens on patient-derived models of recurrent GBM BTICs. These functional screens identified OAS2 as a gene essential for survival of recurrent GBM BTIC models (data not shown). To further validate

the role of OAS2 in GBM progression, the effect of OAS2 depletion on tumor progression at the *in vivo* level was tested. For this purpose, BT972 OAS2 KO and BT972 OAS2 control cells (AAVS1) were intracranially engrafted into the right frontal lobe of the mouse brain and the tumor growth was tracked using weekly MRI imaging until they reached the endpoint (**Figure 4D**). Mice engrafted with OAS2 KO BT972 had significant reduction in tumor burden as shown by histological analysis and MRI imaging (**Figure 4E**) as well as increased survival advantage (**Figure 4F**) compared to the control counterpart (engrafted mouse with BT972 AAVS1), providing another layer of confirmation for the key role of OAS2 in rGBM tumor progression.

Discussion

The field of GBM research currently lacks the quantitative proteomics needed to specifically focus on the direct comparison of primary and recurrent GBMs [315, 319]. To date, the vast majority of molecular datasets of patient GBMs comprise primary tumors. Recently, large consortia have significantly advanced the field of proteogenomics, including in brain malignancies [320-322] but focused almost exclusively on primary treatment-naïve disease. Surprisingly, while the GBM genome and transcriptome have been well elucidated in primary tumors, the GBM proteome and its relation to up-stream genomic alterations are poorly documented.

Previous studies it has been shown that tumor cells in the TME are exposed to IFNγ [323, 324] and that tumor associated-macrophages (TAMs) might be the source of IFNγ production, leading to immune evasion [325]. We identified numerous proteins related to IFNγ signalling that were increased in abundance in rGBM relative to pGBM, including OAS1, OAS2, MX1 and IFIT1. OAS2 is a member of the template-independent nucleotidyltransferase protein family and is an interferon (IFN)-induced antiviral enzyme involved in the antiviral innate immune response [326]. OAS2 has been reported as a prognostic biomarker in breast cancer [327] and causes immunosuppression in oral cancers by down regulating CD3-ζ chain expression through induction of caspase-3 activation which results in non-functional T cells. We show with *in vivo* and *in vitro* CRISPR knockouts that OAS2 is essential for GBM progression through an as-yet unknown mechanism.

Consistent with this broad proteomic change in IFNγ signalling, our data revealed a dominant immunosuppressive phenotype for rGBM, with elevated Siglec-1 (CD169) abundance occurring during tumor evolution under therapeutic pressure. CD169 is a sialic acid receptor expressed on a specific type of macrophages. In triple-negative breast cancer CD169+ macrophages support tumor growth and metastasis by causing immune escape, negatively affecting CD8+ T cell accumulation in tumors and causing the JAK2/STAT3 signaling pathway to be activated upon exposure to tumor cells [318]. TAMs with M2-like phenotype were more abundant at recurrence, as supported by CD3 and CD163 immunohistochemistry on TMAs (**Supplementary Figure 4**). These data provide another layer of confirmation for the crucial role of macrophages in GBM progression and immunosuppression which is associated with poor patient prognosis. This finding is aligned with recent studies reporting the significant role of macrophages in inducing GBM immunosuppression, seen predominantly in GBMs of the mesenchymal subtype [328].

This work describes the first proteomic landscape analysis of rGBM, which could promote the development of new, selective targeted therapies and immunotherapies. This proteomic characterization of rGBM could begin to instruct novel and rational combinatorial poly-therapeutic approaches to provide more effective and personalized treatments for therapy-resistant rGBM.

A

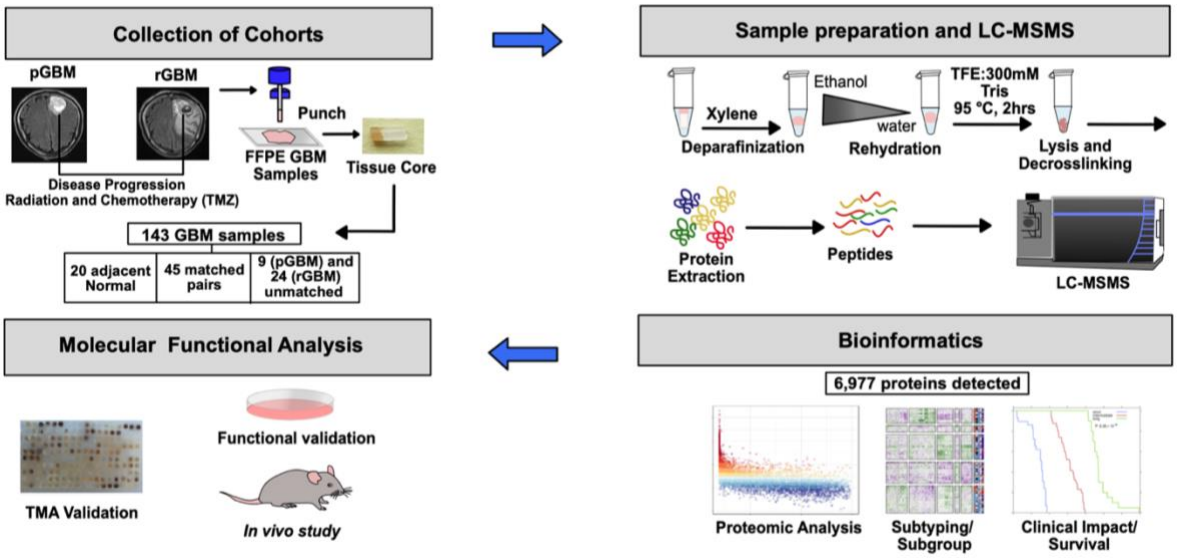
Collection of Cohorts
pGBM
rGBM
Punch
FFPE GBM Samples
Tissue Core
Disease Progression
Radiation and Chemotherapy (TMZ)
143 GBM samples
20 adjacent Normal
45 matched pairs
9 (pGBM) and 24 (rGBM) unmatched
Sample preparation and LC-MSMS
Xylene
Deparafinization
Ethanol
water
Rehydration
TFE:300mM Tris
95 °C, 2hrs
Lysis and Decrosslinking
Protein Extraction
Peptides
LC-MSMS
Molecular Functional Analysis
TMA Validation
Functional validation
In vivo study
Bioinformatics
6,977 proteins detected
Proteomic Analysis
Subtyping/ Subgroup
Clinical Impact/ Survival

B

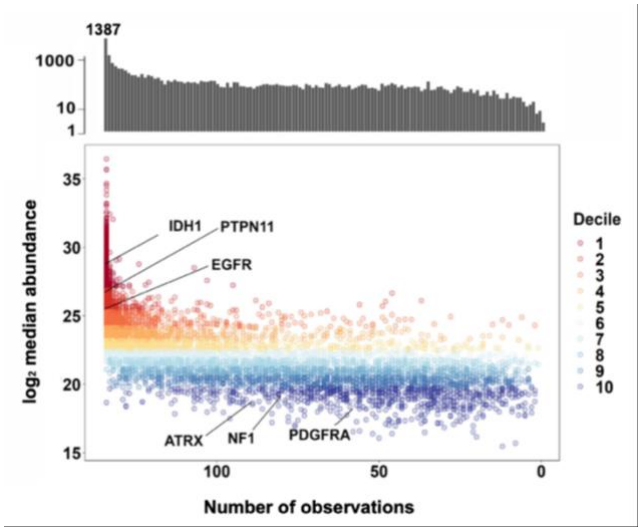
1387
1000
10
1
35
30
25
20
15
log2 median abundance
IDH1
PTPN11
EGFR
ATRX
NF1
PDGFRA
Decile
1
2
3
4
5
6
7
8
9
10
100
50
0
Number of observations

C

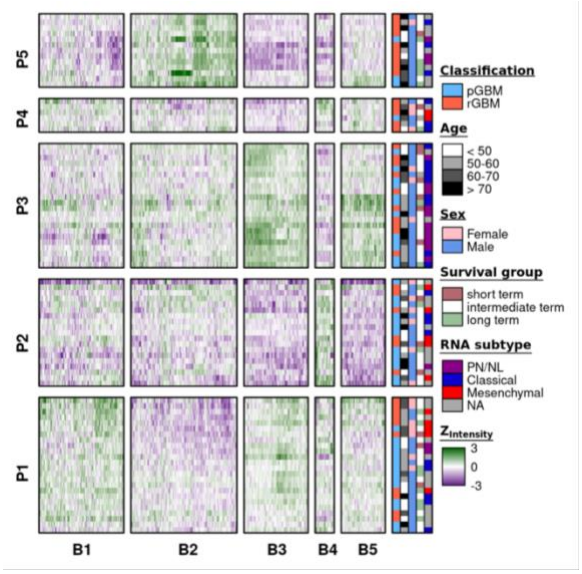
P5
P4
P3
P2
P1
B1
B2
B3
B4
B5
Classification
pGBM
rGBM
Age
< 50
50-60
60-70
> 70
Sex
Female
Male
Survival group
short term
intermediate term
long term
RNA subtype
PN/NL
Classical
Mesenchymal
NA
ZIntensity
3
0
-3

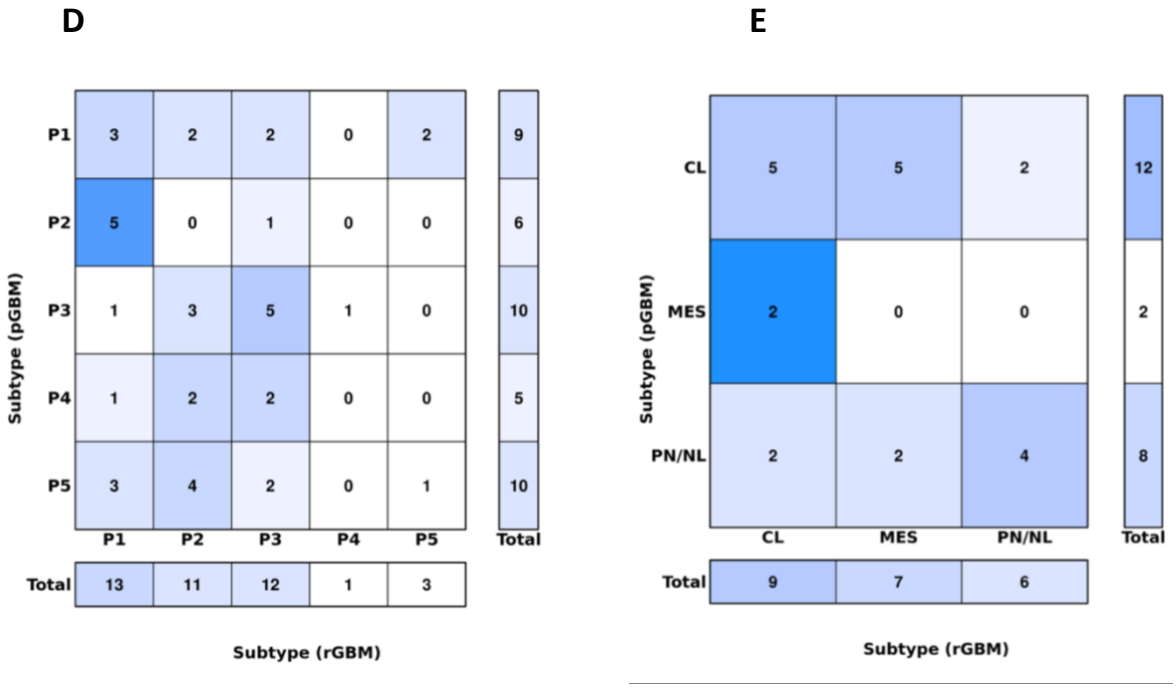

Figure 1. Primary and recurrent GBM have distinct genomic and protein landscapes. **A)** Schematic representation of sample collection and preparation, MS proteomics, target identification and functional analysis workflow. **B)** Distribution of protein quantitation measured as median intensity by the number of samples they are detected in. Bar plot on top represents the total counts of proteins quantified by the number of samples they are present in. Missing values were omitted when calculating the median. **C)** Proteomic subtypes were identified in 40 GBM matched pGBM-rGBM pairs (n = 80). Clinical covariates indicate protein subtype, tumor classification, transcriptomic subtype, patient's sex; age at treatment (years) and survival group (short-term vs. long-term) **D)** pGBM and rGBM samples from the same patient classify as different proteomic (n = 40) and **E)** transcriptomic subtypes (n = 22).

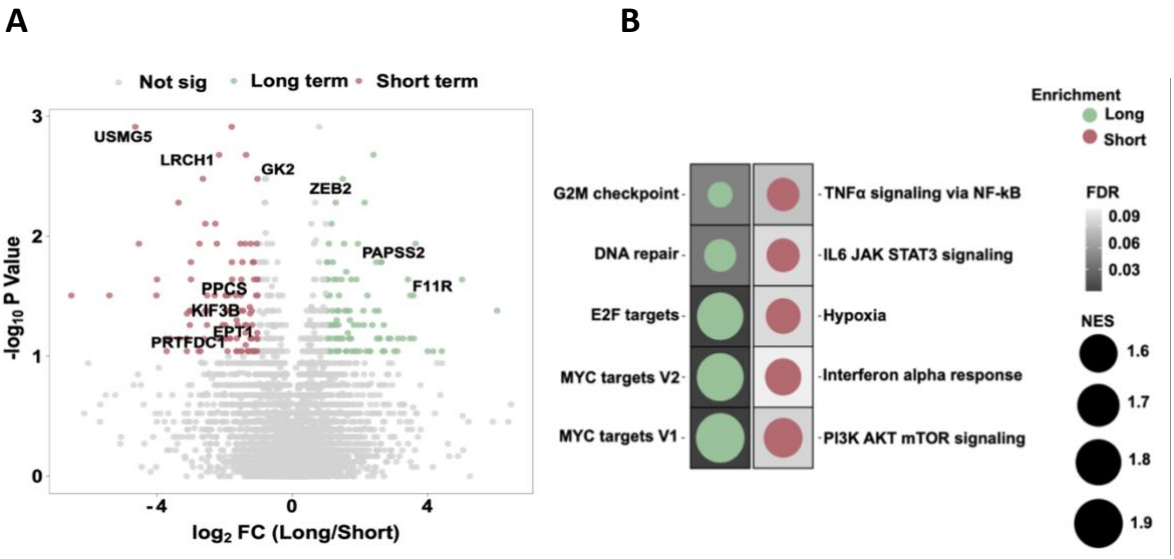
A
Not sig
Long term
Short term
USMG5
LRCH1
GK2
ZEB2
PAPSS2
F11R
PPCS
KIF3B
EPT1
PRTFDC1
-log10 P Value
log2 FC (Long/Short)
B
G2M checkpoint
DNA repair
E2F targets
MYC targets V2
MYC targets V1
TNFα signaling via NF-kB
IL6 JAK STAT3 signaling
Hypoxia
Interferon alpha response
PI3K AKT mTOR signaling
Enrichment
Long
Short
FDR
0.09
0.06
0.03
NES
1.6
1.7
1.8
1.9

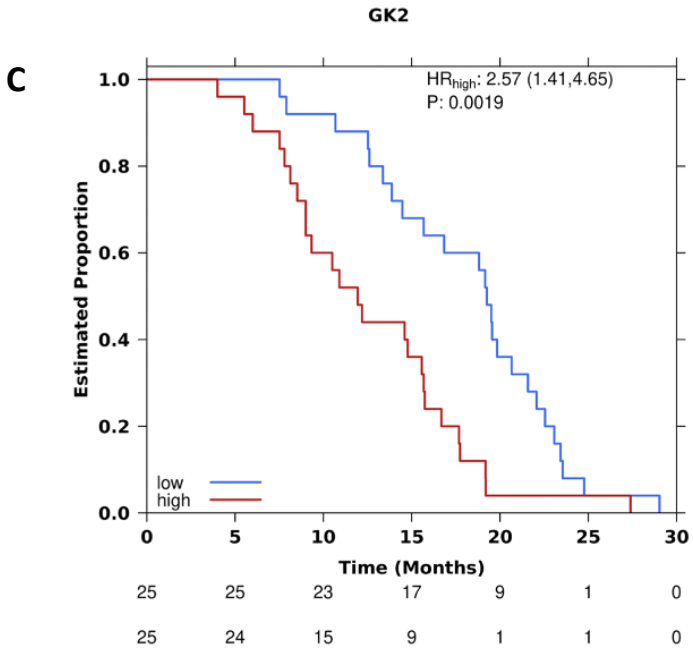
C
GK2
HRhigh: 2.57 (1.41,4.65)
P: 0.0019
Estimated Proportion
low
high
Time (Months)
25 25 23 17 9 1 0
25 24 15 9 1 1 0

Figure 2. Overall survival analysis and proteomic subtypes. A) Differentially abundant proteins between short-term and long-term survivors (**see Methods**). Red dots indicate protein abundance higher in rGBM while green dots indicate protein abundance higher in pGBM. Aquamarine dots indicate that the protein abundance is significantly different between pGBM and rGBM. **B)** Pathway enrichment analysis was performed using GSEA on the gene sets associated with short-term or long-term survival. The bar plots show normalized enrichment scores with the color gradient indicating the FDR values. **C)** Kaplan Meier curve for GK2, where primary pGBM patients were split into groups based on the median GK2 abundance.

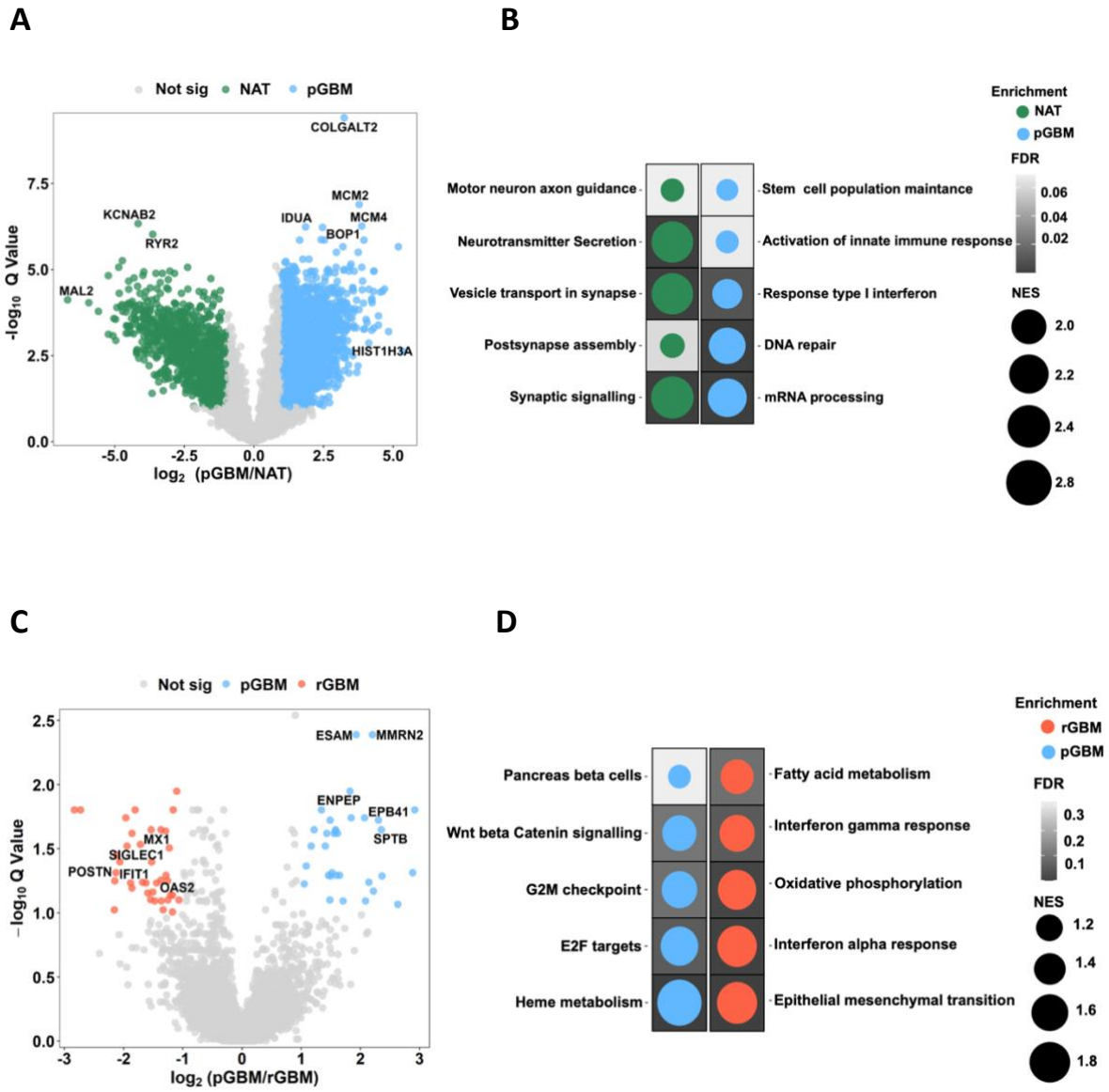

Figure 3: Differential expression analysis between NAT-pGBM and pGBM-rGBM matched pairs. A) Volcano plot displaying differential abundance analysis comparing NAT tissue and pGBM samples. **B)** GSEA analysis showing the pathways upregulated in the NAT and pGBM pairs. The bar plots show normalized enrichment scores with the color

gradient indicating the FDR values. **C)** Volcano plot depicting differential abundance analysis between pGBM and rGBM in matched sample pairs. Proteins significantly enriched in rGBM patients are indicated in red, while proteins enriched in pGBM are indicated in blue (Q value < 0.1; $\log_2$ fold change > 1). **D)** Gene set enrichment analysis (GSEA) showing the top significantly enriched pathways in pGBM *vs*. rGBM. The dot plot shows the normalized enrichment scores (NES) with the background color gradient representing the Q values.

A

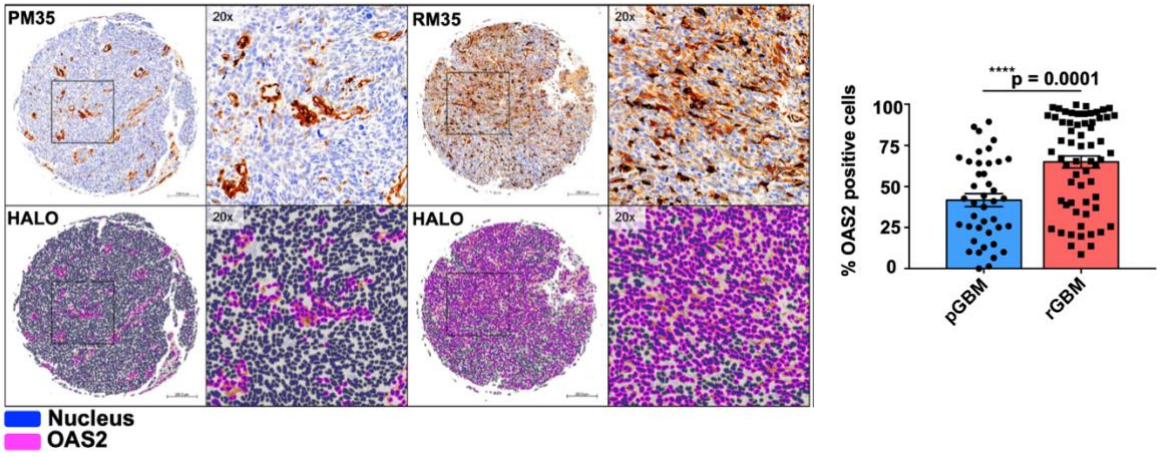
PM35
20x
RM35
20x
HALO
20x
HALO
20x
Nucleus
OAS2
% OAS2 positive cells
p = 0.0001
pGBM
rGBM

B

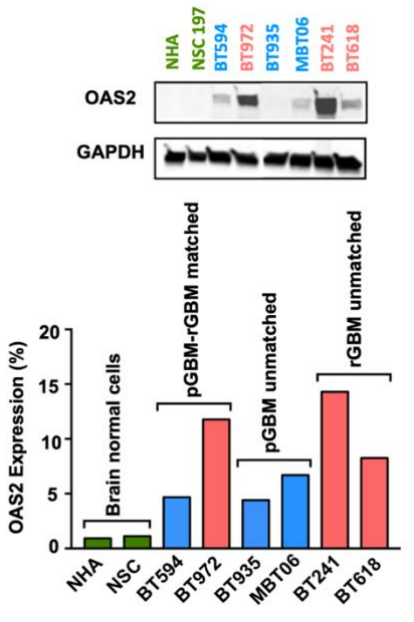
NHA
NSC 197
BT594
BT972
BT935
MBT06
BT241
BT618
OAS2
GAPDH
OAS2 Expression (%)
Brain normal cells
pGBM-rGBM matched
pGBM unmatched
rGBM unmatched
NHA
NSC
BT594
BT972
BT935
MBT06
BT241
BT618

C

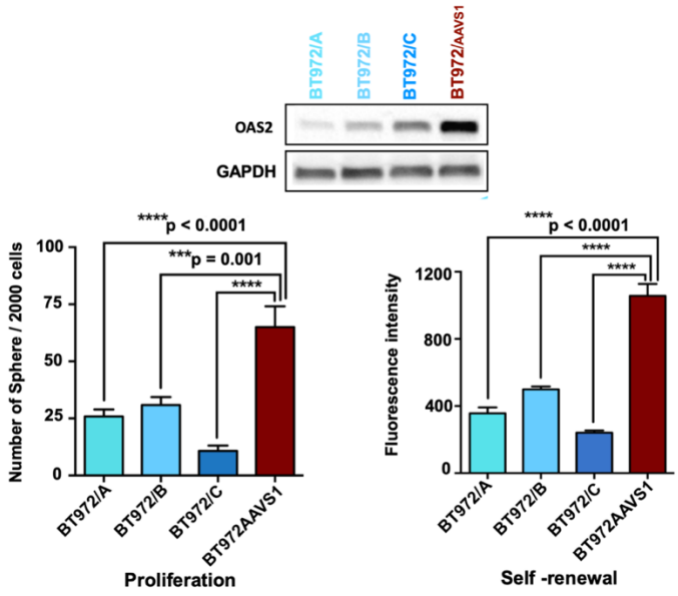
BT972/A
BT972/B
BT972/C
BT972/AAVS1
OAS2
GAPDH
p < 0.0001
p = 0.001
Number of Sphere / 2000 cells
Proliferation
p < 0.0001
Fluorescence intensity
Self -renewal

D

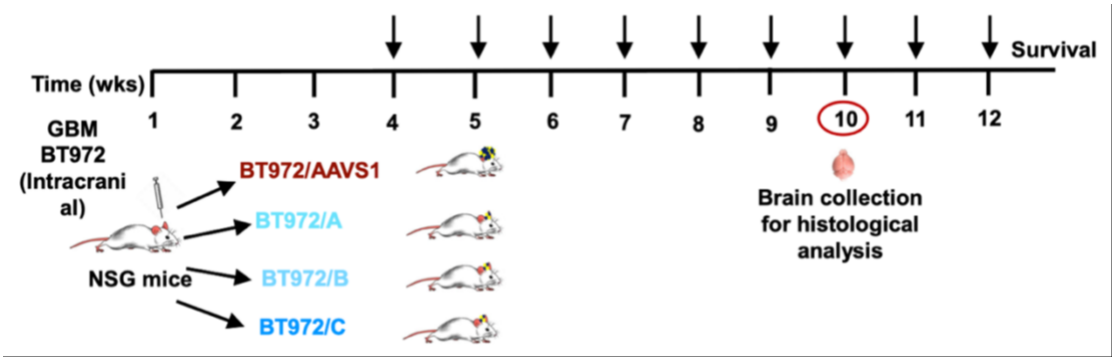
Time (wks)
1
2
3
4
5
6
7
8
9
10
11
12
Survival
GBM
BT972
(Intracrani
al)
NSG mice
BT972/AAVS1
BT972/A
BT972/B
BT972/C
Brain collection
for histological
analysis

E

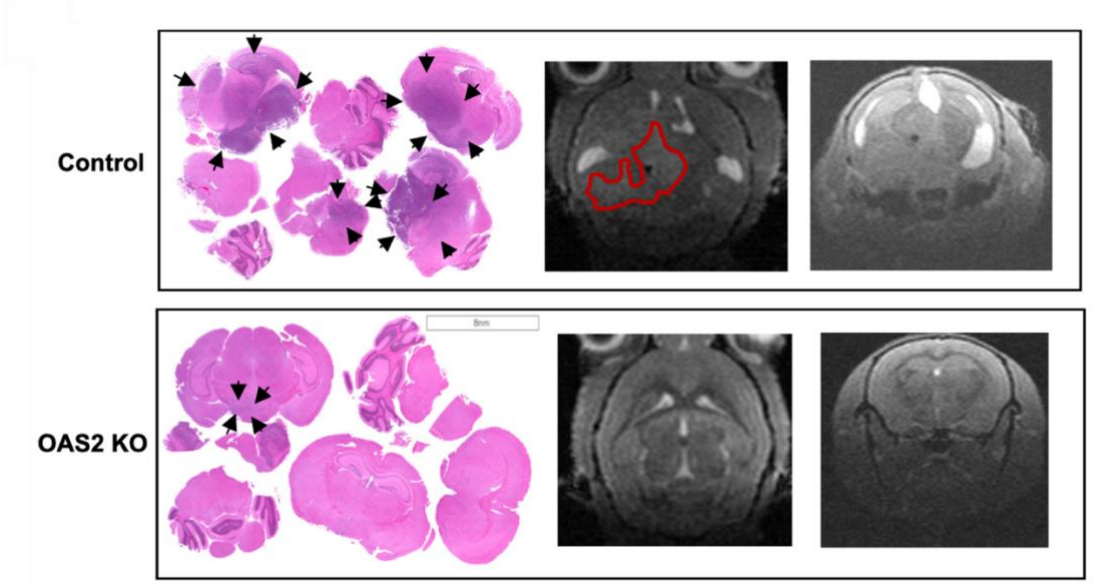
Control
OAS2 KO

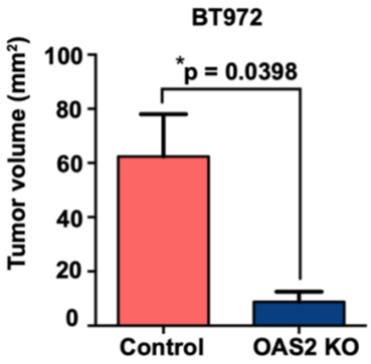
BT972
*p = 0.0398
Tumor volume (mm²)
100
80
60
40
20
0
Control
OAS2 KO

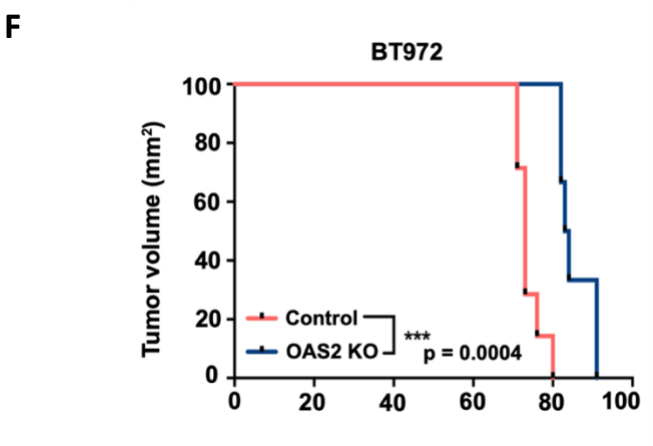

Figure 4: OAS2, an essential gene for rGBM, has significant upregulation at the recurrent stage. A) Immunohistochemical analysis of OAS2 on TMA consisting of both matched and unmatched pGBM-rGBM samples indicated a significantly higher level of OAS2 at the recurrent stage. (The representative image shows pGBM (PM35)-rGBM (RM35) matched samples) (Scale bar: 200 um, P value: *** 0.0002, **** < 0.0001). **B**) Western blotting analysis on the protein lysate of GBM BTIC (pGBM-rGBM matched and unmatched samples) confirmed two-fold increase in OAS2 expression. **C)** BT972, an OAS2 high expressing recurrent GBM BTIC line, was used for functional analysis. OAS2 was knocked out using CRISPR knockout gene editing. Following confirmation of gene knockout (construct A, B and C) by western blotting, the effect of OAS2 on self-renewal and proliferation capacity of OAS2 KO BT972 vs OAS2 WT BT972 (BT972 AAVS1) were measured using secondary sphere formation assay and PrestoBlue proliferation assay, respectively (P value: *** $p < 0.001$, **** $p < 0.0001$) (One way ANOVA). **D)** OAS2 KO BT972 and BT972 control (BT972 AAVS1) (100,000) were intracranially implanted into the right frontal lobe of NSG mice (n=6). The tumor size was tracked weekly using MRI

imaging. **E)** OAS2 KO engrafted mice showed significantly higher tumor burden (P value: * < 0.0398) (mean±SEM, one-tailed t-test) and **F)** consequently lower survival advantage (P value: ***=0.0004) (Log-rank Mantel-Cox Test) compared to control cohort (BT972 AAVS1) engrafted mice.

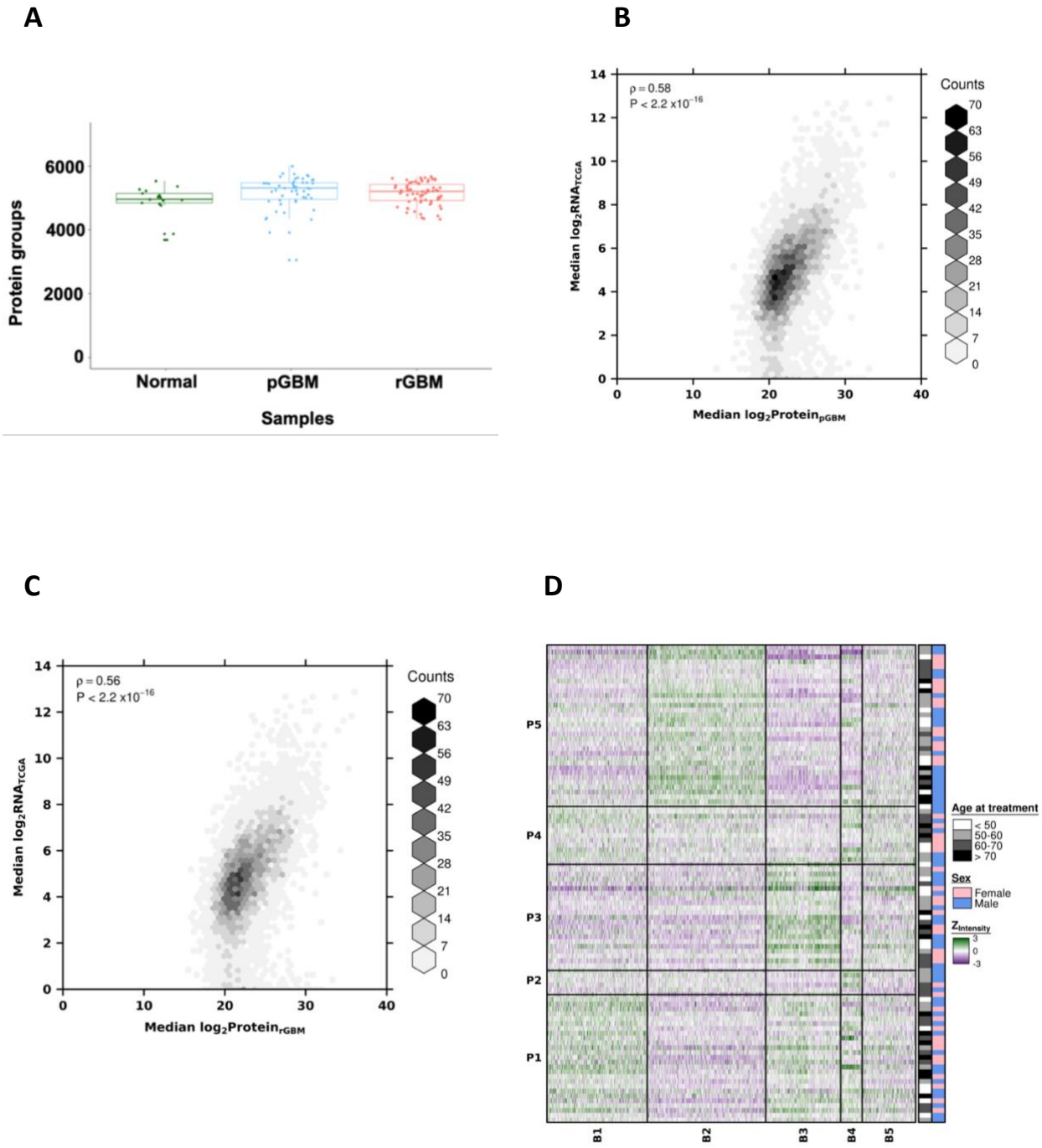
A
Protein groups
6000
4000
2000
0
Normal
pGBM
rGBM
Samples
B
ρ = 0.58
P < 2.2 x10^-16
Median log2RNATCGA
Median log2ProteinpGBM
Counts
70
63
56
49
42
35
28
21
14
7
0
C
ρ = 0.56
P < 2.2 x10^-16
Median log2RNATCGA
Median log2ProteinrGBM
Counts
D
P5
P4
P3
P2
P1
B1
B2
B3
B4
B5
Age at treatment
< 50
50-60
60-70
> 70
Sex
Female
Male
ZIntensity
3
0
-3

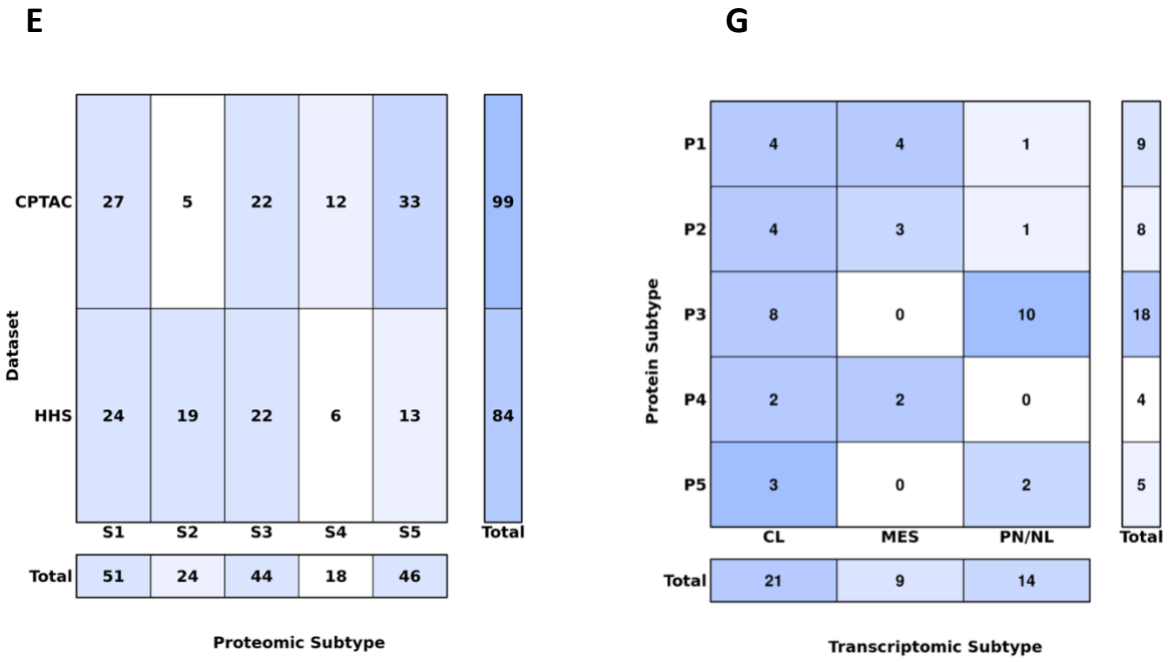
E
CPTAC
HHS
Dataset
27
5
22
12
33
99
24
19
22
6
13
84
S1
S2
S3
S4
S5
Total
Total
51
24
44
18
46
Proteomic Subtype
G
P1
P2
P3
P4
P5
Protein Subtype
4
4
1
9
4
3
1
8
8
0
10
18
2
2
0
4
3
0
2
5
CL
MES
PN/NL
Total
Total
21
9
14
Transcriptomic Subtype

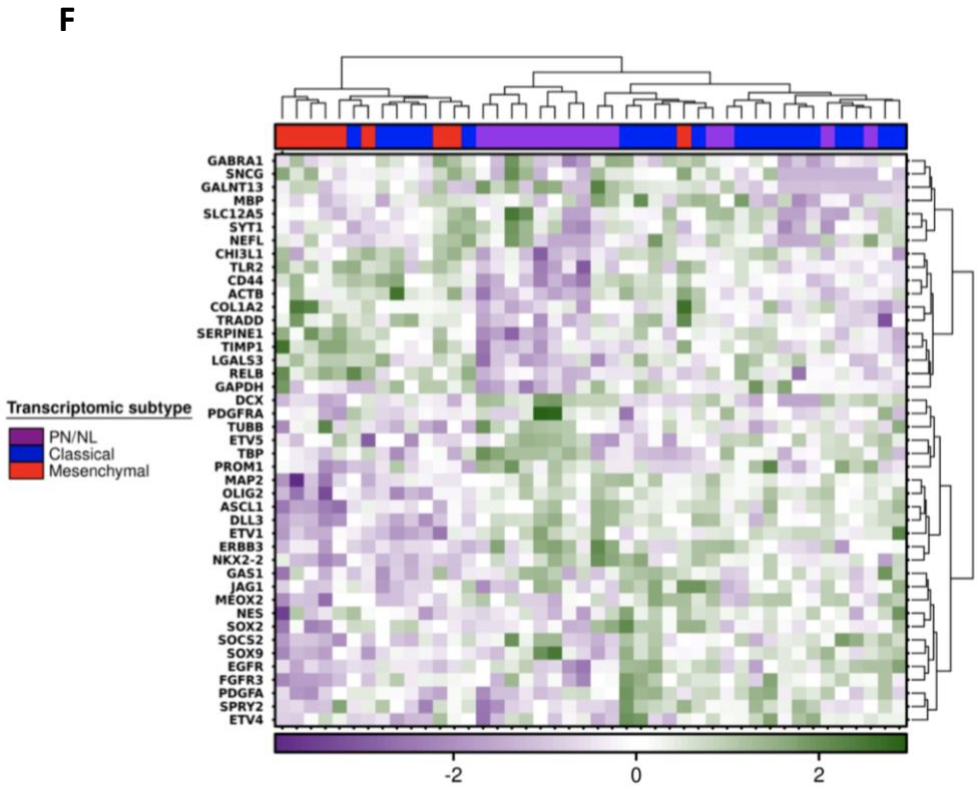
F
Transcriptomic subtype
PN/NL
Classical
Mesenchymal
GABRA1
SNCG
GALNT13
MBP
SLC12A5
SYT1
NEFL
CHI3L1
TLR2
CD44
ACTB
COL1A2
TRADD
SERPINE1
TIMP1
LGALS3
RELB
GAPDH
DCX
PDGFRA
TUBB
ETV5
TBP
PROM1
MAP2
OLIG2
ASCL1
DLL3
ETV1
ERBB3
NKX2-2
GAS1
JAG1
MEOX2
NES
SOX2
SOCS2
SOX9
EGFR
FGFR3
PDGFA
SPRY2
ETV4
-2
0
2

Supplementary Figure 1. Protein identification and comparison of genomic and proteomic subtypes. A) Boxplot showing the number of proteins quantified in each group. **B)** Comparison of the median gene abundance in RNA from primary TCGA samples (n = 166) and the median protein abundance of pGBM (n = 51) and **C)** rGBM (n = 51) in 6,395 matching gene-protein pairs. **D)** Protein subtype classification of CPTAC pGBM samples, using the same proteins in **Figure 1C**. **E)** Comparison of the proportion of samples classified in each proteomic subtype. **F)** NanoString profiles were created in 22 matched pGBM-rGBM tumor pairs to assign transcriptomic subtypes. **G)** Comparison of transcriptomic and proteomic subtypes in matched pGBM-rGBM tumor pairs.

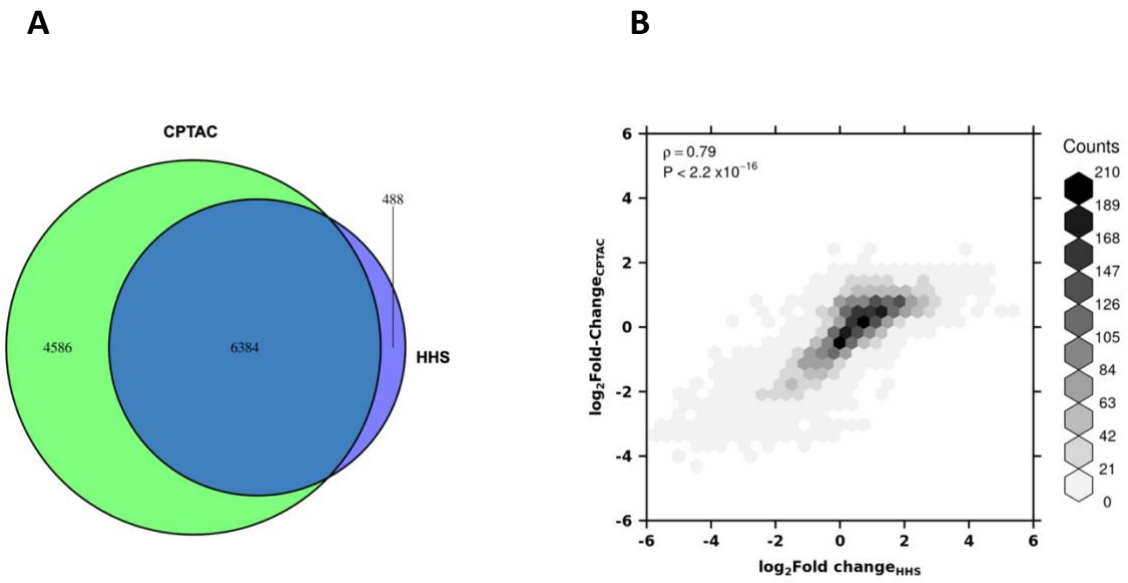

Supplementary Figure 2. Comparison of normal and pGBM samples. **A)** Overlap of proteins identified in CPTAC study and the current study (HHS). **B)** Correlation of the effect sizes from comparisons of adjacent normal (NAT) and pGBM samples in the CPTAC study and the current study (HHS).

A

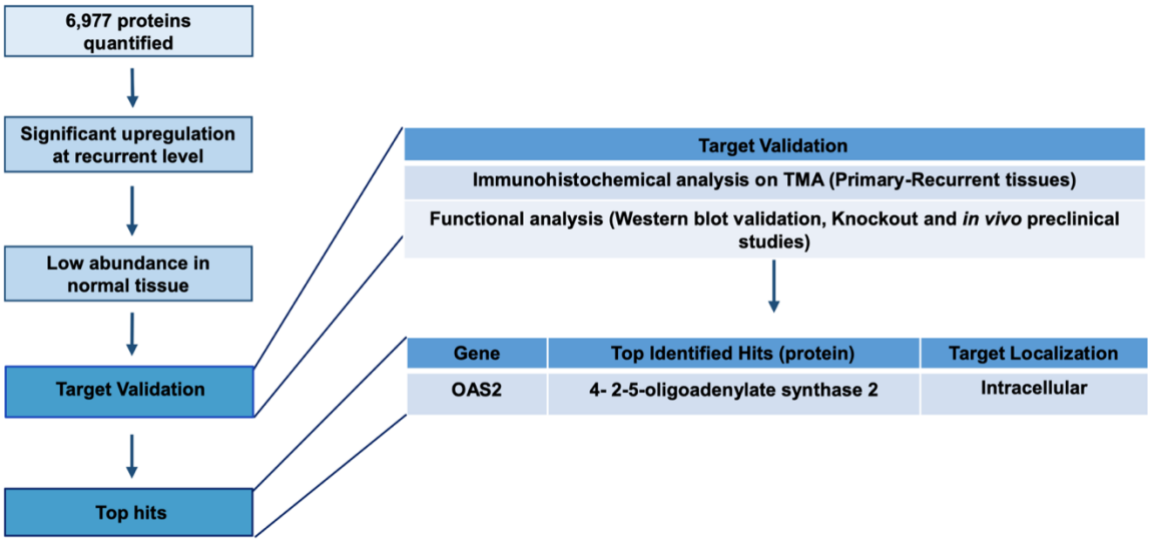
6,977 proteins quantified
Significant upregulation at recurrent level
Low abundance in normal tissue
Target Validation
Top hits
Target Validation
Immunohistochemical analysis on TMA (Primary-Recurrent tissues)
Functional analysis (Western blot validation, Knockout and in vivo preclinical studies)
Gene
Top Identified Hits (protein)
Target Localization
OAS2
4- 2-5-oligoadenylate synthase 2
Intracellular

B

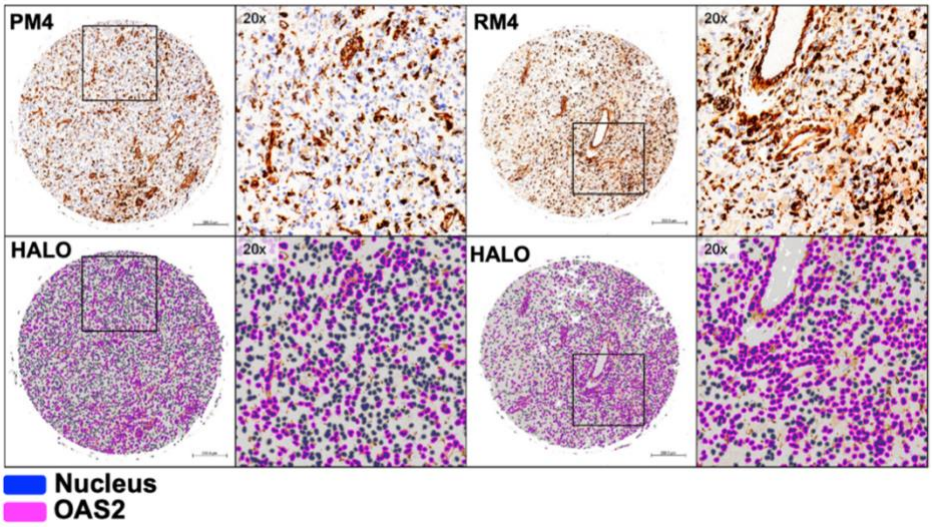
PM4
20x
RM4
20x
HALO
20x
HALO
20x
Nucleus
OAS2

C

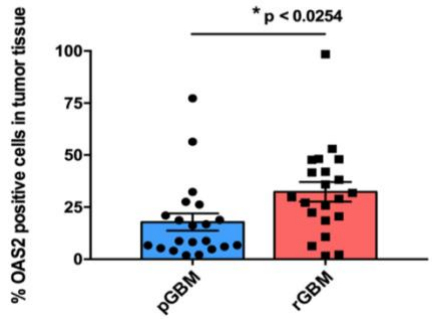
* p < 0.0254
% OAS2 positive cells in tumor tissue
100
75
50
25
0
pGBM
rGBM

D

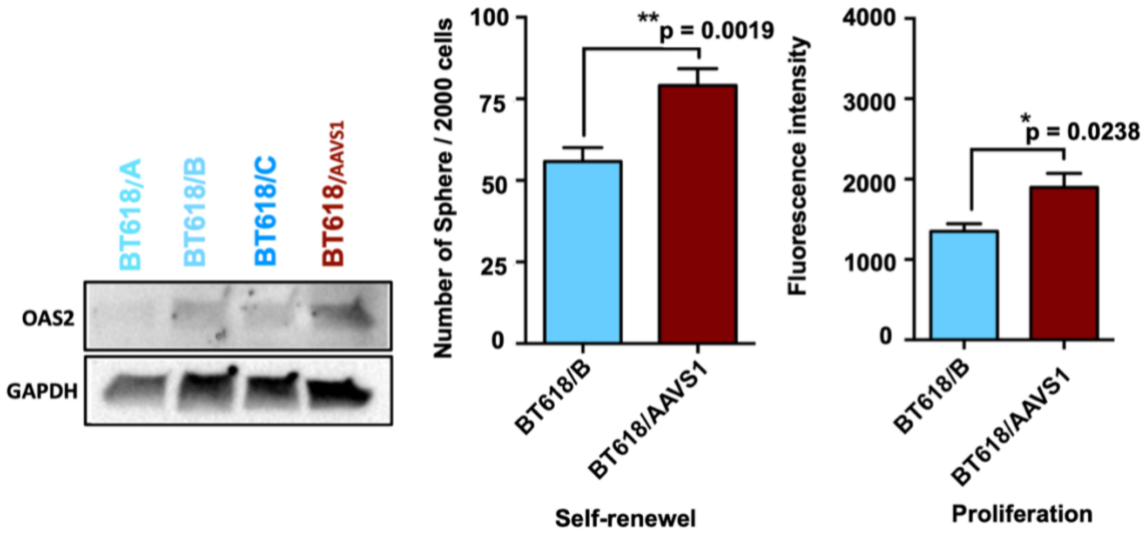

Supplementary Figure 3. Selection and validation of top hits. A) Defined criteria for mining the 6,977 detected proteins for identification of targets for validation. Candidates were validated by immunohistochemical analysis on TMA and functional studies including western blot analysis on primary-recurrent brain tumor initiating cell lines (BTICs), CRISPR KO validation and *in vivo* preclinical studies which introduced OAS2 as the top protein. **B**) Immunohistochemical analysis of OAS2 on TMA construct indicates elevated OAS2 abundance in rGBM tissue. The lower panels show the same cores with pseudo-color, generated using HALO image analysis software, for better visualization. (Scale bar: 200 µm) **C)** Overexpression of OAS2 in rGBM was confirmed by immunohistochemical analysis on a TMA construct consisting of an independent cohort of 20 pGBM-rGBM matched samples. **D)** GBM BTIC line (BT618) shows reduction in stem cell properties including self-renewal and proliferation as measured by secondary sphere formation assay

and PrestoBlue proliferation assay, respectively upon silencing OAS2 gene by CRISPR knockout gene editing. The western blot analysis confirmed OAS2 gene KO in all three constructs (A, B and C) when compared to AAVS1 (control). (P value: ** 0.0019, * 0.0238) (mean±SEM, two-tailed t-test).

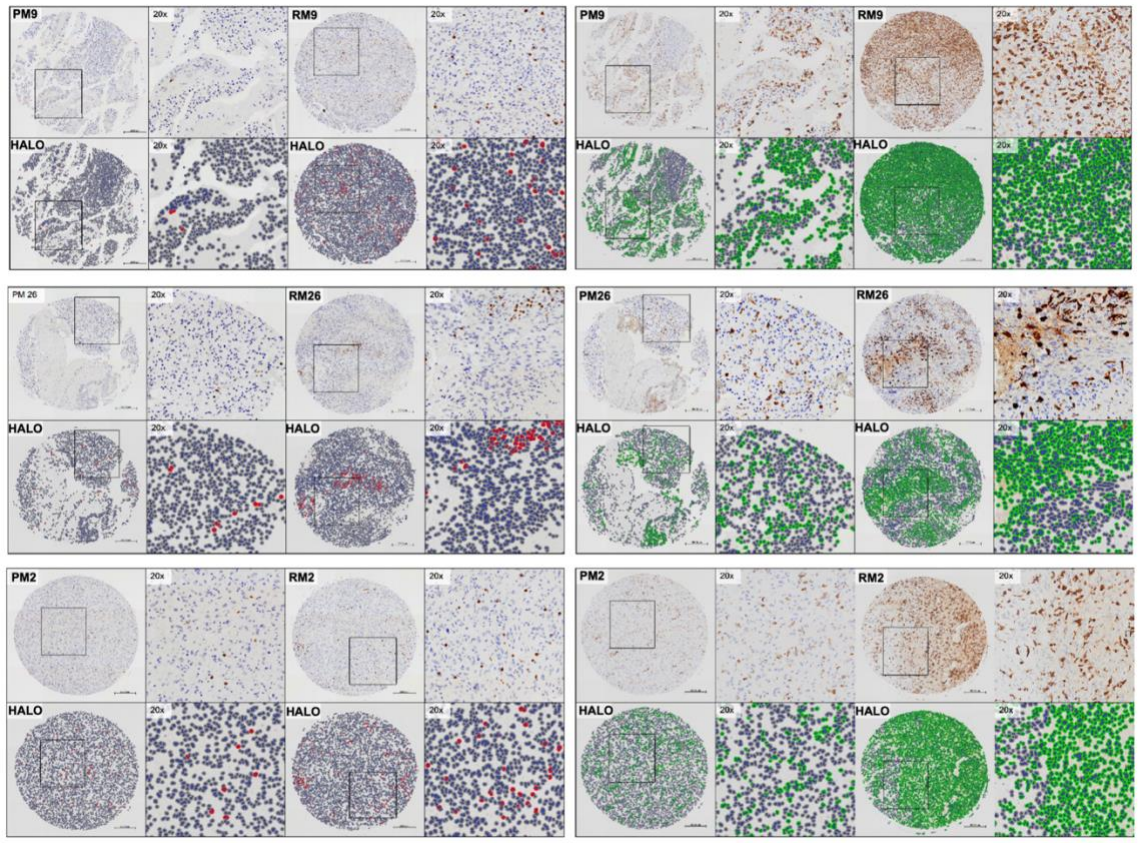
PM9
RM9
HALO
PM 26
RM26
PM26
PM2
RM2
20x
CD3
CD163
Nucleus

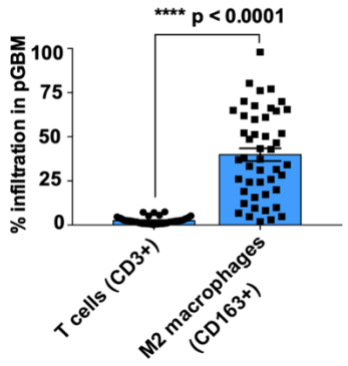
**** p < 0.0001
% infiltration in pGBM
100
75
50
25
0
T cells (CD3+)
M2 macrophages (CD163+)

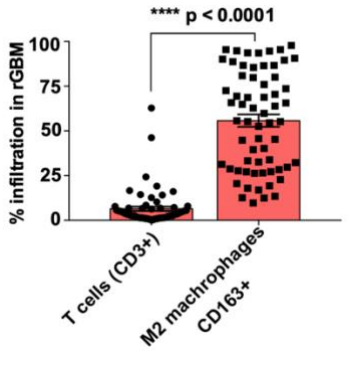
**** p < 0.0001
% infiltration in rGBM
100
75
50
25
0
T cells (CD3+)
M2 machrophages CD163+

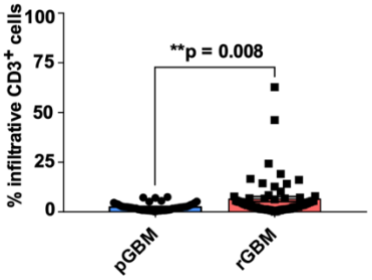
**p = 0.008
% infiltrative CD3+ cells
100
75
50
25
0
pGBM
rGBM

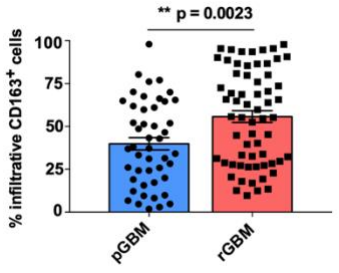
** p = 0.0023
% infiltrative CD163+ cells
100
75
50
25
0
pGBM
rGBM

Supplementary Figure 4. Immunohistochemical analysis of T cell and M2 macrophage infiltration in GBM tissue using Tissue Microarray (TMA) constructs. Analyzing the CD3 and CD163 stained TMA constructs using the HALO image analysis software indicated higher level of **A)** T cell (CD3+ cells highlighted with the red signal) and **B)** M2 macrophage (CD163+ cells highlighted with the green signal) infiltration into the rGBM tissues compared to the pGBM tissues with the M2 macrophages (immunosuppressive cell population) as the dominant cells infiltrated into both the pGBM and the rGBM tissues. PM: Primary Matched, RM: Recurrent Matched

id	sex	age_at_treatment	time_to_recurrence_months	time_to_death_months
GBM01-PM	M	48.1	15.07	22.07
GBM01-RM	M	48.1	15.07	22.07
GBM02-PM	M	60.7	10.2	13.87
GBM02-RM	M	60.7	10.2	13.87
GBM03-PM	M	46.6	3.26	14.6
GBM03-RM	M	46.6	3.26	14.6
GBM04-PM	M	76.1	11.45	15.74
GBM04-RM	M	76.1	11.45	15.74
GBM05-PM	M	53.8	11.87	16.84
GBM05-RM	M	53.8	11.87	16.84
GBM06-PM	M	40.4	2.61	8.13
GBM06-RM	M	40.4	2.61	8.13
GBM07-PM	M	48.7	8.55	9
GBM07-RM	M	48.7	8.55	9
GBM08-PM	M	66.5	3.23	5.52
GBM08-RM	M	66.5	3.23	5.52
GBM09-PM	M	70.4	13.27	19.84
GBM09-PM2	M	70.4	12.97	19.55
GBM09-RM	M	70.4	13.27	19.84
GBM11-PM	M	36.4	17	21.58
GBM11-RM	M	36.4	17	21.58
GBM12-PM	M	55.7	5	18.81
GBM12-RM	M	55.7	5	18.81
GBM14-PM	M	63.6	7.06	8.52
GBM14-RM	M	63.6	7.06	8.52
GBM15-PM	M	55.1	15.19	19.18
GBM15-RM	M	55.1	15.19	19.18
GBM16-PM	M	74.8	5.58	9.33
GBM16-RM	M	74.8	5.58	9.33
GBM17-PM	M	60.6	6.36	24.77
GBM17-RM	M	60.6	6.36	24.77
GBM18-PM	F	54.9	8.27	15.68
GBM18-RM	F	54.9	8.27	15.68
GBM18-PM2	F	54.9	8.27	15.68
GBM19-PM	M	57.4	8.74	12.19
GBM19-RM	M	57.4	8.74	12.19
GBM20-PM	F	52.4	5.97	16.68
GBM20-RM	F	52.4	5.97	16.68
GBM21-PM	F	65.5	8.29	19.5
GBM21-RM	F	65.5	8.29	19.5
GBM21-RM2	F	65.5	17.87	19.5
GBM24-PM2	M	42	0.16	7.52
GBM24-PM	M	42	0.16	7.52
GBM24-RM	M	42	0.16	7.52
GBM26-PM	F	59.8	15.1	17.74
GBM26-RM	F	59.8	15.1	17.74
GBM28-PM	M	54.8	6.45	9
GBM28-RM	M	54.8	6.45	9

GBM29-PM	M	73.6	8.43	10.9
GBM29-RM	M	73.6	8.43	10.9
GBM30-PM	F	50.9	6.9	7.9
GBM30-RM	F	50.9	6.9	7.9
GBM31-PM	M	73.1	7.58	12.52
GBM31-RM	M	73.1	7.58	12.52
GBM32-PM	M	53.8	8.13	10.68
GBM32-RM	M	53.8	8.13	10.68
GBM33-PM	M	55.2	9.57	17.68
GBM33-RM	M	55.2	9.57	17.68
GBM34-PM	M	42.7	7.71	19.26
GBM34-RM	M	42.7	7.71	19.26
GBM35-PM	M	75.9	9.45	13.37
GBM35-RM	M	75.9	9.45	13.37
GBM36-PM	M	72.7	7.83	12.6
GBM36-RM	M	72.7	7.83	12.6
GBM37-PM	M	64.7	16.48	NA
GBM37-RM	M	64.7	16.48	NA
GBM38-PM	M	69.3	8.38	11.94
GBM38-RM	M	69.3	8.38	11.94
GBM39-PM	F	72.4	9.55	10.5
GBM39-RM	F	72.4	9.55	10.5
GBM40-PM	M	59.5	19.33	22.55
GBM40-RM	M	59.5	19.33	22.55
GBM41-PM	F	49.6	2.65	6
GBM41-RM	F	49.6	2.65	6
GBM42-PM	M	40.1	19.1	23.55
GBM42-RM	M	40.1	19.1	23.55
GBM43-PM	M	45.7	1.68	14.47
GBM43-RM	M	45.7	1.68	14.47
GBM44-PM	M	50.9	10.83	15.57
GBM44-RM	M	50.9	10.83	15.57
GBM45-PM	F	66.3	12.94	23.43
GBM45-RM	F	66.3	12.94	23.43
GBM46-RM	F	63.4	12.53	20.66
GBM46-PM	F	63.4	12.53	20.66
GBM01-PNM	M	63.5	4.55	7.8
GBM02-PNM	M	50.6	8.5	62.16
GBM03-PNM	F	66	17.29	29.03
GBM04-PNM	F	76.7	9.61	19.16
GBM05-PNM	M	68.3	9.47	19.19
GBM06-PNM	M	57.5	0	4
GBM07-PNM	F	49.1	16.55	23.07
GBM08-PNM	F	55.8	8.39	27.39
GBM09-PNM	F	61.4	12	14.77
GBM01-RNM	M	51.6	0.35	13.65
GBM02-RNM	F	64.2	10.93	20.77
GBM04-RNM	M	63.3	6.32	23.52
GBM05-RNM	M	47.6	11.07	14.06
GBM06-RNM	M	53.9	0	1.03
GBM07-RNM	M	37.6	16.06	25.97

GBM08-RNM	F	59.5	9.21	17.45
GBM09-RNM	M	52.5	2.57	17.23
GBM06-RNM2	M	53.9	0	1.03
GBM11-RNM	M	69.2	14.87	16.48
GBM12-RNM	F	29.1	6.23	14.13
GBM13-RNM	M	65.2	27.03	34.77
GBM14-RNM	M	50.1	10.23	10.45
GBM14-RNM2	M	50.1	7.46	10.45
GBM15-RNM	M	40.8	7.07	8.94
GBM16-RNM	F	74.4	0	5.48
GBM17-RNM	F	57.3	5.39	14.1
GBM19-RNM	M	75.7	15.65	16.67
GBM20-RNM	M	57.8	2.83	6.32
GBM21-RNM	F	53.4	11.6	12.32
GBM22-RNM	M	61.5	4	5.29
GBM24-RNM	M	54.4	11.33	19.35
GBM25-RNM	M	48	1.35	1.35
GBM01-N	M	67.5	NA	7.74
GBM03-N	F	74.4	NA	5.48
GBM04-N	M	61.5	NA	5.29
GBM06-N	M	54.4	NA	2.55
GBM07-N	M	48	NA	NA
GBM09-N	F	63.4	NA	20.66
GBM10-N	M	40.1	NA	23.55
GBM11-N	M	60.7	NA	13.87
GBM12-N	M	49.3	NA	6.97
GBM14-N	M	63.9	NA	17.2
GBM15-N	M	67.5	NA	11.83
GBM16-N	F	52.9	NA	10.74
GBM17-N	M	45.7	NA	14.47
GBM18-N	F	63.4	NA	20.66
GBM19-N	M	58.1	NA	3.48
GBM20-N	M	53.8	NA	10.68
GBM21-N	M	67.5	NA	11.83

Table 1: Patient demographics of HHS patients. Patient demographics indicating the clinico-pathological information of each patient at both primary and recurrent stage

Accession #	Gene Name	Class Name	Description
NM_001101.3	ACTB	Housekeeping	ACTB
NM_002046.3	GAPDH	Housekeeping	GAPDH
NM_003194.4	TBP	Housekeeping	TBP
NM_178014.2	TUBB	Housekeeping	TUBB
NM_004316.3	ASCL1	Endogenous	ASCL1
NM_001195553.1	DCX	Endogenous	DCX
NM_203486.2	DLL3	Endogenous	DLL3
NM_052917.2	GALNT13	Endogenous	GALNT13
NM_002374.3	MAP2	Endogenous	MAP2
NM_002509.2	NKX2-2	Endogenous	NKX2-2
NM_005806.2	OLIG2	Endogenous	OLIG2
NM_003106.2	SOX2	Endogenous	SOX2
NM_001005915.1	ERBB3	Endogenous	ERBB3
NM_000806.5	GABRA1	Endogenous	GABRA1
NM_006158.5	NEFL	Endogenous	NEFL
NM_001134771.2	SLC12A5	Endogenous	SLC12A5
NM_003087.3	SNCG	Endogenous	SNCG
NM_005639.3	SYT1	Endogenous	SYT1
NM_022965.2	FGFR3	Endogenous	FGFR3
NM_002048.2	GAS1	Endogenous	GAS1
NM_000214.2	JAG1	Endogenous	JAG1
NM_005924.5	MEOX2	Endogenous	MEOX2
NM_006617.1	NES	Endogenous	NES
NM_002607.5	PDGFA	Endogenous	PDGFA
NM_003877.3	SOCS2	Endogenous	SOCS2
NM_000346.2	SOX9	Endogenous	SOX9
NM_005842.2	SPRY2	Endogenous	SPRY2
NM_000089.3	COL1A2	Endogenous	COL1A2
NM_002306.2	LGALS3	Endogenous	LGALS3
NM_006509.2	RELB	Endogenous	RELB
NM_000602.4	SERPINE1	Endogenous	SERPINE1
NM_003254.2	TIMP1	Endogenous	TIMP1
NM_003264.3	TLR2	Endogenous	TLR2
NM_003789.2	TRADD	Endogenous	TRADD

Supplementary Table 1: The custom codeset of probes for NanoString gene expression analysis to determine GBM samples genomic subtype. The custom codeset of 70 probes representing housekeeping genes (4) and classifier genes (30) corresponding to the classical (CL), mesenchymal (MES), proneural (PN), and neural (NL) subtypes.

Chapter 4: Discussion and future direction

4.1. Summary of Results

Glioblastoma (GBM) is characterized by extensive cellular and genetic heterogeneity which evolves through disease progression and under therapeutic pressure. This necessitates a detailed understanding of the evolutionary dynamics of tumor progression as well as characterization of pathways and molecular players driving GBM recurrence as crucial steps towards identification of therapeutic targets for designing and developing rational therapies against this deadly disease.

This thesis has focused on generating detailed molecular profiles of rGBM using advanced proteomics technologies which led to characterization of molecular mechanisms underlying GBM recurrence as well as identification and validation of novel, rational targets and predictive biomarkers for this treatment-refractory disease. In addition, the efficacy of Dual Antigen T cell engagers (DATEs) as a novel and empiric immunotherapeutic modality for targeting hypoxia niche in GBM at the preclinical stage was investigated.

In Chapter 2, I showed the importance of targeting hypoxic tumor microenvironment in solid tumors specifically in GBM and RCC. This was shown by using a novel targeted immunotherapeutic approach against the hypoxia-inducible enzyme, CA9. Previous studies have indicated that CA9 expression and activation lead to poor patient prognosis due to its effect on tumor cell metabolic alterations and response to therapy [274, 329]. We saw that majority of treatment- resistant BTIC populations isolated from various tumors had a high level of CA9 expression which was associated with poor patient survival. Moreover, upon

exposing CA9-low expressing BTICs to hypoxic conditions, we saw CA9 elevation which was associated with higher levels of self-renewal and proliferation. These findings confirmed the potential utility of CA9 as a therapeutic target for GBM. Current existing therapeutic modalities against CA9 are only effective when used in combination with other therapeutic agents including TMZ [274], underscoring an urgent need to develop effective therapeutic modalities against CA9 in solid tumors. To improve the potency of TAA-targeted Ab therapy we constructed CA9-specific DATE for the first time. DATEs act as a tumor-specific immune stimulus and bring circulating T cells into close proximity of tumor cells. This initiates an antigen-like stimulation signal within the recruited T cells, leading to immune targeting and eventually destruction of the antigen-expressing tumor cells. Our data revealed the potent cytotoxicity effect of the constructed CA9 DATE against tumor cells in both GBM and RCC models at *in vitro* and *in vivo* level. We first showed the specificity of CA9 DATE for both CD3 and CA9 antigens. Binding of CA9 DATEs to both T cells and tumor cells via surface-expressed antigens led to T cell activation which was detected by elevated level of T cell activation markers including CD25 and CD69, resulting in induction of severe cytotoxicity in tumor cells in both GBM and RCC models. Moreover, intratumoral administration of CA9 DATE in patient-derived xenograft models of GBM and RCC resulted in significant reduction of tumor burden as well as increased survival. In summary, through this work we showed the potency and efficacy of CA9 DATE, as an antibody-based targeted therapy against solid tumors with high level of CA9 expression particularly GBM and RCC.

With respect to the data generated in Chapter 3, we were able to decipher the evolutionary pattern of the GBM proteome landscape from primary to the recurrent state using advanced proteomics technologies. Studies conducted in the past decade using multi-omics analysis on patient samples indicated that GBM evolves significantly under therapeutic pressure in such a way that the genetic and molecular landscape of rGBM doesn't resemble its primary counterpart [70, 305]. However, the majority of studies focused on characterization of the molecular landscape of GBM, have only identified the malignant modifications associated with pGBM. The field currently lacks an in-depth understanding of how GBM evolves through therapy to become a very different tumor at recurrence [315, 319]. Therefore, we undertook this study to increase our understanding of aberrant pathways specific to rGBM, for biomarker development and therapeutic intervention. Through this research we were able to identify and validate novel targets and predictive biomarkers for rGBM which indicated rGBM is heavily associated with immunosuppression. In fact, our data revealed pathways involved in immunoregulation, including Epithelial to Mesenchymal transition and IFN-γ pathways which were highly elevated in the rGBM proteome compared to pGBM. We also found that proteins related to IFNγ signalling such as OAS2 were differentially enriched across all rGBM samples. This led us to further investigation of the role of OAS2 in GBM pathogenesis. Using CRISPR knockout studies we showed OAS2 has a direct effect on CSC cardinal features including self-renewal and proliferation. Moreover, orthotopic engraftment of OAS2 WT and KO in immunocompromised mice showed a dramatic reduction in tumor burden as well as increased survival advantage for OAS2 KO mice, indicating the significant role of OAS2 in GBM progression. In addition,

we showed enrichment of the immunosuppressive macrophage population in rGBM by identifying CD163 (M2-like macrophage marker) as well as CD169 (marker small subpopulation of macrophages with immunosuppressive role) expression in rGBM, as another layer of confirmation for high level of immunosuppression at the recurrent state which is associated with patient poor prognosis. In another part of our study, we performed overall survival analysis by categorizing patients into short-term vs long-term survivors. Comparing their protein landscapes indicated that the hypoxia pathway, PI3k-AKT-MTOR pathway, Interferon α response and IL6-JAK-STAT3 pathways were upregulated in short-term survivors compared to long-term survivors, emphasizing their putative role in GBM progression.

In conclusion, for the first time we were able to use clinically annotated patient tumor tissues and advanced proteomics technologies to identify the proteomic landscape of rGBM. This allows for development of diagnostic and/or predictive biomarkers as well as new selective molecular targeted therapies. Moreover, this would be extremely complementary and instructive for the development of new polytherapeutic paradigms for GBM patients at the recurrent level which will improve future patient survival.

In summary, the studies conducted throughout my Ph.D. revealed new aberrant pathways driving rGBM. Target validation experiments and exploration of mechanisms indicated the crucial role of both CSCs and TIME in GBM progression and treatment resistance. Moreover, I showed the efficacy of a novel immunotherapeutic modality, the CA9 DATE, against both the hypoxic tumor microenvironment of GBM and $CA9^{+}$ BTICs. All in all, this thesis provides a great resource for identifying new targets in treatment-resistant rGBM

as well as instruction of novel and rational combinatorial polytherapeutic approaches, to one day generate more effective and personalized treatments for therapy-resistant rGBM.

4.2. Future Directions

Project 1 (chapter 2):

Investigating the effect of CA9 DATE therapy on tumor microenvironment, particularly on tumor immune microenvironment and its ability in recruiting T cells to the tumor site is a crucial step in assessing its therapeutic efficacy. To further explore this and preclinically validate CA9 DATEs, another important experiment that can be done is generating both GBM and ccRCC models using NOG-EXL humanized mice. Following mice intra-tumoral treatment with CA9 DATEs, the tumor will be harvested for CYTOF and sciRNAseq analysis. The analysis of gene expression patterns at single cell resolution following CA9 DATE therapy would allow us to study tumor intrinsic features and characterize the infiltrated immune cell population into the tumor at the single cell level in addition to identification of the pathways affected by CA9 DATE treatment. This all will result in understanding CA9 DATEs mechanism of action on tumor growth inhibition and provide key information to establish signatures that predict response to this particular immunotherapy.

Project 2 (chapter 3):

To be able to expand our understanding of GBM evolution through therapy across multiple sample types, in addition to 143 FFPE-embedded GBM samples we have also collected 5

fresh-frozen patient-matched pGBM and rGBM tissues as well as 7 unmatched pGBMs (17 total samples) and foresee receiving the matched rGBM. These samples are significantly larger (approximately 5x5 mm) in size than the FFPE punctures used in the proteomics study. Access to these samples will provide us with a one-of-a-kind resource of matched pGBM-rGBM tumor pairs for in-depth proteomics. We will perform total proteome, N-glycoproteomic and phosphoproteomic analyses on these samples to obtain the most in-depth interrogation of the GBM proteome to date. The top enriched targets at the recurrent state from this study as well as FFPE proteomics analysis will be chosen to be further validated on the TMA using multiplexed ion beam imaging by time of flight (MIBI-TOF) which allows for spatial and compositional profiling of up to 45 targets. Using this technology, we will be able to study the cell-cell and receptor-ligand interactions on intact tumor tissues.

In addition, as majority of the identified targets from the FFPE data set are macrophage associated markers and it has been repeatedly shown that macrophages play a significant role in GBM immunosuppression, the next step would be developing a therapeutic modality for co-targeting CSCs and macrophage population simultaneously. This would be extremely complementary and instructive for the development of new poly-therapeutic paradigms for rGBM.

Project 3

Immunotherapeutics have emerged as potent anticancer agents owing to recent advances in the understanding of tumor antigens and immune checkpoint modulators and can lead to efficient tumor killing and long-term surveillance against cancer cells. Tumor vaccines and

adoptive cell transfer-based cancer immunotherapies have proven to be safe, showing a trend toward prolonged survival. However, the efficacy of these promising immunotherapies is negatively affected by GBM immunosuppressive microenvironment. Thus, therapeutic strategies that render tumor cells more sensitive to immune cell killing, neutralize immunosuppression, or recruit active immune killing mechanisms, will be critical for enhancing treatment outcomes in GBM patients.

Camilo *et al.* previously showed that SoC alters the GBM patients' immune system towards a suppressive state, including an increase in functional regulatory T cells (Tregs) and decrease in effector $CD8^+$ T cells and NK cells [330]. It has also been shown that radiation therapy alters the TIME and makes GBM more aggressive [331]. Moreover, Mohme *et al.* found a signature of immune exhaustion in GBM patients in both primary and recurrent GBMs. Interestingly, reduced T cell receptor (TCR) diversity with an activated memory T cell phenotype was noted in recurrent GBM patients, suggesting recurrent GBM patients may have a distinct TCR clonality profile as compared to primary GBM patients [332]. Therefore, profiling GBM and its associated TIME will be important to advance immunotherapeutic strategies.

Our hypothesis is that detailed profiling of the TIME in relation to tumor cell state can reveal immune regulatory genes as important drivers of recurrent GBM and new targets that can lead to efficient tumor killing and long-term surveillance against cancer cells. Our observations, models, and targets aim to generate pre-clinical data showing enhanced efficacy of poly- or immune-therapies to achieve desired clinical outcomes for rGBM patients.

To conduct this study, we will employ the technologies which would allow for surveying the immune constitution of GBM from patient samples:

1- *Single-cell sequencing using a combinatorial barcode indexing strategy (sci-RNA-seq3) on patient-matched pGBM and rGBM fresh frozen samples as well as syngeneic mouse models of GBM.* The sci-RNA-seq3 platform [333, 334] provides us a robust, powerful, and cost-effective approach for the systematic in-depth characterization and understanding of tumor heterogeneity and the TIME evolution from primary to recurrent state over the course of treatment using at least 10 matched pGBM and rGBM samples as well as 2 two syngeneic brain tumor models derived from mice, CT-2A and GL261, which have stem cell like phenotype. The syngeneic mouse models will be generated by implanting CT-2A or GL261 into the right frontal lobes of fully immunocompetent mice (C57BL/6 mice). Growing cells to mid and large sizes, allows for profiling the dynamics of the TIME as tumors grow in size. In a pilot experiment, we successfully detected diverse cell populations, representing GBM tumor cells, immune cells, and surrounding brain cells. Importantly, data from this pilot experiment demonstrated the existence of diverse cellular states within the tumors, including OPC-like, NPC-like, AC-like, and MES-like tumor cells, which is highly consistent with the recent human GBM study [72]. Interestingly, the two mouse models showed different compositions of cell populations. For example, NPC-like tumor cells are dominated by GL261 models, while MES-like tumor cells show a higher proportion of cells from the CT2A model. This will be important to better understand these two different

syngeneic mouse models as well as different human GBMs. In addition to tumor cells, we also profiled and characterized the TIME, including both immune populations (e.g., microglia, macrophages, and nuocytes) and surrounding brain stroma (e.g., different neurons and glia cells).

2- *Flow cytometric analyses of immune isolated cells patient-matched pGBM and rGBM from fresh tumor tissues.* In this approach, we used fresh patient tumor tissue immediately following tumor resection. We then separated the immune cell fraction from the tumor cell fraction using antibody-based depletion. The immune cell fraction using a phenotyping panel for both innate and adaptive immune cells in matched pGBM and rGBM samples will be characterize. The flow cytometry panel includes CD68 (macrophages), CD163 (microglia), CD11b and HLA-DR (myeloid-derived suppressor cells, MDSC) and CD4 and CD25 (Tregs) to further investigate the immunosuppressive signature in rGBM.

3- *Immunohistochemistry on FFPE patient-matched pGBM and rGBM samples.* A tissue microarray built by 143 samples, including matched, unmatched and normal control tissues will be used for Immunohistochemical analysis. This results in spatial and compositional profiling of immune cell infiltrates. Profiles of T cells, microglia, myeloid cells and bone marrow-derived macrophages (BMDMs) will provide visual evidence of changes in the distribution of immune cells in recurrent tumors. These samples will be further examined by image-based mass cytometry.

This study would allow us to survey the TIME in human rGBM models in detail, establish a resource of co-isogenic GBM models that recapitulate features of human rGBM including

the TIME, and validate promising targeting strategies that render tumor cells more susceptible to immune killing. Eventually the data coming out of this project will be used to generate pre-clinical data showing enhanced efficacy of poly- or immune-therapies to achieve desired clinical outcomes for rGBM patients.

References

1. Louis, D.N., et al., *The 2016 World Health Organization Classification of Tumors of the Central Nervous System: a summary.* Acta Neuropathol, 2016. **131**(6): p. 803-20.
2. Walker, E.V., F.G. Davis, and C.f. affiliates, *Malignant primary brain and other central nervous system tumors diagnosed in Canada from 2009 to 2013.* Neuro Oncol, 2019. **21**(3): p. 360-369.
3. Mikkelsen, V.E., et al., *The histological representativeness of glioblastoma tissue samples.* Acta Neurochir (Wien), 2021. **163**(7): p. 1911-1920.
4. Ohgaki, H. and P. Kleihues, *The definition of primary and secondary glioblastoma.* Clin Cancer Res, 2013. **19**(4): p. 764-72.
5. D'Alessio, A., et al., *Pathological and Molecular Features of Glioblastoma and Its Peritumoral Tissue.* Cancers (Basel), 2019. **11**(4).
6. Louis, D.N., et al., *The 2021 WHO Classification of Tumors of the Central Nervous System: a summary.* Neuro Oncol, 2021.
7. Bao, S., et al., *Glioma stem cells promote radioresistance by preferential activation of the DNA damage response.* Nature, 2006. **444**(7120): p. 756-60.
8. Chen, J., et al., *A restricted cell population propagates glioblastoma growth after chemotherapy.* Nature, 2012. **488**(7412): p. 522-6.
9. Ostrom, Q.T., et al., *CBTRUS Statistical Report: Primary Brain and Other Central Nervous System Tumors Diagnosed in the United States in 2009-2013.* Neuro Oncol, 2016. **18**(suppl_5): p. v1-v75.
10. Chinot, O.L., et al., *Bevacizumab plus radiotherapy-temozolomide for newly diagnosed glioblastoma.* N Engl J Med, 2014. **370**(8): p. 709-22.
11. Gilbert, M.R., et al., *A randomized trial of bevacizumab for newly diagnosed glioblastoma.* N Engl J Med, 2014. **370**(8): p. 699-708.
12. Weller, M., et al., *EANO guideline for the diagnosis and treatment of anaplastic gliomas and glioblastoma.* Lancet Oncol, 2014. **15**(9): p. e395-403.
13. Weller, M., et al., *Standards of care for treatment of recurrent glioblastoma--are we there yet?* Neuro Oncol, 2013. **15**(1): p. 4-27.
14. Fernandes, C., et al., *Current Standards of Care in Glioblastoma Therapy*, in *Glioblastoma*, S. De Vleeschouwer, Editor. 2017: Brisbane (AU).
15. Wolbers, J.G., *Novel strategies in glioblastoma surgery aim at safe, supra-maximum resection in conjunction with local therapies.* Chin J Cancer, 2014. **33**(1): p. 8-15.
16. Sanai, N., et al., *An extent of resection threshold for newly diagnosed glioblastomas.* J Neurosurg, 2011. **115**(1): p. 3-8.
17. Li, Y.M., et al., *The influence of maximum safe resection of glioblastoma on survival in 1229 patients: Can we do better than gross-total resection?* J Neurosurg, 2016. **124**(4): p. 977-88.
18. Panciani, P.P., et al., *5-aminolevulinic acid and neuronavigation in high-grade glioma surgery: results of a combined approach.* Neurocirugia (Astur), 2012. **23**(1): p. 23-8.

19. Stupp, R., et al., *Radiotherapy plus concomitant and adjuvant temozolomide for glioblastoma.* N Engl J Med, 2005. **352**(10): p. 987-96.
20. Gilbert, M.R., et al., *Dose-dense temozolomide for newly diagnosed glioblastoma: a randomized phase III clinical trial.* J Clin Oncol, 2013. **31**(32): p. 4085-91.
21. Taal, W., et al., *Single-agent bevacizumab or lomustine versus a combination of bevacizumab plus lomustine in patients with recurrent glioblastoma (BELOB trial): a randomised controlled phase 2 trial.* Lancet Oncol, 2014. **15**(9): p. 943-53.
22. Friedman, H.S., et al., *Bevacizumab alone and in combination with irinotecan in recurrent glioblastoma.* J Clin Oncol, 2009. **27**(28): p. 4733-40.
23. Kreisl, T.N., et al., *Phase II trial of single-agent bevacizumab followed by bevacizumab plus irinotecan at tumor progression in recurrent glioblastoma.* J Clin Oncol, 2009. **27**(5): p. 740-5.
24. Piccioni, D.E. and A. Lai, *Deferred use of bevacizumab for recurrent glioblastoma is not associated with diminished efficacy.* Neuro Oncol, 2014. **16**(10): p. 1427-8.
25. Niyazi, M., et al., *ESTRO-ACROP guideline "target delineation of glioblastomas".* Radiother Oncol, 2016. **118**(1): p. 35-42.
26. Shaw, E., et al., *Single dose radiosurgical treatment of recurrent previously irradiated primary brain tumors and brain metastases: final report of RTOG protocol 90-05.* Int J Radiat Oncol Biol Phys, 2000. **47**(2): p. 291-8.
27. Cihoric, N., et al., *Current status and perspectives of interventional clinical trials for glioblastoma - analysis of ClinicalTrials.gov.* Radiat Oncol, 2017. **12**(1): p. 1.
28. Brown, C.E., et al., *Bioactivity and Safety of IL13Ralpha2-Redirected Chimeric Antigen Receptor CD8+ T Cells in Patients with Recurrent Glioblastoma.* Clin Cancer Res, 2015. **21**(18): p. 4062-72.
29. Brown, C.E., et al., *Regression of Glioblastoma after Chimeric Antigen Receptor T-Cell Therapy.* N Engl J Med, 2016. **375**(26): p. 2561-9.
30. Ahmed, N., et al., *HER2-Specific Chimeric Antigen Receptor-Modified Virus-Specific T Cells for Progressive Glioblastoma: A Phase 1 Dose-Escalation Trial.* JAMA Oncol, 2017. **3**(8): p. 1094-1101.
31. O'Rourke, D.M., et al., *A single dose of peripherally infused EGFRvIII-directed CAR T cells mediates antigen loss and induces adaptive resistance in patients with recurrent glioblastoma.* Sci Transl Med, 2017. **9**(399).
32. Goff, S.L., et al., *Pilot Trial of Adoptive Transfer of Chimeric Antigen Receptor-transduced T Cells Targeting EGFRvIII in Patients With Glioblastoma.* J Immunother, 2019. **42**(4): p. 126-135.
33. Reardon, D.A., et al., *Effect of Nivolumab vs Bevacizumab in Patients With Recurrent Glioblastoma: The CheckMate 143 Phase 3 Randomized Clinical Trial.* JAMA Oncol, 2020. **6**(7): p. 1003-1010.
34. Sahebjam, S., et al., *Hypofractionated stereotactic re-irradiation with pembrolizumab and bevacizumab in patients with recurrent high-grade gliomas: results from a phase I study.* Neuro Oncol, 2021. **23**(4): p. 677-686.

35. Nayak, L., et al., *Randomized Phase II and Biomarker Study of Pembrolizumab plus Bevacizumab versus Pembrolizumab Alone for Patients with Recurrent Glioblastoma.* Clin Cancer Res, 2021. **27**(4): p. 1048-1057.
36. Schalper, K.A., et al., *Neoadjuvant nivolumab modifies the tumor immune microenvironment in resectable glioblastoma.* Nat Med, 2019. **25**(3): p. 470-476.
37. Grossmann, P., et al., *Quantitative imaging biomarkers for risk stratification of patients with recurrent glioblastoma treated with bevacizumab.* Neuro Oncol, 2017. **19**(12): p. 1688-1697.
38. Sampson, J.H., et al., *Immunologic escape after prolonged progression-free survival with epidermal growth factor receptor variant III peptide vaccination in patients with newly diagnosed glioblastoma.* J Clin Oncol, 2010. **28**(31): p. 4722-9.
39. Sampson, J.H., et al., *Greater chemotherapy-induced lymphopenia enhances tumor-specific immune responses that eliminate EGFRvIII-expressing tumor cells in patients with glioblastoma.* Neuro Oncol, 2011. **13**(3): p. 324-33.
40. Schuster, J., et al., *A phase II, multicenter trial of rindopepimut (CDX-110) in newly diagnosed glioblastoma: the ACT III study.* Neuro Oncol, 2015. **17**(6): p. 854-61.
41. Weller, M., et al., *Rindopepimut with temozolomide for patients with newly diagnosed, EGFRvIII-expressing glioblastoma (ACT IV): a randomised, double-blind, international phase 3 trial.* Lancet Oncol, 2017. **18**(10): p. 1373-1385.
42. Reardon, D.A., et al., *Rindopepimut with Bevacizumab for Patients with Relapsed EGFRvIII-Expressing Glioblastoma (ReACT): Results of a Double-Blind Randomized Phase II Trial.* Clin Cancer Res, 2020. **26**(7): p. 1586-1594.
43. Mitchell, D.A., et al., *Tetanus toxoid and CCL3 improve dendritic cell vaccines in mice and glioblastoma patients.* Nature, 2015. **519**(7543): p. 366-9.
44. Batich, K.A., et al., *Long-term Survival in Glioblastoma with Cytomegalovirus pp65-Targeted Vaccination.* Clin Cancer Res, 2017. **23**(8): p. 1898-1909.
45. Batich, K.A., et al., *Once, Twice, Three Times a Finding: Reproducibility of Dendritic Cell Vaccine Trials Targeting Cytomegalovirus in Glioblastoma.* Clin Cancer Res, 2020. **26**(20): p. 5297-5303.
46. Platten, M., et al., *A vaccine targeting mutant IDH1 in newly diagnosed glioma.* Nature, 2021. **592**(7854): p. 463-468.
47. Liau, L.M., et al., *First results on survival from a large Phase 3 clinical trial of an autologous dendritic cell vaccine in newly diagnosed glioblastoma.* J Transl Med, 2018. **16**(1): p. 142.
48. Crane, C.A., et al., *Individual patient-specific immunity against high-grade glioma after vaccination with autologous tumor derived peptides bound to the 96 KD chaperone protein.* Clin Cancer Res, 2013. **19**(1): p. 205-14.
49. Bloch, O., et al., *Heat-shock protein peptide complex-96 vaccination for recurrent glioblastoma: a phase II, single-arm trial.* Neuro Oncol, 2014. **16**(2): p. 274-9.
50. Ji, N., et al., *Heat shock protein peptide complex-96 vaccination for newly diagnosed glioblastoma: a phase I, single-arm trial.* JCI Insight, 2018. **3**(10).

51. Bloch, O., et al., *Autologous Heat Shock Protein Peptide Vaccination for Newly Diagnosed Glioblastoma: Impact of Peripheral PD-L1 Expression on Response to Therapy.* Clin Cancer Res, 2017. **23**(14): p. 3575-3584.
52. Ghiaseddin, A.P., et al., *Tumor Treating Fields in the Management of Patients with Malignant Gliomas.* Curr Treat Options Oncol, 2020. **21**(9): p. 76.
53. Lee, S.Y., *Temozolomide resistance in glioblastoma multiforme.* Genes Dis, 2016. **3**(3): p. 198-210.
54. Hegi, M.E., et al., *Correlation of O6-methylguanine methyltransferase (MGMT) promoter methylation with clinical outcomes in glioblastoma and clinical strategies to modulate MGMT activity.* J Clin Oncol, 2008. **26**(25): p. 4189-99.
55. Zhang, J., M.F. Stevens, and T.D. Bradshaw, *Temozolomide: mechanisms of action, repair and resistance.* Curr Mol Pharmacol, 2012. **5**(1): p. 102-14.
56. Wick, W., et al., *MGMT testing--the challenges for biomarker-based glioma treatment.* Nat Rev Neurol, 2014. **10**(7): p. 372-85.
57. Wick, W., M. Platten, and M. Weller, *New (alternative) temozolomide regimens for the treatment of glioma.* Neuro Oncol, 2009. **11**(1): p. 69-79.
58. Beroukhim, R., et al., *Assessing the significance of chromosomal aberrations in cancer: methodology and application to glioma.* Proc Natl Acad Sci U S A, 2007. **104**(50): p. 20007-12.
59. Bredel, M., et al., *High-resolution genome-wide mapping of genetic alterations in human glial brain tumors.* Cancer Res, 2005. **65**(10): p. 4088-96.
60. Kotliarov, Y., et al., *High-resolution global genomic survey of 178 gliomas reveals novel regions of copy number alteration and allelic imbalances.* Cancer Res, 2006. **66**(19): p. 9428-36.
61. Zhang, Y., et al., *The p53 Pathway in Glioblastoma.* Cancers (Basel), 2018. **10**(9).
62. Brennan, C.W., et al., *The somatic genomic landscape of glioblastoma.* Cell, 2013. **155**(2): p. 462-77.
63. Parsons, D.W., et al., *An integrated genomic analysis of human glioblastoma multiforme.* Science, 2008. **321**(5897): p. 1807-12.
64. Fan, Q.W., et al., *EGFR phosphorylates tumor-derived EGFRvIII driving STAT3/5 and progression in glioblastoma.* Cancer Cell, 2013. **24**(4): p. 438-49.
65. Kim, Y., et al., *Platelet-derived growth factor receptors differentially inform intertumoral and intratumoral heterogeneity.* Genes Dev, 2012. **26**(11): p. 1247-62.
66. Verhaak, R.G., et al., *Integrated genomic analysis identifies clinically relevant subtypes of glioblastoma characterized by abnormalities in PDGFRA, IDH1, EGFR, and NF1.* Cancer Cell, 2010. **17**(1): p. 98-110.
67. Sharma, A., et al., *Angiogenic Gene Signature Derived from Subtype Specific Cell Models Segregate Proneural and Mesenchymal Glioblastoma.* Front Oncol, 2017. **7**: p. 146.
68. Colman, H., et al., *A multigene predictor of outcome in glioblastoma.* Neuro Oncol, 2010. **12**(1): p. 49-57.

69. Sottoriva, A., et al., *Intratumor heterogeneity in human glioblastoma reflects cancer evolutionary dynamics.* Proc Natl Acad Sci U S A, 2013. **110**(10): p. 4009-14.
70. Patel, A.P., et al., *Single-cell RNA-seq highlights intratumoral heterogeneity in primary glioblastoma.* Science, 2014. **344**(6190): p. 1396-401.
71. Szerlip, N.J., et al., *Intratumoral heterogeneity of receptor tyrosine kinases EGFR and PDGFRA amplification in glioblastoma defines subpopulations with distinct growth factor response.* Proc Natl Acad Sci U S A, 2012. **109**(8): p. 3041-6.
72. Neftel, C., et al., *An Integrative Model of Cellular States, Plasticity, and Genetics for Glioblastoma.* Cell, 2019. **178**(4): p. 835-849 e21.
73. DeCordova, S., et al., *Molecular Heterogeneity and Immunosuppressive Microenvironment in Glioblastoma.* Front Immunol, 2020. **11**: p. 1402.
74. Singh, S.K., et al., *Identification of human brain tumour initiating cells.* Nature, 2004. **432**(7015): p. 396-401.
75. Dalerba, P., R.W. Cho, and M.F. Clarke, *Cancer stem cells: models and concepts.* Annu Rev Med, 2007. **58**: p. 267-84.
76. Singh, S.K., et al., *Identification of a cancer stem cell in human brain tumors.* Cancer Res, 2003. **63**(18): p. 5821-8.
77. Clarke, M.F. and M. Fuller, *Stem cells and cancer: two faces of eve.* Cell, 2006. **124**(6): p. 1111-5.
78. Liu, G., et al., *Analysis of gene expression and chemoresistance of CD133+ cancer stem cells in glioblastoma.* Mol Cancer, 2006. **5**: p. 67.
79. Galli, R., et al., *Isolation and characterization of tumorigenic, stem-like neural precursors from human glioblastoma.* Cancer Res, 2004. **64**(19): p. 7011-21.
80. Hemmati, H.D., et al., *Cancerous stem cells can arise from pediatric brain tumors.* Proc Natl Acad Sci U S A, 2003. **100**(25): p. 15178-83.
81. Bonnet, D. and J.E. Dick, *Human acute myeloid leukemia is organized as a hierarchy that originates from a primitive hematopoietic cell.* Nat Med, 1997. **3**(7): p. 730-7.
82. Lee, J.H., et al., *Human glioblastoma arises from subventricular zone cells with low-level driver mutations.* Nature, 2018. **560**(7717): p. 243-247.
83. Ogden, A.T., et al., *Identification of A2B5+CD133- tumor-initiating cells in adult human gliomas.* Neurosurgery, 2008. **62**(2): p. 505-14; discussion 514-5.
84. Son, M.J., et al., *SSEA-1 is an enrichment marker for tumor-initiating cells in human glioblastoma.* Cell Stem Cell, 2009. **4**(5): p. 440-52.
85. Anido, J., et al., *TGF-beta Receptor Inhibitors Target the CD44(high)/Id1(high) Glioma-Initiating Cell Population in Human Glioblastoma.* Cancer Cell, 2010. **18**(6): p. 655-68.
86. Chen, R., et al., *A hierarchy of self-renewing tumor-initiating cell types in glioblastoma.* Cancer Cell, 2010. **17**(4): p. 362-75.
87. McCord, A.M., et al., *CD133+ glioblastoma stem-like cells are radiosensitive with a defective DNA damage response compared with established cell lines.* Clin Cancer Res, 2009. **15**(16): p. 5145-53.

88. Pallini, R., et al., *Cancer stem cell analysis and clinical outcome in patients with glioblastoma multiforme.* Clin Cancer Res, 2008. **14**(24): p. 8205-12.
89. Tomita, T., et al., *Clinicopathological significance of expression of nestin, a neural stem/progenitor cell marker, in human glioma tissue.* Brain Tumor Pathol, 2014. **31**(3): p. 162-71.
90. Zhang, M., et al., *Nestin and CD133: valuable stem cell-specific markers for determining clinical outcome of glioma patients.* J Exp Clin Cancer Res, 2008. **27**: p. 85.
91. Bjerkvig, R., et al., *Opinion: the origin of the cancer stem cell: current controversies and new insights.* Nat Rev Cancer, 2005. **5**(11): p. 899-904.
92. Ehtesham, M., et al., *CXCR4 mediates the proliferation of glioblastoma progenitor cells.* Cancer Lett, 2009. **274**(2): p. 305-12.
93. Persano, L., et al., *Glioblastoma cancer stem cells: role of the microenvironment and therapeutic targeting.* Biochem Pharmacol, 2013. **85**(5): p. 612-622.
94. Dirkse, A., et al., *Stem cell-associated heterogeneity in Glioblastoma results from intrinsic tumor plasticity shaped by the microenvironment.* Nat Commun, 2019. **10**(1): p. 1787.
95. Beier, D., J.B. Schulz, and C.P. Beier, *Chemoresistance of glioblastoma cancer stem cells--much more complex than expected.* Mol Cancer, 2011. **10**: p. 128.
96. Hsieh, A., R. Ellsworth, and D. Hsieh, *Hedgehog/GLI1 regulates IGF dependent malignant behaviors in glioma stem cells.* J Cell Physiol, 2011. **226**(4): p. 1118-27.
97. Okada, M., et al., *JNK contributes to temozolomide resistance of stem-like glioblastoma cells via regulation of MGMT expression.* Int J Oncol, 2014. **44**(2): p. 591-9.
98. Persano, L., et al., *BMP2 sensitizes glioblastoma stem-like cells to Temozolomide by affecting HIF-1alpha stability and MGMT expression.* Cell Death Dis, 2012. **3**: p. e412.
99. Beier, D., et al., *Temozolomide preferentially depletes cancer stem cells in glioblastoma.* Cancer Res, 2008. **68**(14): p. 5706-15.
100. Eramo, A., et al., *Chemotherapy resistance of glioblastoma stem cells.* Cell Death Differ, 2006. **13**(7): p. 1238-41.
101. Xi, G., et al., *CD133 and DNA-PK regulate MDR1 via the PI3K- or Akt-NF-kappaB pathway in multidrug-resistant glioblastoma cells in vitro.* Oncogene, 2016. **35**(2): p. 241-50.
102. Mimeault, M. and S.K. Batra, *Recent progress on tissue-resident adult stem cell biology and their therapeutic implications.* Stem Cell Rev, 2008. **4**(1): p. 27-49.
103. Wang, K., et al., *Hedgehog/Gli1 signaling pathway regulates MGMT expression and chemoresistance to temozolomide in human glioblastoma.* Cancer Cell Int, 2017. **17**: p. 117.
104. Shi, L., et al., *MicroRNA-125b-2 confers human glioblastoma stem cells resistance to temozolomide through the mitochondrial pathway of apoptosis.* Int J Oncol, 2012. **40**(1): p. 119-29.

105. Kumar, V., et al., *The Role of Notch, Hedgehog, and Wnt Signaling Pathways in the Resistance of Tumors to Anticancer Therapies.* Front Cell Dev Biol, 2021. **9**: p. 650772.
106. Da Ros, M., et al., *Glioblastoma Chemoresistance: The Double Play by Microenvironment and Blood-Brain Barrier*. Int J Mol Sci, 2018. **19**(10).
107. Uribe, D., et al., *Multidrug resistance in glioblastoma stem-like cells: Role of the hypoxic microenvironment and adenosine signaling.* Mol Aspects Med, 2017. **55**: p. 140-151.
108. Pistollato, F., et al., *Intratumoral hypoxic gradient drives stem cells distribution and MGMT expression in glioblastoma.* Stem Cells, 2010. **28**(5): p. 851-62.
109. Li, Z., et al., *Hypoxia-inducible factors regulate tumorigenic capacity of glioma stem cells.* Cancer Cell, 2009. **15**(6): p. 501-13.
110. Seidel, S., et al., *A hypoxic niche regulates glioblastoma stem cells through hypoxia inducible factor 2 alpha.* Brain, 2010. **133**(Pt 4): p. 983-95.
111. Sun, X., et al., *Hypoxia-mediated cancer stem cell resistance and targeted therapy.* Biomed Pharmacother, 2020. **130**: p. 110623.
112. Hjelmeland, A.B., et al., *Acidic stress promotes a glioma stem cell phenotype.* Cell Death Differ, 2011. **18**(5): p. 829-40.
113. Wang, J., et al., *CD133 negative glioma cells form tumors in nude rats and give rise to CD133 positive cells.* Int J Cancer, 2008. **122**(4): p. 761-8.
114. Dahan, P., et al., *Ionizing radiations sustain glioblastoma cell dedifferentiation to a stem-like phenotype through survivin: possible involvement in radioresistance.* Cell Death Dis, 2014. **5**: p. e1543.
115. Fleurence, J., et al., *Impairing temozolomide resistance driven by glioma stem-like cells with adjuvant immunotherapy targeting O-acetyl GD2 ganglioside.* Int J Cancer, 2020. **146**(2): p. 424-438.
116. Kitabayashi, T., et al., *Identification of GSK3beta inhibitor kenpaullone as a temozolomide enhancer against glioblastoma.* Sci Rep, 2019. **9**(1): p. 10049.
117. Morgan, M.A. and T.S. Lawrence, *Molecular Pathways: Overcoming Radiation Resistance by Targeting DNA Damage Response Pathways.* Clin Cancer Res, 2015. **21**(13): p. 2898-904.
118. Pilie, P.G., et al., *State-of-the-art strategies for targeting the DNA damage response in cancer.* Nat Rev Clin Oncol, 2019. **16**(2): p. 81-104.
119. Schulz, A., et al., *Cancer Stem Cells and Radioresistance: DNA Repair and Beyond.* Cancers (Basel), 2019. **11**(6).
120. Balbous, A., et al., *A radiosensitizing effect of RAD51 inhibition in glioblastoma stem-like cells.* BMC Cancer, 2016. **16**: p. 604.
121. King, H.O., et al., *RAD51 Is a Selective DNA Repair Target to Radiosensitize Glioma Stem Cells.* Stem Cell Reports, 2017. **8**(1): p. 125-139.
122. De Bacco, F., et al., *MET inhibition overcomes radiation resistance of glioblastoma stem-like cells.* EMBO Mol Med, 2016. **8**(5): p. 550-68.
123. Tamura, K., et al., *Expansion of CD133-positive glioma cells in recurrent de novo glioblastomas after radiotherapy and chemotherapy.* J Neurosurg, 2013. **119**(5): p. 1145-55.

124. Tamura, K., et al., *Accumulation of CD133-positive glioma cells after high-dose irradiation by Gamma Knife surgery plus external beam radiation.* J Neurosurg, 2010. **113**(2): p. 310-8.
125. Qazi, M.A., et al., *Intratumoral heterogeneity: pathways to treatment resistance and relapse in human glioblastoma.* Ann Oncol, 2017. **28**(7): p. 1448-1456.
126. Abbott, N.J., L. Ronnback, and E. Hansson, *Astrocyte-endothelial interactions at the blood-brain barrier.* Nat Rev Neurosci, 2006. **7**(1): p. 41-53.
127. Abbott, N.J., *Blood-brain barrier structure and function and the challenges for CNS drug delivery.* J Inherit Metab Dis, 2013. **36**(3): p. 437-49.
128. Davies, D.C., *Blood-brain barrier breakdown in septic encephalopathy and brain tumours.* J Anat, 2002. **200**(6): p. 639-46.
129. Papadopoulos, M.C., et al., *Emerging molecular mechanisms of brain tumour oedema.* Br J Neurosurg, 2001. **15**(2): p. 101-8.
130. Phoenix, T.N., et al., *Medulloblastoma Genotype Dictates Blood Brain Barrier Phenotype.* Cancer Cell, 2016. **29**(4): p. 508-522.
131. Sevenich, L., et al., *Analysis of tumour- and stroma-supplied proteolytic networks reveals a brain-metastasis-promoting role for cathepsin S.* Nat Cell Biol, 2014. **16**(9): p. 876-88.
132. Jain, R.K., et al., *Angiogenesis in brain tumours.* Nat Rev Neurosci, 2007. **8**(8): p. 610-22.
133. Jain, R.K., *Normalization of tumor vasculature: an emerging concept in antiangiogenic therapy.* Science, 2005. **307**(5706): p. 58-62.
134. Tong, R.T., et al., *Vascular normalization by vascular endothelial growth factor receptor 2 blockade induces a pressure gradient across the vasculature and improves drug penetration in tumors.* Cancer Res, 2004. **64**(11): p. 3731-6.
135. Winkler, F., et al., *Kinetics of vascular normalization by VEGFR2 blockade governs brain tumor response to radiation: role of oxygenation, angiopoietin-1, and matrix metalloproteinases.* Cancer Cell, 2004. **6**(6): p. 553-63.
136. Wurmser, A.E., et al., *Cell fusion-independent differentiation of neural stem cells to the endothelial lineage.* Nature, 2004. **430**(6997): p. 350-6.
137. Hu, B., et al., *Epigenetic Activation of WNT5A Drives Glioblastoma Stem Cell Differentiation and Invasive Growth.* Cell, 2016. **167**(5): p. 1281-1295 e18.
138. Lathia, J.D., et al., *Cancer stem cells in glioblastoma.* Genes Dev, 2015. **29**(12): p. 1203-17.
139. Pietras, A., et al., *Osteopontin-CD44 signaling in the glioma perivascular niche enhances cancer stem cell phenotypes and promotes aggressive tumor growth.* Cell Stem Cell, 2014. **14**(3): p. 357-69.
140. Quail, D.F. and J.A. Joyce, *The Microenvironmental Landscape of Brain Tumors.* Cancer Cell, 2017. **31**(3): p. 326-341.
141. Wolburg, H., et al., *Brain endothelial cells and the glio-vascular complex.* Cell Tissue Res, 2009. **335**(1): p. 75-96.
142. Sofroniew, M.V., *Astrocyte barriers to neurotoxic inflammation.* Nat Rev Neurosci, 2015. **16**(5): p. 249-63.

143. Quail, D.F., et al., *The tumor microenvironment underlies acquired resistance to CSF-1R inhibition in gliomas.* Science, 2016. **352**(6288): p. aad3018.
144. Le, D.M., et al., *Exploitation of astrocytes by glioma cells to facilitate invasiveness: a mechanism involving matrix metalloproteinase-2 and the urokinase-type plasminogen activator-plasmin cascade.* J Neurosci, 2003. **23**(10): p. 4034-43.
145. Liu, C., et al., *Mosaic analysis with double markers reveals tumor cell of origin in glioma.* Cell, 2011. **146**(2): p. 209-21.
146. Venkatesh, H.S., et al., *Neuronal Activity Promotes Glioma Growth through Neuroligin-3 Secretion.* Cell, 2015. **161**(4): p. 803-16.
147. Neman, J., et al., *Human breast cancer metastases to the brain display GABAergic properties in the neural niche.* Proc Natl Acad Sci U S A, 2014. **111**(3): p. 984-9.
148. Pombo Antunes, A.R., et al., *Understanding the glioblastoma immune microenvironment as basis for the development of new immunotherapeutic strategies.* Elife, 2020. **9**.
149. Louveau, A., T.H. Harris, and J. Kipnis, *Revisiting the Mechanisms of CNS Immune Privilege.* Trends Immunol, 2015. **36**(10): p. 569-577.
150. Galea, I., I. Bechmann, and V.H. Perry, *What is immune privilege (not)?* Trends Immunol, 2007. **28**(1): p. 12-8.
151. Russo, M.V. and D.B. McGavern, *Immune Surveillance of the CNS following Infection and Injury.* Trends Immunol, 2015. **36**(10): p. 637-650.
152. Davies, L.C., et al., *Tissue-resident macrophages.* Nat Immunol, 2013. **14**(10): p. 986-95.
153. Hussain, S.F., et al., *The role of human glioma-infiltrating microglia/macrophages in mediating antitumor immune responses.* Neuro Oncol, 2006. **8**(3): p. 261-79.
154. Hambardzumyan, D., D.H. Gutmann, and H. Kettenmann, *The role of microglia and macrophages in glioma maintenance and progression.* Nat Neurosci, 2016. **19**(1): p. 20-7.
155. Bennett, M.L., et al., *New tools for studying microglia in the mouse and human CNS.* Proc Natl Acad Sci U S A, 2016. **113**(12): p. E1738-46.
156. Bowman, R.L., et al., *Macrophage Ontogeny Underlies Differences in Tumor-Specific Education in Brain Malignancies.* Cell Rep, 2016. **17**(9): p. 2445-2459.
157. Burns, J.M., et al., *A novel chemokine receptor for SDF-1 and I-TAC involved in cell survival, cell adhesion, and tumor development.* J Exp Med, 2006. **203**(9): p. 2201-13.
158. Rempel, S.A., et al., *Identification and localization of the cytokine SDF1 and its receptor, CXC chemokine receptor 4, to regions of necrosis and angiogenesis in human glioblastoma.* Clin Cancer Res, 2000. **6**(1): p. 102-11.
159. Zhu, X., et al., *Systemic delivery of neutralizing antibody targeting CCL2 for glioma therapy.* J Neurooncol, 2011. **104**(1): p. 83-92.

160. Chang, A.L., et al., *CCL2 Produced by the Glioma Microenvironment Is Essential for the Recruitment of Regulatory T Cells and Myeloid-Derived Suppressor Cells.* Cancer Res, 2016. **76**(19): p. 5671-5682.
161. Coniglio, S.J., et al., *Microglial stimulation of glioblastoma invasion involves epidermal growth factor receptor (EGFR) and colony stimulating factor 1 receptor (CSF-1R) signaling.* Mol Med, 2012. **18**: p. 519-27.
162. De, I., et al., *CSF1 Overexpression Promotes High-Grade Glioma Formation without Impacting the Polarization Status of Glioma-Associated Microglia and Macrophages.* Cancer Res, 2016. **76**(9): p. 2552-60.
163. Wei, J., et al., *Osteopontin mediates glioblastoma-associated macrophage infiltration and is a potential therapeutic target.* J Clin Invest, 2019. **129**(1): p. 137-149.
164. Zhou, W., et al., *Periostin secreted by glioblastoma stem cells recruits M2 tumour-associated macrophages and promotes malignant growth.* Nat Cell Biol, 2015. **17**(2): p. 170-82.
165. Friedberg, M.H., et al., *Specific matrix metalloproteinase profiles in the cerebrospinal fluid correlated with the presence of malignant astrocytomas, brain metastases, and carcinomatous meningitis.* Cancer, 1998. **82**(5): p. 923-30.
166. Markovic, D.S., et al., *Gliomas induce and exploit microglial MT1-MMP expression for tumor expansion.* Proc Natl Acad Sci U S A, 2009. **106**(30): p. 12530-5.
167. Ye, X.Z., et al., *Tumor-associated microglia/macrophages enhance the invasion of glioma stem-like cells via TGF-beta1 signaling pathway.* J Immunol, 2012. **189**(1): p. 444-53.
168. Qi, L., et al., *IL-10 secreted by M2 macrophage promoted tumorigenesis through interaction with JAK2 in glioma.* Oncotarget, 2016. **7**(44): p. 71673-71685.
169. Wang, T., et al., *Regulation of the innate and adaptive immune responses by Stat-3 signaling in tumor cells.* Nat Med, 2004. **10**(1): p. 48-54.
170. Van Meir, E.G., *Cytokines and tumors of the central nervous system.* Glia, 1995. **15**(3): p. 264-88.
171. Platten, M., W. Wick, and M. Weller, *Malignant glioma biology: role for TGF-beta in growth, motility, angiogenesis, and immune escape.* Microsc Res Tech, 2001. **52**(4): p. 401-10.
172. Fontana, A., et al., *Expression of TGF-beta 2 in human glioblastoma: a role in resistance to immune rejection?* Ciba Found Symp, 1991. **157**: p. 232-8; discussion 238-41.
173. Crane, C.A., et al., *Soluble factors secreted by glioblastoma cell lines facilitate recruitment, survival, and expansion of regulatory T cells: implications for immunotherapy.* Neuro Oncol, 2012. **14**(5): p. 584-95.
174. Bhat, K.P.L., et al., *Mesenchymal differentiation mediated by NF-kappaB promotes radiation resistance in glioblastoma.* Cancer Cell, 2013. **24**(3): p. 331-46.

175. Wang, Q., et al., *Tumor Evolution of Glioma-Intrinsic Gene Expression Subtypes Associates with Immunological Changes in the Microenvironment.* Cancer Cell, 2017. **32**(1): p. 42-56 e6.
176. Raychaudhuri, B., et al., *Myeloid-derived suppressor cell accumulation and function in patients with newly diagnosed glioblastoma.* Neuro Oncol, 2011. **13**(6): p. 591-9.
177. Raychaudhuri, B., et al., *Myeloid derived suppressor cell infiltration of murine and human gliomas is associated with reduction of tumor infiltrating lymphocytes.* J Neurooncol, 2015. **122**(2): p. 293-301.
178. Dubinski, D., et al., *CD4+ T effector memory cell dysfunction is associated with the accumulation of granulocytic myeloid-derived suppressor cells in glioblastoma patients.* Neuro Oncol, 2016. **18**(6): p. 807-18.
179. Di Tomaso, T., et al., *Immunobiological characterization of cancer stem cells isolated from glioblastoma patients.* Clin Cancer Res, 2010. **16**(3): p. 800-13.
180. Kamran, N., et al., *Immunosuppressive Myeloid Cells' Blockade in the Glioma Microenvironment Enhances the Efficacy of Immune-Stimulatory Gene Therapy.* Mol Ther, 2017. **25**(1): p. 232-248.
181. Zhang, P., et al., *Therapeutic targeting of tumor-associated myeloid cells synergizes with radiation therapy for glioblastoma.* Proc Natl Acad Sci U S A, 2019. **116**(47): p. 23714-23723.
182. Orrego, E., et al., *Distribution of tumor-infiltrating immune cells in glioblastoma.* CNS Oncol, 2018. **7**(4): p. CNS21.
183. Woroniecka, K. and P.E. Fecci, *T-cell exhaustion in glioblastoma.* Oncotarget, 2018. **9**(82): p. 35287-35288.
184. Wherry, E.J., et al., *Molecular signature of CD8+ T cell exhaustion during chronic viral infection.* Immunity, 2007. **27**(4): p. 670-84.
185. Koyama, S., et al., *Adaptive resistance to therapeutic PD-1 blockade is associated with upregulation of alternative immune checkpoints.* Nat Commun, 2016. **7**: p. 10501.
186. Woroniecka, K., et al., *T-Cell Exhaustion Signatures Vary with Tumor Type and Are Severe in Glioblastoma.* Clin Cancer Res, 2018. **24**(17): p. 4175-4186.
187. Woroniecka, K.I., et al., *T-cell Dysfunction in Glioblastoma: Applying a New Framework.* Clin Cancer Res, 2018. **24**(16): p. 3792-3802.
188. Allan, S.E., et al., *The role of 2 FOXP3 isoforms in the generation of human CD4+ Tregs.* J Clin Invest, 2005. **115**(11): p. 3276-84.
189. Colombo, M.P. and S. Piconese, *Regulatory-T-cell inhibition versus depletion: the right choice in cancer immunotherapy.* Nat Rev Cancer, 2007. **7**(11): p. 880-7.
190. Jacobs, J.F., et al., *Prognostic significance and mechanism of Treg infiltration in human brain tumors.* J Neuroimmunol, 2010. **225**(1-2): p. 195-9.
191. Heimberger, A.B., et al., *Incidence and prognostic impact of FoxP3+ regulatory T cells in human gliomas.* Clin Cancer Res, 2008. **14**(16): p. 5166-72.
192. Elliott, L.H., W.H. Brooks, and T.L. Roszman, *Activation of immunoregulatory lymphocytes obtained from patients with malignant gliomas.* J Neurosurg, 1987. **67**(2): p. 231-6.

193. Jordan, J.T., et al., *Preferential migration of regulatory T cells mediated by glioma-secreted chemokines can be blocked with chemotherapy.* Cancer Immunol Immunother, 2008. **57**(1): p. 123-31.
194. Desbaillets, I., et al., *Human astrocytomas and glioblastomas express monocyte chemoattractant protein-1 (MCP-1) in vivo and in vitro.* Int J Cancer, 1994. **58**(2): p. 240-7.
195. Humphries, W., et al., *The role of tregs in glioma-mediated immunosuppression: potential target for intervention.* Neurosurg Clin N Am, 2010. **21**(1): p. 125-37.
196. Simon, M.C. and B. Keith, *The role of oxygen availability in embryonic development and stem cell function.* Nat Rev Mol Cell Biol, 2008. **9**(4): p. 285-96.
197. Pistollato, F., et al., *Oxygen tension controls the expansion of human CNS precursors and the generation of astrocytes and oligodendrocytes.* Mol Cell Neurosci, 2007. **35**(3): p. 424-35.
198. Colwell, N., et al., *Hypoxia in the glioblastoma microenvironment: shaping the phenotype of cancer stem-like cells.* Neuro Oncol, 2017. **19**(7): p. 887-896.
199. Sheehan, J.P., et al., *Improving the radiosensitivity of radioresistant and hypoxic glioblastoma.* Future Oncol, 2010. **6**(10): p. 1591-601.
200. Chiche, J., M.C. Brahimi-Horn, and J. Pouyssegur, *Tumour hypoxia induces a metabolic shift causing acidosis: a common feature in cancer.* J Cell Mol Med, 2010. **14**(4): p. 771-94.
201. Rankin, E.B. and A.J. Giaccia, *The role of hypoxia-inducible factors in tumorigenesis.* Cell Death Differ, 2008. **15**(4): p. 678-85.
202. Nakazawa, M.S., B. Keith, and M.C. Simon, *Oxygen availability and metabolic adaptations.* Nat Rev Cancer, 2016. **16**(10): p. 663-73.
203. Barsoum, I.B., et al., *A mechanism of hypoxia-mediated escape from adaptive immunity in cancer cells.* Cancer Res, 2014. **74**(3): p. 665-74.
204. Bronisz, A., et al., *Hypoxic Roadmap of Glioblastoma-Learning about Directions and Distances in the Brain Tumor Environment.* Cancers (Basel), 2020. **12**(5).
205. Lee, S.B., et al., *An ID2-dependent mechanism for VHL inactivation in cancer.* Nature, 2016. **529**(7585): p. 172-7.
206. Dang, E.V., et al., *Control of T(H)17/T(reg) balance by hypoxia-inducible factor 1.* Cell, 2011. **146**(5): p. 772-84.
207. Sedlakova, O., et al., *Carbonic anhydrase IX, a hypoxia-induced catalytic component of the pH regulating machinery in tumors.* Front Physiol, 2014. **4**: p. 400.
208. Agnihotri, S. and G. Zadeh, *Metabolic reprogramming in glioblastoma: the influence of cancer metabolism on epigenetics and unanswered questions.* Neuro Oncol, 2016. **18**(2): p. 160-72.
209. McDonald, P.C., et al., *Recent developments in targeting carbonic anhydrase IX for cancer therapeutics.* Oncotarget, 2012. **3**(1): p. 84-97.
210. Darvin, P., et al., *Immune checkpoint inhibitors: recent progress and potential biomarkers.* Exp Mol Med, 2018. **50**(12): p. 1-11.
211. Roberts, Z.J., et al., *Axicabtagene ciloleucel, a first-in-class CAR T cell therapy for aggressive NHL.* Leuk Lymphoma, 2018. **59**(8): p. 1785-1796.

212. Weenink, B., et al., *Immunotherapy in Glioblastoma: Current Shortcomings and Future Perspectives.* Cancers (Basel), 2020. **12**(3).
213. Prasad, S., et al., *Effective Eradication of Glioblastoma Stem Cells by Local Application of an AC133/CD133-Specific T-cell-Engaging Antibody and CD8 T Cells.* Cancer Res, 2015. **75**(11): p. 2166-76.
214. Choi, B.D., et al., *Human regulatory T cells kill tumor cells through granzyme-dependent cytotoxicity upon retargeting with a bispecific antibody.* Cancer Immunol Res, 2013. **1**(3): p. 163.
215. Choi, B.D., et al., *Systemic administration of a bispecific antibody targeting EGFRvIII successfully treats intracerebral glioma.* Proc Natl Acad Sci U S A, 2013. **110**(1): p. 270-5.
216. Rosenberg, S.A., et al., *Use of tumor-infiltrating lymphocytes and interleukin-2 in the immunotherapy of patients with metastatic melanoma. A preliminary report.* N Engl J Med, 1988. **319**(25): p. 1676-80.
217. Sadelain, M., *CAR therapy: the CD19 paradigm.* J Clin Invest, 2015. **125**(9): p. 3392-400.
218. June, C.H., et al., *CAR T cell immunotherapy for human cancer.* Science, 2018. **359**(6382): p. 1361-1365.
219. Kuwana, Y., et al., *Expression of chimeric receptor composed of immunoglobulin-derived V regions and T-cell receptor-derived C regions.* Biochem Biophys Res Commun, 1987. **149**(3): p. 960-8.
220. Gross, G., T. Waks, and Z. Eshhar, *Expression of immunoglobulin-T-cell receptor chimeric molecules as functional receptors with antibody-type specificity.* Proc Natl Acad Sci U S A, 1989. **86**(24): p. 10024-8.
221. Abate-Daga, D. and M.L. Davila, *CAR models: next-generation CAR modifications for enhanced T-cell function.* Mol Ther Oncolytics, 2016. **3**: p. 16014.
222. Chmielewski, M. and H. Abken, *TRUCKs: the fourth generation of CARs.* Expert Opin Biol Ther, 2015. **15**(8): p. 1145-54.
223. Garrido, F., et al., *The urgent need to recover MHC class I in cancers for effective immunotherapy.* Curr Opin Immunol, 2016. **39**: p. 44-51.
224. Han, X., et al., *Multi-antigen-targeted chimeric antigen receptor T cells for cancer therapy.* J Hematol Oncol, 2019. **12**(1): p. 128.
225. Land, C.A., et al., *Chimeric antigen receptor T-cell therapy in glioblastoma: charging the T cells to fight.* J Transl Med, 2020. **18**(1): p. 428.
226. O'Leary, M.C., et al., *FDA Approval Summary: Tisagenlecleucel for Treatment of Patients with Relapsed or Refractory B-cell Precursor Acute Lymphoblastic Leukemia.* Clin Cancer Res, 2019. **25**(4): p. 1142-1146.
227. Brown, C.E., et al., *Stem-like tumor-initiating cells isolated from IL13Ralpha2 expressing gliomas are targeted and killed by IL13-zetakine-redirected T Cells.* Clin Cancer Res, 2012. **18**(8): p. 2199-209.
228. Morgan, R.A., et al., *Recognition of glioma stem cells by genetically modified T cells targeting EGFRvIII and development of adoptive cell therapy for glioma.* Hum Gene Ther, 2012. **23**(10): p. 1043-53.

229. Ahmed, N., et al., *HER2-specific T cells target primary glioblastoma stem cells and induce regression of autologous experimental tumors.* Clin Cancer Res, 2010. **16**(2): p. 474-85.
230. Miao, H., et al., *EphA2 promotes infiltrative invasion of glioma stem cells in vivo through cross-talk with Akt and regulates stem cell properties.* Oncogene, 2015. **34**(5): p. 558-67.
231. Mount, C.W., et al., *Potent antitumor efficacy of anti-GD2 CAR T cells in H3-K27M(+) diffuse midline gliomas.* Nat Med, 2018. **24**(5): p. 572-579.
232. Golinelli, G., et al., *Targeting GD2-positive glioblastoma by chimeric antigen receptor empowered mesenchymal progenitors.* Cancer Gene Ther, 2020. **27**(7-8): p. 558-570.
233. Majzner, R.G., et al., *CAR T Cells Targeting B7-H3, a Pan-Cancer Antigen, Demonstrate Potent Preclinical Activity Against Pediatric Solid Tumors and Brain Tumors.* Clin Cancer Res, 2019. **25**(8): p. 2560-2574.
234. Wang, D., et al., *Chlorotoxin-directed CAR T cells for specific and effective targeting of glioblastoma.* Sci Transl Med, 2020. **12**(533).
235. Jin, L., et al., *CD70, a novel target of CAR T-cell therapy for gliomas.* Neuro Oncol, 2018. **20**(1): p. 55-65.
236. Vora, P., et al., *The Rational Development of CD133-Targeting Immunotherapies for Glioblastoma.* Cell Stem Cell, 2020. **26**(6): p. 832-844 e6.
237. Grupp, S.A., et al., *Chimeric antigen receptor-modified T cells for acute lymphoid leukemia.* N Engl J Med, 2013. **368**(16): p. 1509-1518.
238. Akhavan, D., et al., *CAR T cells for brain tumors: Lessons learned and road ahead.* Immunol Rev, 2019. **290**(1): p. 60-84.
239. Lim, M., et al., *Current state of immunotherapy for glioblastoma.* Nat Rev Clin Oncol, 2018. **15**(7): p. 422-442.
240. Pardoll, D.M., *The blockade of immune checkpoints in cancer immunotherapy.* Nat Rev Cancer, 2012. **12**(4): p. 252-64.
241. Fife, B.T. and J.A. Bluestone, *Control of peripheral T-cell tolerance and autoimmunity via the CTLA-4 and PD-1 pathways.* Immunol Rev, 2008. **224**: p. 166-82.
242. Sharpe, A.H. and K.E. Pauken, *The diverse functions of the PD1 inhibitory pathway.* Nat Rev Immunol, 2018. **18**(3): p. 153-167.
243. Jackson, C.M., J. Choi, and M. Lim, *Mechanisms of immunotherapy resistance: lessons from glioblastoma.* Nat Immunol, 2019. **20**(9): p. 1100-1109.
244. Zhang, N., et al., *Treatment Progress of Immune Checkpoint Blockade Therapy for Glioblastoma.* Front Immunol, 2020. **11**: p. 592612.
245. Fecci, P.E., A.B. Heimberger, and J.H. Sampson, *Immunotherapy for primary brain tumors: no longer a matter of privilege.* Clin Cancer Res, 2014. **20**(22): p. 5620-9.
246. Yap, T.A., et al., *Intratumor heterogeneity: seeing the wood for the trees.* Sci Transl Med, 2012. **4**(127): p. 127ps10.
247. McGranahan, N. and C. Swanton, *Biological and therapeutic impact of intratumor heterogeneity in cancer evolution.* Cancer Cell, 2015. **27**(1): p. 15-26.

248. Johnson, B.E., et al., *Mutational analysis reveals the origin and therapy-driven evolution of recurrent glioma.* Science, 2014. **343**(6167): p. 189-193.
249. Qazi, M.A., et al., *A novel stem cell culture model of recurrent glioblastoma.* J Neurooncol, 2016. **126**(1): p. 57-67.
250. Iorgulescu, J.B., et al., *Immunotherapy for glioblastoma: going viral.* Nat Med, 2018. **24**(8): p. 1094-1096.
251. Szopa, W., et al., *Diagnostic and Therapeutic Biomarkers in Glioblastoma: Current Status and Future Perspectives.* Biomed Res Int, 2017. **2017**: p. 8013575.
252. Cancer Genome Atlas Research, N., *Comprehensive genomic characterization defines human glioblastoma genes and core pathways.* Nature, 2008. **455**(7216): p. 1061-8.
253. Liang, Y., et al., *Gene expression profiling reveals molecularly and clinically distinct subtypes of glioblastoma multiforme.* Proc Natl Acad Sci U S A, 2005. **102**(16): p. 5814-9.
254. Chen, Z. and D. Hambardzumyan, *Immune Microenvironment in Glioblastoma Subtypes.* Front Immunol, 2018. **9**: p. 1004.
255. Tomaszewski, W., et al., *Brain Tumor Microenvironment and Host State: Implications for Immunotherapy.* Clin Cancer Res, 2019. **25**(14): p. 4202-4210.
256. Omuro, A. and L.M. DeAngelis, *Glioblastoma and other malignant gliomas: a clinical review.* JAMA, 2013. **310**(17): p. 1842-50.
257. Stupp, R. and D.C. Weber, *The role of radio- and chemotherapy in glioblastoma.* Onkologie, 2005. **28**(6-7): p. 315-7.
258. Ostrom, Q.T., et al., *American Brain Tumor Association Adolescent and Young Adult Primary Brain and Central Nervous System Tumors Diagnosed in the United States in 2008-2012.* Neuro Oncol, 2016. **18 Suppl 1**: p. i1-i50.
259. Stupp, R., et al., *Effects of radiotherapy with concomitant and adjuvant temozolomide versus radiotherapy alone on survival in glioblastoma in a randomised phase III study: 5-year analysis of the EORTC-NCIC trial.* Lancet Oncol, 2009. **10**(5): p. 459-66.
260. Hegi, M.E., et al., *MGMT gene silencing and benefit from temozolomide in glioblastoma.* N Engl J Med, 2005. **352**(10): p. 997-1003.
261. Noroxe, D.S., H.S. Poulsen, and U. Lassen, *Hallmarks of glioblastoma: a systematic review.* ESMO Open, 2016. **1**(6): p. e000144.
262. Wen, P.Y. and S. Kesari, *Malignant gliomas in adults.* N Engl J Med, 2008. **359**(5): p. 492-507.
263. Liu, G., et al., *Analysis of gene expression and chemoresistance of CD133+ cancer stem cells in glioblastoma*, in *Mol Cancer*. 2006. p. 67.
264. Cooper, L.A., et al., *The tumor microenvironment strongly impacts master transcriptional regulators and gene expression class of glioblastoma.* Am J Pathol, 2012. **180**(5): p. 2108-19.
265. Pastorekova, S. and R.J. Gillies, *The role of carbonic anhydrase IX in cancer development: links to hypoxia, acidosis, and beyond.* Cancer Metastasis Rev, 2019. **38**(1-2): p. 65-77.

266. Lee, S.H. and J.R. Griffiths, *How and Why Are Cancers Acidic? Carbonic Anhydrase IX and the Homeostatic Control of Tumour Extracellular pH.* Cancers (Basel), 2020. **12**(6).
267. Proescholdt, M.A., et al., *Function of carbonic anhydrase IX in glioblastoma multiforme.* Neuro Oncol, 2012. **14**(11): p. 1357-66.
268. Said, H.M., et al., *Modulation of carbonic anhydrase 9 (CA9) in human brain cancer.* Curr Pharm Des, 2010. **16**(29): p. 3288-99.
269. Heaton, J.T., S.M. Farabaugh, and S.E. Brauth, *Effect of syringeal denervation in the budgerigar (Melopsittacus undulatus): the role of the syrinx in call production.* Neurobiol Learn Mem, 1995. **64**(1): p. 68-82.
270. Soyupak, B., et al., *CA9 expression as a prognostic factor in renal clear cell carcinoma.* Urol Int, 2005. **74**(1): p. 68-73.
271. Liao, S.Y., M.I. Lerman, and E.J. Stanbridge, *Expression of transmembrane carbonic anhydrases, CAIX and CAXII, in human development.* BMC Dev Biol, 2009. **9**: p. 22.
272. Ivanov, S., et al., *Expression of hypoxia-inducible cell-surface transmembrane carbonic anhydrases in human cancer.* Am J Pathol, 2001. **158**(3): p. 905-19.
273. McIntyre, A., et al., *Carbonic anhydrase IX promotes tumor growth and necrosis in vivo and inhibition enhances anti-VEGF therapy.* Clin Cancer Res, 2012. **18**(11): p. 3100-11.
274. Boyd, N.H., et al., *Addition of carbonic anhydrase 9 inhibitor SLC-0111 to temozolomide treatment delays glioblastoma growth in vivo.* JCI Insight, 2017. **2**(24).
275. Touisni, N., et al., *Glycosyl coumarin carbonic anhydrase IX and XII inhibitors strongly attenuate the growth of primary breast tumors.* J Med Chem, 2011. **54**(24): p. 8271-7.
276. Zatovicova, M., et al., *Monoclonal antibody G250 targeting CA : Binding specificity, internalization and therapeutic effects in a non-renal cancer model.* Int J Oncol, 2014. **45**(6): p. 2455-67.
277. Lam, J.S., et al., *G250: a carbonic anhydrase IX monoclonal antibody.* Curr Oncol Rep, 2005. **7**(2): p. 109-15.
278. Zatovicova, M., et al., *Carbonic anhydrase IX as an anticancer therapy target: preclinical evaluation of internalizing monoclonal antibody directed to catalytic domain.* Curr Pharm Des, 2010. **16**(29): p. 3255-63.
279. Baeuerle, P.A., P. Kufer, and R. Bargou, *BiTE: Teaching antibodies to engage T-cells for cancer therapy.* Curr Opin Mol Ther, 2009. **11**(1): p. 22-30.
280. Klein, J.S., et al., *Examination of the contributions of size and avidity to the neutralization mechanisms of the anti-HIV antibodies b12 and 4E10.* Proc Natl Acad Sci U S A, 2009. **106**(18): p. 7385-90.
281. Brischwein, K., et al., *Strictly target cell-dependent activation of T cells by bispecific single-chain antibody constructs of the BiTE class.* J Immunother, 2007. **30**(8): p. 798-807.

282. Herrmann, I., et al., *Highly efficient elimination of colorectal tumor-initiating cells by an EpCAM/CD3-bispecific antibody engaging human T cells.* PLoS One, 2010. **5**(10): p. e13474.
283. Hoffmann, P., et al., *Serial killing of tumor cells by cytotoxic T cells redirected with a CD19-/CD3-bispecific single-chain antibody construct.* Int J Cancer, 2005. **115**(1): p. 98-104.
284. Venugopal, C., et al., *Processing of primary brain tumor tissue for stem cell assays and flow sorting.* J Vis Exp, 2012(67).
285. Lobo, N.C., et al., *Efficient generation of patient-matched malignant and normal primary cell cultures from clear cell renal cell carcinoma patients: clinically relevant models for research and personalized medicine.* BMC Cancer, 2016. **16**: p. 485.
286. Qazi, M., et al., *Generation of murine xenograft models of brain tumors from primary human tissue for in vivo analysis of the brain tumor-initiating cell.* Methods Mol Biol, 2014. **1210**: p. 37-49.
287. Benej, M., S. Pastorekova, and J. Pastorek, *Carbonic anhydrase IX: regulation and role in cancer.* Subcell Biochem, 2014. **75**: p. 199-219.
288. Heddleston, J.M., et al., *The hypoxic microenvironment maintains glioblastoma stem cells and promotes reprogramming towards a cancer stem cell phenotype.* Cell Cycle, 2009. **8**(20): p. 3274-84.
289. Oosterwijk, E., et al., *Monoclonal antibody G 250 recognizes a determinant present in renal-cell carcinoma and absent from normal kidney.* Int J Cancer, 1986. **38**(4): p. 489-94.
290. Dorai, T., et al., *The role of carbonic anhydrase IX overexpression in kidney cancer.* Eur J Cancer, 2005. **41**(18): p. 2935-47.
291. Shiheido, H., et al., *Modulation of the human T cell response by a novel non-mitogenic anti-CD3 antibody.* PLoS One, 2014. **9**(4): p. e94324.
292. Sathornsumetee, S., et al., *Tumor angiogenic and hypoxic profiles predict radiographic response and survival in malignant astrocytoma patients treated with bevacizumab and irinotecan.* J Clin Oncol, 2008. **26**(2): p. 271-8.
293. Matolay, O., et al., *[The role of carbonic anhydrase IX in the progression of malignant tumors - a potential therapeutic target?].* Magy Onkol, 2021. **65**(2): p. 157-166.
294. Lou, Y., et al., *Targeting tumor hypoxia: suppression of breast tumor growth and metastasis by novel carbonic anhydrase IX inhibitors.* Cancer Res, 2011. **71**(9): p. 3364-76.
295. Chiche, J., et al., *Hypoxia-inducible carbonic anhydrase IX and XII promote tumor cell growth by counteracting acidosis through the regulation of the intracellular pH.* Cancer Res, 2009. **69**(1): p. 358-68.
296. Cazzamalli, S., et al., *Enhanced Therapeutic Activity of Non-Internalizing Small-Molecule-Drug Conjugates Targeting Carbonic Anhydrase IX in Combination with Targeted Interleukin-2.* Clin Cancer Res, 2018. **24**(15): p. 3656-3667.
297. Chames, P., et al., *Therapeutic antibodies: successes, limitations and hopes for the future.* Br J Pharmacol, 2009. **157**(2): p. 220-33.

298. Baeuerle, P.A. and C. Reinhardt, *Bispecific T-cell engaging antibodies for cancer therapy.* Cancer Res, 2009. **69**(12): p. 4941-4.
299. Suryadevara, C.M., et al., *Are BiTEs the "missing link" in cancer therapy?* Oncoimmunology, 2015. **4**(6): p. e1008339.
300. Sheridan, C., *Amgen's bispecific antibody puffs across finish line.* Nat Biotechnol, 2015. **33**(3): p. 219-21.
301. Bargou, R., et al., *Tumor regression in cancer patients by very low doses of a T cell-engaging antibody.* Science, 2008. **321**(5891): p. 974-7.
302. Wolf, E., et al., *BiTEs: bispecific antibody constructs with unique anti-tumor activity.* Drug Discov Today, 2005. **10**(18): p. 1237-44.
303. Molhoj, M., et al., *CD19-/CD3-bispecific antibody of the BiTE class is far superior to tandem diabody with respect to redirected tumor cell lysis.* Mol Immunol, 2007. **44**(8): p. 1935-43.
304. Kim, H., et al., *Whole-genome and multisector exome sequencing of primary and post-treatment glioblastoma reveals patterns of tumor evolution.* Genome Res, 2015. **25**(3): p. 316-27.
305. Meyer, M., et al., *Single cell-derived clonal analysis of human glioblastoma links functional and genomic heterogeneity.* Proc Natl Acad Sci U S A, 2015. **112**(3): p. 851-6.
306. Korber, V., et al., *Evolutionary Trajectories of IDH(WT) Glioblastomas Reveal a Common Path of Early Tumorigenesis Instigated Years ahead of Initial Diagnosis.* Cancer Cell, 2019. **35**(4): p. 692-704 e12.
307. Cox, J. and M. Mann, *MaxQuant enables high peptide identification rates, individualized p.p.b.-range mass accuracies and proteome-wide protein quantification.* Nat Biotechnol, 2008. **26**(12): p. 1367-72.
308. Cox, J., et al., *Accurate proteome-wide label-free quantification by delayed normalization and maximal peptide ratio extraction, termed MaxLFQ.* Mol Cell Proteomics, 2014. **13**(9): p. 2513-26.
309. Wojtowicz, E.E., et al., *Ectopic miR-125a Expression Induces Long-Term Repopulating Stem Cell Capacity in Mouse and Human Hematopoietic Progenitors.* Cell Stem Cell, 2016. **19**(3): p. 383-96.
310. Wilkerson, M.D. and D.N. Hayes, *ConsensusClusterPlus: a class discovery tool with confidence assessments and item tracking.* Bioinformatics, 2010. **26**(12): p. 1572-3.
311. Romaniuk, P.J., et al., *A comparison of the solution structures and conformational properties of the somatic and oocyte 5S rRNAs of Xenopus laevis.* Nucleic Acids Res, 1988. **16**(5): p. 2295-312.
312. Chen, H. and P.C. Boutros, *VennDiagram: a package for the generation of highly-customizable Venn and Euler diagrams in R.* BMC Bioinformatics, 2011. **12**: p. 35.
313. Hart, T., et al., *Evaluation and Design of Genome-Wide CRISPR/SpCas9 Knockout Screens.* G3 (Bethesda), 2017. **7**(8): p. 2719-2727.
314. P'ng, C., et al., *BPG: Seamless, automated and interactive visualization of scientific data.* BMC Bioinformatics, 2019. **20**(1): p. 42.

315. Sinha, A., et al., *The Proteogenomic Landscape of Curable Prostate Cancer.* Cancer Cell, 2019. **35**(3): p. 414-427 e6.
316. Wang, L.B., et al., *Proteogenomic and metabolomic characterization of human glioblastoma.* Cancer Cell, 2021. **39**(4): p. 509-528 e20.
317. Dar, A.A., et al., *Extracellular 2'5'-oligoadenylate synthetase 2 mediates T-cell receptor CD3-zeta chain down-regulation via caspase-3 activation in oral cancer.* Immunology, 2016. **147**(2): p. 251-64.
318. Jing, W., et al., *Breast cancer cells promote CD169(+) macrophage-associated immunosuppression through JAK2-mediated PD-L1 upregulation on macrophages.* Int Immunopharmacol, 2020. **78**: p. 106012.
319. Casey, A.E., et al., *Mammary molecular portraits reveal lineage-specific features and progenitor cell vulnerabilities.* J Cell Biol, 2018. **217**(8): p. 2951-2974.
320. Vasaikar, S., et al., *Proteogenomic Analysis of Human Colon Cancer Reveals New Therapeutic Opportunities.* Cell, 2019. **177**(4): p. 1035-1049 e19.
321. Yang, M., et al., *Proteogenomics and Hi-C reveal transcriptional dysregulation in high hyperdiploid childhood acute lymphoblastic leukemia.* Nat Commun, 2019. **10**(1): p. 1519.
322. Zhu, Y., et al., *Discovery of coding regions in the human genome by integrated proteogenomics analysis workflow.* Nat Commun, 2018. **9**(1): p. 903.
323. Hoekstra, M.E., et al., *Long-distance modulation of bystander tumor cells by CD8(+) T cell-secreted IFNgamma.* Nat Cancer, 2020. **1**(3): p. 291-301.
324. Thibaut, R., et al., *Bystander IFN-gamma activity promotes widespread and sustained cytokine signaling altering the tumor microenvironment.* Nat Cancer, 2020. **1**(3): p. 302-314.
325. Gangoso, E., et al., *Glioblastomas acquire myeloid-affiliated transcriptional programs via epigenetic immunoediting to elicit immune evasion.* Cell, 2021. **184**(9): p. 2454-2470 e26.
326. Choi, U.Y., et al., *Oligoadenylate synthase-like (OASL) proteins: dual functions and associations with diseases.* Exp Mol Med, 2015. **47**: p. e144.
327. Zhang, Y. and C. Yu, *Prognostic characterization of OAS1/OAS2/OAS3/OASL in breast cancer.* BMC Cancer, 2020. **20**(1): p. 575.
328. Hara, T., et al., *Interactions between cancer cells and immune cells drive transitions to mesenchymal-like states in glioblastoma.* Cancer Cell, 2021. **39**(6): p. 779-792 e11.
329. Cetin, B., et al., *Carbonic anhydrase IX is a prognostic biomarker in glioblastoma multiforme.* Neuropathology, 2018. **38**(5): p. 457-462.
330. Fadul, C.E., et al., *Immune modulation effects of concomitant temozolomide and radiation therapy on peripheral blood mononuclear cells in patients with glioblastoma multiforme.* Neuro Oncol, 2011. **13**(4): p. 393-400.
331. Gupta, K. and T.C. Burns, *Radiation-Induced Alterations in the Recurrent Glioblastoma Microenvironment: Therapeutic Implications.* Front Oncol, 2018. **8**: p. 503.

332. Mohme, M., et al., *Immunophenotyping of Newly Diagnosed and Recurrent Glioblastoma Defines Distinct Immune Exhaustion Profiles in Peripheral and Tumor-infiltrating Lymphocytes.* Clin Cancer Res, 2018. **24**(17): p. 4187-4200.
333. Cao, J., et al., *Comprehensive single-cell transcriptional profiling of a multicellular organism.* Science, 2017. **357**(6352): p. 661-667.
334. Cao, J., et al., *The single-cell transcriptional landscape of mammalian organogenesis.* Nature, 2019. **566**(7745): p. 496-502.